# Abstract

YELVERTON, TIFFANY LEIGH BERRY. Soot Formation in Laminar Jet Diffusion Flames at Elevated Pressures. (Under the direction of Dr. William L. Roberts.)

Fossil fuels, which have a finite and depleting source, are currently needed to provide energy for most practical combustion devices across the world. Due to the ever increasing demand for these combustion devices, it is essential that research focus on finding ways to make these combustion processes more efficient. In order to ensure thermodynamic efficiency and high power output, these combustion devices typically operate at elevated pressures, which have been shown to increase the pollutant (particularly soot and nitrogen oxides) production. One way to ensure these combustion devices are working as efficiently as possible is to reduce or eliminate the production of these pollutants. Therefore the following investigation was completed in order to better understand the growth and production of soot caused by combustion inefficiencies.

The current investigation uses five individual, but interrelated, experiments in order to analyze soot formation in hydrocarbon-air diffusion flames at elevated pressures, where most common combustion devices operate. The investigations were conducted in a co-flow laminar diffusion flame burner, and utilized two hydrocarbon fuels (methane and ethylene) in pure and diluted form. The addition of diluent (helium, nitrogen, argon, or carbon dioxide) to the fuel stream enabled the investigation to focus on the reduction of soot formation within these flames, and thus focus on gaining a better understanding of soot growth and production in commonly used combustion devices such as automobiles, military vehicles, aircraft, and non-mobile combustion devices.

Through this investigation several interesting observation were made from the analysis of pressure and dilution effects on ethylene and methane flames. It was shown that the addition of inert diluent to the fuel stream does decrease the flame's propensity to soot, with carbon dioxide proving to be a superior soot suppressant compared to helium. It was also shown in heavily diluted flames that in some instances there is not only a chemical effect on the sooting tendencies of diluted flames, but also a purely diffusion driven effect. Each of the individual experiments is discussed in detail, with further observations and conclusions, in the following chapters.

# Soot Formation in Laminar Jet Diffusion Flames at Elevated Pressures

by
Tiffany Leigh Berry Yelverton

A dissertation submitted to the Graduate Faculty of
North Carolina State University
in partial fulfillment of the
requirements for the Degree of
Doctor of Philosophy

Mechanical Engineering

Raleigh, North Carolina

2008

APPROVED BY:

_____

Dr. William L. Roberts
Chair of Supervisory Committee

_____

Dr. Tarek Echekki
Member of Supervisory Committee

_____

Dr. Kevin M. Lyons
Member of Supervisory Committee

_____

Dr. Tiegang Fang
Member of Supervisory Committee

_____

Dr. Adrianna de Souza e'Silva
Member of Supervisory Committee

# Dedication

***…to my whole family, especially the two men in my life:***

***my daddy, my hero***

***and***

***my husband, the love of my life…***

# Biography

The author was born Tiffany Leigh Berry on December 31, 1980 in Raleigh, North Carolina, daughter of Billy and Dorothy Berry and younger sister of Adrienne Lynn (Berry) Bauer. She graduated in 1999 from Cary High School, but prior to her senior year had already applied to attend North Carolina State University to pursue a degree in Aerospace Engineering. Upon completion of her undergraduate studies in May 2003, she decided to continue her education and applied and was accepted to the Aerospace Engineering program for her Master of Science. During her first year of graduate school she decided that she wanted to pursue a Doctorate degree in order to one day return to academia. With the help of her advisor, Dr. William L. Roberts, a research proposal was determined that allowed many phases of her research to be conducted that would carry her through both of her graduate degree programs. She completed her Master of Science in Aerospace Engineering in July 2005, and began her Doctorate studies in Mechanical Engineering, which was better suited for her combustion research.

Therefore, Tiffany graduates as a Doctor of Philosophy in Mechanical Engineering in August 2008. While working towards her Ph.D. she was lucky enough to marry her best friend, William Yelverton, and thus she will graduate Tiffany Leigh Berry Yelverton. Although Tiffany's plans for returning to academia at some point are not completely out of the question, she is currently seeking to stay in research as a postdoctoral researcher, not at the university, but rather with the National Risk Management Research Laboratory of the Environmental Protection Agency in Research Triangle Park under the technical advisement of Bill Linak, Ph.D.

# Acknowledgements

The author would like to acknowledge her advisor, Dr. William L. Roberts, whose love of research, and knowledge of combustion and thermal sciences has been a great source of help throughout these many years in which they have worked together; her committee for their help and guidance; Sean Danby (especially for all his help in coding) Carlye Rojas, Ranjith Kumar, Wes Boyette and Dan Cassidy for all their help and support throughout many trials and tribulations of research, for being such great friends, and for always making the AERL fun; Bill Linak and Bob Seila at the Environmental Protection Agency, for their seemingly unending help and understanding that experimental research knows no timeline; Neervi Shah, Malia McCarthy, and Jane Vignovic for being there to listen to her complain and to offer her comfort or a batch of margaritas.

The author would like to acknowledge most of all her family; her parents Billy and Dorothy Berry who have provided more support (both emotional and financial) than any child could ever ask for, as well as for teaching her all the values needed to succeed in life: believe in yourself, believe in your family, care for others, and always work as hard as you can so that all your dreams can come true; her sister, and best friend, Adrienne Bauer for always comforting her and watching over her since childhood; her dogs: Spice (who passed away during graduate school), Duke, and Bella, who always made home such a happy and crazy place to be; and last but certainly not least, her husband Will Yelverton for all his love, patience, understanding of just how trying accomplishing dreams can be, and his commitment to their life together and all the adventures that soon await them.

# Table of Contents

# List of Tables

# List of Figures

# 1 Introduction

In a society that depends heavily of a depleting supply of non-renewable fossil fuels in order to make energy for heat and work, eliminating inefficiencies from combustion devices that run on these fossil fuels is becoming more and more critical. It is known that diffusion-flame-driven devices are much more fuel efficient than premixed-flame-driven devices, but with this increased efficiency comes the disadvantage of more pollutant formation, particularly soot and $NO_x$. Since these diffusion-flame-driven devices can provide a more efficient means to meet energy demands, research efforts should be focused on reducing or eliminating the pollutant formation from these combustion devices while maintaining fuel efficiency. Of these pollutants formed through the combustion process, particulate matter is of greatest concern. Particulate matter, such as soot, is a risk not only to the environment, but also to human health. Soot has been proven to be a carcinogen and a mutagen as well as causing more long-term illnesses such as chronic bronchitis (Sydbom et al., 2001; Comstock et al., 1998; Morgan et al., 1997; Scheepers et al., 1992). Because of these environmental and human health effects soot entails, the Environmental Protection Agency (EPA) continues to stringently monitor and regulate particulate emissions from all sources, both mobile and stationary. Heavy-duty Diesel engines continue to come under strict regulations for emissions from the EPA, and Diesel engine manufacturers find it difficult to keep up with these ever changing emission regulations. Through research it is possible to get a better, more complete, understanding of the soot formation process at elevated pressures, where the majority of combustion devices operate. Soot is an indicator of

the interactions between combustion chemistry, transport, and fluid mechanics, but a complete understanding of these interactions is not known by the combustion community at this time. The majority of the research conducted currently is accomplished at atmospheric conditions and not at elevated pressures where these devices operate. The lack of research at elevated pressures is due mostly to cost, time, and safety issues. Despite these drawbacks, this research is necessary to increase the pool of knowledge in order to reduce or eliminate soot production from these diffusion-flame-driven devices.

The current research used ethylene and methane, both pure and diluted (individually with helium, nitrogen, argon and carbon dioxide) from 1 to 16 atmospheres to investigate smoke point height, fuel exit velocity profile effects, soot surface temperatures, hydrocarbon species concentrations, and soot volume fraction. Each of these investigations was conducted in order to gain the necessary information to evaluate the hydrogen absorption carbon addition (HACA) soot growth mechanism at elevated pressures. This soot growth mechanism is widely accepted in the combustion community, but has not been thoroughly investigated at elevated pressures where most practical combustion devices operate. Each phase of the experiments is documented within this paper and as the experimental apparatus changes for each experiment is it noted. In most cases, except where noted, the air to fuel velocity ratio remains at unity and the flames are kept at their smoke point. By limiting these experiments to velocity-matched and smoke point conditions, this research eliminates possible causes for discrepancies from laboratory to laboratory and makes the data reproducible and easier to compare and contrast to the research of other investigations. Below, each of the phases of the current investigation are discussed in detail, including the

reason for that particular phase of the experiment, each individual experimental apparatus, the results and discussion obtained from each phase, and finally the conclusions that are apparent from each phase as well as the overall conclusions reached from the entire investigation.

## 1.1 Soot Formation and Growth

Recent research has focused on a better understanding of soot growth and formation. Investigators have determined that a better understanding of chemical kinetics transport, and fluid mechanics would greatly increase the combustion community's understanding of soot formation. Although some understanding exists for the chemical kinetics, transport, and fluid mechanics, the interactions between these three functions are also of great interest and not very well understood at all, and it has been determined that, as a community, our research efforts should be focused on these interactions (Frenklach, 2002; Richter & Howard, 2000).

Diffusion flames and premixed flames have very contrasting qualities that must be understood prior to being able to conduct research. Diffusion flames, as stated earlier, will produce more soot than premixed flames. This is due to the fundamental controlling mechanisms present in diffusion flames. In diffusion flames, the fuel and the oxidizer are stored separately and do not come into contact with one another until they reach the primary reaction zone. The fuel and oxidizer then diffuse into the reaction zone due to the concentration gradient, called Fickian diffusion. While the fuel and oxidizer are stored separately, the fuel undergoes pyrolysis without the presence of oxidizer, which allows for less soot precursor to be oxidized. In contract, in a premixed flame the fuel is heated with the

oxidizer present and then the fuel and oxidizer enter the reaction zone together. Furthermore, in the premixed flame soot is created when the oxidizer is absent, as it is responsible for the converting of hydrocarbons into carbon monoxide and diatomic hydrogen. It has been shown by Wagner (1981) experimentally that if the ratio of carbon to oxygen atoms for the flame is greater than 0.5, the premixed flame will produce soot. The converse of Wagner's findings also holds true such that soot will not be produced if a non-soot-yielding ratio of carbon to oxygen atoms is maintained in the mixture region. Controlling and maintaining the ratio of carbon to oxygen atoms in the mixing region in a diffusion flame is typically not possible, which makes an environment more suitable for soot production.

Whether dealing with a diffusion or premixed flame, soot formation begins in the same manner, in the preheat zone. It is in the preheat zone that the large molecules decompose into smaller hydrocarbon pieces because of increases in temperature that occur in this zone. Soot precursors are formed because of this pyrolysis and take the form of acetylene ($C_2H_2$). Hydrocarbon fuels that have a low propensity to form soot, such as methane ($CH_4$), have low soot production because they have a more difficult path to thermally decompose into acetylene. However, more complex hydrocarbons, such as ethylene ($C_2H_4$), have a much easier path to thermally decompose into acetylene and thus have a much higher propensity to form soot. After the precursors to soot are created, the acetylene molecules combine in groups of three to form benzene rings ($C_6H_6$). Several of these benzene rings then combine to form polycyclic aromatic hydrocarbons, typically referred to as PAHs. Then the process of polymerization begins and the rings of benzene lose hydrogen atoms. This loss of hydrogen atoms causes hydroxyl and water to form and

the rings become unsaturated. As this process continues, the carbon to hydrogen atom ratio increases and causes the rings to group together forming the soot particle, often called a soot spherule. These soot spherules continue to grow in size up to roughly 30 to 50 nm in diameter. Just one of the many things researchers do not understand about soot formation is why the soot spherule's growth discontinues at this range of diameters. However, after the soot spherules reach this diameter range, they begin to join together to form agglomerates, which end up containing hundreds to thousands of soot spherules. Then these agglomerates join together to form clusters, which result in soot particles (Figure 1.1). These soot particles have an estimated empirical formula of $C_8H$.

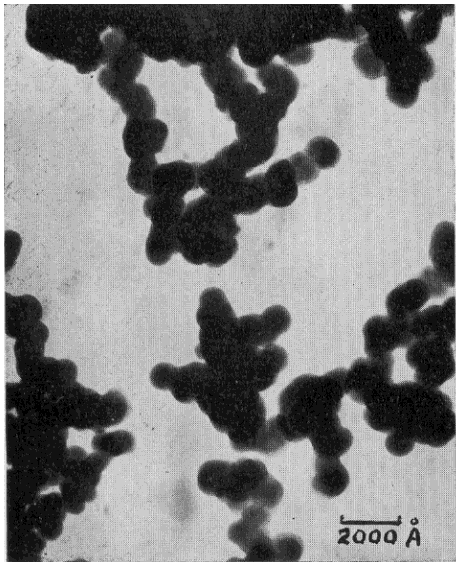


**Figure 1.1: Soot spherules forming agglomerates (Gaydon & Wolfhard, 1970)**

The formation of soot can be a rapid process, especially when using a fuel with a high propensity to soot and having the flame in an elevated pressure condition. However, there is a simple method of soot removal, through oxidation, that combats the soot formation and

growth. The visibly yellow portion of a flame (a candle for instance) is the soot incandescence. If the soot in this soot incandescence region is oxidized prior to diffusing across the flame front, the flame with cease to emit visible smoke. This is how the distinction between soot and smoke becomes apparent. Any carbon that leaves the flame is smoke, but any carbon that stays within the flame and is oxidized, forming CO or $CO_2$, is considered soot. Early investigations by Schalla and co-workers (1955) looked at the difference between smoke and soot production in diffusion flames at atmospheric and elevated pressures.

## 1.2 Effects of Elevated Pressure on Soot Formation

A very well known and well researched aspect of diffusion-flame-driven devices is that the soot production increases, while soot oxidation decreases, with increasing pressure (Flower & Bowman, 1986). However, as mentioned previously, experimental research at elevated pressures is limited because of its timely, costly, and dangerous nature. More recent research is moving towards experimental research at elevated pressures, such as the current research, in order to better understand pollutant formation from combustion devices at their normal operating conditions. Researchers, although they do not fully understand why, agree that increasing the pressure surrounding a diffusion flame increases the reaction rates and the diffusion coefficient of the flame, thus leading to increased soot production. Other researchers, who have focused on spray combustion and premixed-flame-driven combustion, have seen increases in soot production in these devices when the environment surrounding the flames increase in pressure (McArragher & Tan, 1972; Schalla & McDonald, 1955;

Kadota et al., 1977; Miller & Maahs, 1977; Millberg, 1959; Fischer & Moss, 1998; Heidermann et al., 1999).

Previous research by McCrain and Roberts (2005), conducted in a similar burner and vessel configuration as the current research at elevated pressures, was able to measure the effects of elevating pressure. Working with laminar diffusion flames, they were able to measure the soot volume fraction, $f_v$. The current work also investigates the soot volume fraction in laminar diffusion flames at elevated pressures, but uses a different technique, described below in detail in §1.7, from McCrain and Roberts (2005) who used laser induced incandescence (LII) and extinction measurements.

Increasing the pressure inside the vessel has a few impacts on the flame. With the reaction rates increasing in proportion to the pressure and the diffusion rates increasing as the gradients become steeper, the flame becomes thinner, less stable, and shorter. These changes to the flame were expected, and similar findings involving pressure effects on flames were reported by Miller and Maahs (1977). They showed that hydrodynamics disrupt the flame and make it more sensitive to extinction because the diffusion of reactants cannot occur quickly enough to restore the flame.

## 1.3 Smoke Point

The smoke point of a flame has been recognized in the combustion community, for many years, as a fundamental measure of a fuel's propensity to soot. Smoke point has been used to determine the quality of various liquid fuels. In the current research smoke point is defined as the flame height immediately prior to the flame emitting visible smoke. In Figure

1.2, it is possible to see the distinct difference between two flames at and just slightly above their smoke points. The flame on the left has a volumetric fuel flow rate of 76 sccm and an air co-flow rate of 16.6 SLPM. The flame on the right, which is slightly above its smoke point, has a volumetric fuel flow rate of 98 sccm and an air co-flow rate of 21.7 SPLM. In each flame the air to fuel velocity ratio is unity. In the flame on the right, which is just above its smoke point, it is possible to see visible smoke from the tip and feathering of the flame (called wings) near the tip which is a sign of a flame reaching and exceeding its smoke point.

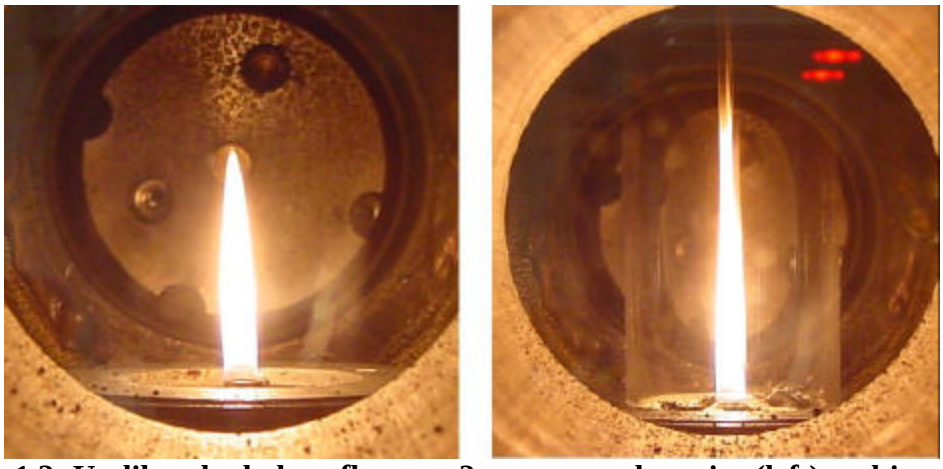

**Figure 1.2: Undiluted ethylene flame at 2 atm at smoke point (left) and just above smoke point (right)**

The smoke point can also be described as the position of the flame where the soot production and soot oxidation directly offset one another. It should be noted that the current research was conducted with gaseous fuels rather than liquid fuels. There is limited experimental research published regarding the smoke point of gaseous fuels, and even fewer publications exist that focused on smoke points of diluted fuels or the effects of pressure (Dai & Faeth, 2000; Urban et al., 2000; Lin & Faeth, 1996; Glassman, 1988; Gomez & Glassman, 1984;

Glassman & Yaccarino, 1981; Schalla et al., 1954). Furthermore, only slightly more research on smoke points, using numerical simulation has been conducted and published (Guo et al., 2002; Delichatsios, 1994; Kent, 1986). The work of Schalla and co-workers (1955), mentioned previously, examined the smoke and soot production in diffusion flames and recorded flame heights at smoke points for ethylene and ethane flames from 0.5 to 20 atmospheres. They worked with not only wick-fed liquid fuels but also with gaseous fuels. Although they had no way of metering and recording the fuel flow rates, they were able to measure the flame's height at its smoke point. They reported that the flame height decreased, nearly linearly, with the increasing pressure for gaseous fuels. At the time they believed this effect to be caused by diffusion rates and the rate of mixing of the fuel and air. Dai and Faeth (2000) investigated laminar diffusion flames and the air to fuel velocity ratios effects at sub-atmospheric pressures to find that the flame's height at its smoke point is twice as long as a soot-free (blue) flame under the same conditions. Urban and co-workers (2000) also tested with laminar diffusion flames, but in microgravity conditions, and reported that contrary to normal gravity conditions, the smoke point occurred in two configurations: closed-tip flames with soot emissions along the flame axis and open-tip flames with soot emissions from an annular ring about the flame axis.

In the current experimental research diffusion flames are investigated and the luminous flame height and mass flow rates were recorded at the smoke point of pure and diluted flames. Since the current research sought to investigate combustion devices at normal operating conditions, the smoke point measurements were conducted not only at

atmospheric conditions, but also at elevated pressures up to 8 atmospheres for ethylene and up to 16 atmospheres for methane.

## 1.4 Fuel Exit Velocity Profile and Dilution Effects

The investigation into the effects of the fuel exit velocity profile was not initially anticipated as a phase of this research. However, after the smoke point data was collected and compared to that of previous researchers, it was necessary to investigate the fuel exit velocity profile and the effects of different inert diluents in order to explain the discrepancy between the current experiment and the experiments of previous researchers.

### 1.4.1 Diluent and Dilution

Previous researchers have investigated the effects of dilution on smoke point in laminar diffusion flames at atmospheric pressures. McLintock (1968) investigated the effects on smoke point and sooting tendencies by adding inert diluent to either the fuel or oxidizer stream. It was found that dramatic differences in the smoke point existed when using different diluents, with carbon dioxide ($CO_2$) having a very strong ability to suppress soot production and helium (He) having a very weak to no ability to suppress soot production. Both nitrogen ($N_2$) and argon (Ar) fell in between $CO_2$ and He, but much closer to He, in their ability to suppress soot formation. For McLintock's experiments the air co-flow velocity was held constant with an initial fuel-to-air velocity ratio of approximately 1.4, which increased with dilution level. At the initial fuel-to-air velocity ratio, McLintock found that the slope of $CO_2$ and He addition were 0.75 and approximately zero, respectively, when

plotting the volumetric fuel flow rate at the smoke point versus the volumetric diluent flow rate.

Glassman and co-workers (1998, 1980) found similar trends when using these diluents in a highly over-ventilated environment (with unreported, but presumed constant, air co-flow velocity), but showed $CO_2$ having an even stronger soot suppression effect than McLintock (1968) had reported. Glassman and co-workers plotted the volumetric fuel flow rate versus the volumetric diluent rate and found a slope of 1.10 for $CO_2$ and a slope of 0.2 for He. Although the results of Glassman and McLintock differ slightly, the observation that $CO_2$ is much more efficient than He at suppressing soot is consistent. Since the findings of the current experiments differ, showing very little difference in soot suppression at the smoke point height using $CO_2$ versus He, from those of previous investigations, this experiment to investigate fuel exit velocity profiles and dilution was added as a phase in the research.

Previous investigations into dilution of a fuel or oxidizer stream have shown that there is both a thermal effect, scaling with molar heat capacity of a diluent, and a dilution effect, scaling with the molecular and thermal diffusivities of a diluent (Guo et al., 2000, 2004). Many researchers have used the same diluents for investigation as the ones chosen for the current experiments: He, Ar, $N_2$, and $CO_2$. The use of these diluents, to investigate the effects of diluent addition to ethylene and methane flames, makes it possible to cover a broad range of diffusivities and heat capacities (Table 1.1).

**Table 1.1: Transport properties of the four diluents at 20 degrees Celsius**

| | Helium | Carbon Dioxide | Argon | Nitrogen |
|---|---|---|---|---|
| Specific Heat Capactiy (J/kg C) | 5193 | 846 | 520 | 1042 |
| Kinematic Viscosity ($cm^2/s$) | 1.15 | 0.08 | 0.12 | 0.15 |
| Thermal Diffusivity ($cm^2/s$) | 1.59 | 0.10 | 0.18 | 0.19 |
| Binary Diffusion Coefficient into $N_2$ ($cm^2/s$) | 0.71 | 0.16 | 0.20 | 0.22 |

With the addition of any of these diluents, to a fuel or oxidizer stream, there is a change in the viscosity and therefore the shear layer growth and entrainment is effected. Therefore, it is expected that He should have more of an effect on entrainment and mixing than $CO_2$, with $N_2$ and Ar falling between them. Table 1.1 shows the kinematic viscosities, thermal and molecular diffusivities, and the specific heats of the four diluents (Kanury, 1994). From the values in this table it is made clear the property differences between He and $CO_2$, such that they differ by a factor of 15 in both kinematic and thermal diffusivity but only a factor of 5 in molecular diffusivity. This provides a unique effect on the ethylene when either of the two diluents is used.

The transport and thermal effects on soot suppression by a given diluent is important to consider, but the possible chemical effects must also be considered. Glassman (1998) and Schug (1980) both postulated that there were chemical effects with the addition of $CO_2$ in addition to the thermal and transport effects. Later, in 2001, Liu and co-workers showed computationally that these chemical effects do suppress soot formation by reducing both the concentration of acetylene and the flame temperature. Also, they showed that the process of

converting $CO_2$, by hydrogen atom, to carbon monoxide and hydroxyl prompts the oxidation of soot precursors in the formation region. They further found that not only does the addition of $CO_2$ to the fuel stream reduce soot formation, but this addition also reduces $NO_x$ formation through suppression of the temperature.

### 1.4.2 Exit Velocity Profiles

As stated previously, the initial intent of this particular experiment was not to study the effects of fuel exit velocity profile on smoke point, but rather to identify potential reasons for the discrepancies observed with dilution compared with the findings of previous researchers.

Faeth and co-workers identified and aerodynamic means of affecting the diffusion flame by reducing the shear layer effects between the fuel and the air co-flow (Lin & Faeth, 1996; Dai & Faeth, 2000). They were able to show that the closer to unity the fuel-to-air velocity ratio falls, the effect of the shear layer becomes smaller and nearly negligible. Prior to Faeth's work, Roper and co-workers (1977) reported that smoke point was insensitive to the fuel to air velocity ratio as long as the flame was highly over-ventilated. This led some researchers to conclude that for gaseous fuel laminar flames, the smoke point and soot concentrations are dominated by buoyancy and molecular diffusion, and are insensitive to viscous effects. Ultimately, this was proven to not be the case.

Faeth and co-workers (1996, 2000) showed the velocity ratio to have great effect on determining smoke point characteristics of a particular fuel. The found that in these laminar diffusion flames, when the fuel flow rates are increased, it height of the flame lengthens. They also showed that the soot emissions could be suppressed, and possibly eliminated, by

substantially increasing the air co-flow rates. For the majority of the current research, and research conducted by Berry and Roberts (2006), a plug flow fuel exit velocity profile and a fuel to air velocity ratio of unity was employed. As stated above the plug flow fuel exit velocity profile was necessary to eliminate oscillations in the flames as pressure within the vessel was increased, and the velocity ratio of unity was used to minimize shear layer effects. In contrast, many of the researchers completing similar experiments have used parabolic fuel exit velocity profiles and a plug flow air exit velocity. In most of the experiments of other researchers, the velocity matching between fuel and air, if it ever occurred, only occurred at the initial undiluted conditions. Therefore, as diluent was added to their fuel stream the fuel exit velocity increased, maintaining the over-ventilated status, but the air co-flow velocity remained constant.

When the velocities are not matched, shear layer and entrainment scales with the viscosity and therefore the diluent choice becomes important. Smooke (2005) showed, experimentally and computationally, the importance of the velocity ratio in diffusion flames. Their investigation was performed in a velocity matched parabolic velocity profile flame at atmospheric conditions.

The Froude number (G) determines whether the flame is momentum or buoyancy dominated, as it is a dimensionless ratio between inertial and gravity forces. The Froude number was calculated for the current investigation using the atmospheric, undiluted ethylene flame and had a value equal to 0.21, and thus it is buoyancy controlled. With increasing pressure causes a decrease in Froude number, thus all of the flames in this investigation are buoyancy dominated.

## 1.5 Soot Surface Temperature

In order to reach the overall goal of investigating the accuracy of the HACA mechanism at elevated pressures it was necessary to complete soot surface temperature measurements from the flames at and above atmospheric pressure. These measurements are necessary to understand the structure of the flame, as temperature can affect the concentrations of species among other characteristics of the flames. Experiments by previous researchers have focused on soot surface temperature measurements but only at atmospheric pressure conditions (Hall & Bonczyk, 1990; Cignoli et al., 2001; Xu et al., 2003). More recent research, conducted by Thomson and co-workers (2005) has focused on these measurements with elevating pressure and has shown an overall decrease in soot surface temperature as pressure increases. Also, they observed that the temperature increased axially from the base to the tip of the flame. Throughout the current experiment the same trends in soot surface temperatures were recognized; however, a major difference between the current experiment and those of previous researchers is that the current measurements were taken at the flame's smoke point.

## 1.6 Hydrocarbon Species Concentrations

Yet another essential piece of information that was required to analyze the HACA mechanism at elevated pressures was species concentrations. This experiment focused on hydrocarbon species only, but future experiments to be conducted in the near future by another research assistant will focus on concentrations of major species such as water, carbon dioxide and carbon monoxide, as well as radical species concentrations. These species

concentrations were measured by extracting samples from ethylene flames and analyzing them with gas chromatography with a flame ionization detector (GC-FID). Unlike the previous experiments discussed thus far in the current investigation, the flame for this experiment were not at their smoke point; however, they were velocity matched such that the reactant flow (fuel plus diluent) velocity was matched with the air co-flow velocity. The samples were extracted through a probe and in order to avoid clogging of the probe, it was necessary to use very heavily diluted flames, 80% by volume. However, these flames remained highly over-ventilated and buoyancy dominated at all pressure conditions.

Hydrocarbon species have been investigated by many researchers in the last ten to fifteen years both computationally (Smooke et al., 1999; McEnally et al., 2000) and experimentally (McEnally & Pfefferle, 1999; Kim et al., 2004 & 2008). However, excluding the most recent work by Kim and co-workers (2008), these measurements have been accomplished at atmospheric pressures. Also, in each of the investigations by previous researchers the species concentration measurements have been taken along the centerline of the flame. The current research extracted samples not only along the centerline, but also along the surface of the flame. Nearly all of the samples collected were within the blue (soot-free) region of the flame with only a few samples reaching in to the soot incandescence (yellow) region of the flame.

## 1.7 Soot Volume Fraction and Pyrometry

Soot mass yield is one characteristic that can be useful in determining the parameters of soot. One such value of soot mass yield is the measure of soot volume fraction within a

flame. There are several experimental methods that can be incorporated to measure soot volume fraction such as LII, laser extinction, and pyrometry, to name a few. Of all the research that has been conducted over the years pertaining to soot volume fraction, some of which has been conducted at elevated pressures, it is clear that the researchers are in agreement that as pressure increasing the soot volume fraction also increases.

One of the first investigations into soot volume fraction at elevated pressures was conducted by Flower and Bowman (1986). They were able to measure soot volume fraction from 1 to 10 at atmospheres, showing experimentally that as the pressure increases the rates of soot production and growth also increase. Flower and Bowman collected line integrated soot volume fraction measurements using laser scattering techniques, but unfortunately these measurements to not provide results that are spatially or temporally resolved.

As mentioned previously, more recent experiments have been conducted, with a similar burner and pressure vessel to that used in the current investigation, to investigate not only soot volume fraction, but the effects elevated pressure has on soot volume fraction. McCrain and Roberts (2005) used a diffusion flame, with undiluted methane or ethylene, to measure integrated and peak soot volume fraction. The technique chosen for these measurements were LII and extinction. They found that integrated $f_v$ of methane scales approximately as $P^{1.0}$, and for ethylene approximately as $P^{1.2}$. They also found that peak $f_v$ for methane and ethylene scales approximately as $P^{1.2}$ and $P^{1.7}$, respectively. This research was conducted in the same pressure vessel as the current research, and the measurements were taken up to twenty-five atmospheres for methane and up to sixteen atmospheres for

ethylene. Their work was unique in the fact that no other researchers had ever measured peak soot volume fraction.

### 1.7.1 Refractive Index of Soot

The refractive index of soot has been widely disputed over the past half of a century, especially in laboratory scale experiments. In 1969, Dalzell and Sarofim published a journal article describing the best value to be used for the index of refraction for soot, 1.57-i0.56. This value became widely accepted and many researchers still continue to use this particular index of refraction. However, more recent investigations into the refractive index of soot have led researchers to choose their value to be more specific to their particular laboratory set-up. Chang and Charalampopoulos (1990) experimentally showed that there is a wavelength dependence for the soot refractive index. They combined classical and dynamic light scattering measurements and the Kramers-Kronig relations to express refractive index of soot for specific wavelengths, thus making the decision for the refractive index assumption specific to experimental apparatus. They performed these measurements and calculations for a range of wavelengths and then were able to determine an equation (Eq. 1.1) that can be used to calculate the refractive index of soot for a given experiment.

$$m = n - ik$$

$$\begin{aligned} where: n &= 1.811 + 0.1263\ln(l) + 0.027\ln^2(l) + 0.0417\ln^3(l) \\ k &= 0.5821 + 0.1213\ln(l) + 0.2309\ln^2(l) - 0.01\ln^3(l) \end{aligned} \qquad \textbf{(1.1)}$$

For the pyrometry and laser extinction methods used in the current experiments, using the above equation, the refractive index of soot was determined to be 1.75-i0.57.

### 1.7.2 Two Wavelength Emission Technique

This technique for measuring the temperature profile and soot volume fraction along the centerline of the flame has been shown to be rather accurate (De Iuliis et al., 1998; Cignoli et al., 2001; Boiarciuc et al., 2006). Boiarcius (2006) conducted measurements of soot volume fraction and particle size estimates using both the two color emission method and the classic method of LII and found that the two color emission technique is just as accurate, but requires less time and equipment. Cignoli and co-workers (2001) extended on the two-color pyrometry (discussed in §1.5) technique and used mathematical equations to solve for the soot volume fraction based on the emissions of the flame, emission from a known source (a tungsten lamp), the temperature profile, and the spectral properties of soot to measure the soot volume fraction in flames. Although the current experiment employs a black body calibrator to create a temperature calibration for the flame's profile, the same equations used by Cignoli et al. (2001) and De Iuliis et al. (1998) was used to determine soot volume fraction for the flames in the current experiment. As stated previously (§1.5), the two-color pyrometry yielded a temperature profile of each flame. The same fourth-order equation, based on Planck's equation, was used, but a new calibration was necessary according to the needed camera settings for these measurements in order to generate a temperature profile. Then, using that temperature profile, and updating and adding to the previous MATLAB program (Appendix 11.2) the following modified equation for calculation of soot volume fraction (Cignoli et al., 2001; DeIuliis et al., 1998):

$$f_v = \frac{\ell_{abs}}{L} \ln\left[1 - 0.99 \frac{E_{Sl}}{E_{L\,l}} * \exp\left\{\frac{-c}{l}\left(\frac{1}{T_L} - \frac{1}{T_s}\right)\right\}\right] \qquad \textbf{(1.2)}$$

where, $l_{abs}$ is the natural length of absorption at a given wavelength with respect to soot spectral properties (calculated), L is the width of the flame under consideration (measured), $E_{S?}$ is the integration process over the optical path (measured), $E_{L?}$ is the intensity of the calibrated lamp emission (given), c is Planck's constant (given), ? is the wavelength of the filter (in µm), $T_L$ is the lamp or black body calibrator temperature (measured), and $T_S$ is the soot temperature determined from the image ratio (measured), the soot volume fraction is calculated.

### 1.7.3 Laser Extinction and Tomographic Inversion Technique

The laser extinction method is the same method employed by McCrain and Roberts (2005) to yield average soot volume fraction, and used by many other researchers. This method uses a helium-neon (HeNe) laser beam and passes the beam through the flame. When the laser beam passes through the flame the energy is removed by molecules or particles, such as soot. The soot particles scatter and absorb the laser energy and the beam becomes attenuated. Another beam is passed directly above the flame, but parallel to the beam passing through the flame to yield an unattenuated beam. The ratio of the attenuated and unattenuated beam can be used to calculate average soot volume fraction. D'Alessio and co-workers (1972) used the extinction method, assuming the soot particles fall within a

Rayleigh scattering regime (where d<<?) to solve for average soot volume fraction using the following equation:

$$f_{sv,ave} = \left( \frac{l}{6pL} \right) \frac{\ln(I / I_o)}{\mathrm{Im}\left\{(m^2 - 1)/(m^2 + 2)\right\}} \qquad \textbf{(1.3)}$$

where in this case, ?=632 nm (He-Ne laser beam), L is the path length, I is the attenuated intensity, $I_0$ is the unattenuated intensity, and m is the refractive index of soot. As stated above, in §1.7.1, the value used in this particular experiment for the refractive index of soot is 1.75-i0.57.

Once the extinction measurements were completed, these values for average soot volume fraction for each flame is used, along with a tomographic inversion technique, to solve for the soot distribution at a given height in the flame. Other researchers have previously used this technique to investigate soot volume fraction and distribution at atmospheric and elevated pressures (Bento et al., 2006, Quay et al., 1994).

# 2 General Experimental Apparatus

For the majority of the experiments throughout this investigation the co-flow burner and the pressure vessel remained the same. However, at times during certain experiments the co-flow burner was modified, and in one experiment a second co-flow burner was utilized. This section details the co-flow burner, pressure vessel, chimney, and ignition most often used throughout this investigation. In the following chapters, when applicable, changes or modifications to the burner or chimney that were necessary for each particular experiment are documented.

## 2.1 Co-Flow Diffusion Flame Burner and Chimney

The burner, modeled as the classic over-ventilated Burke-Schumann (1928) laminar diffusion flame, used for this investigation has a fuel tube diameter of 4.5 mm and an air co-flow diameter of 65 mm (shown in Figure 2.1).

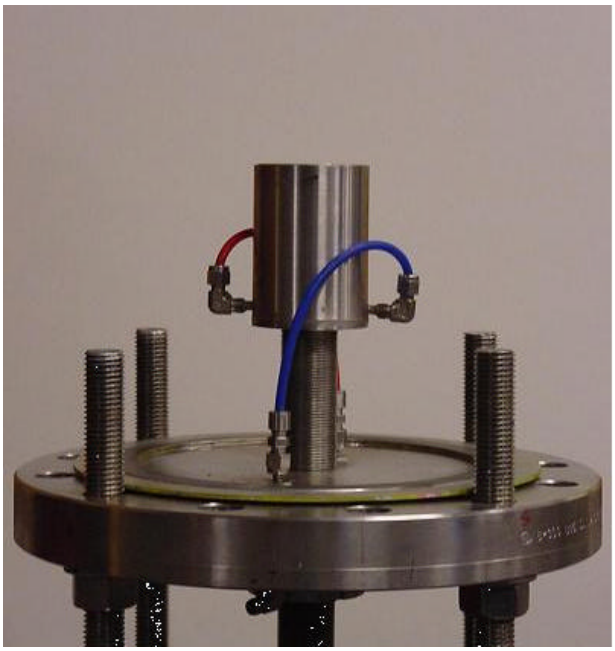

**Figure 2.1: Co-flow diffusion flame burner cup**

In order to minimize pressure fluctuation effects on the fuel flow rate, stainless steel wool (0000 gage) was inserted into the fuel tube. This created an isolated pressure drop and a uniform, also referred to as plug or top-hat, exit velocity profile. The steel wool was necessary for measurements made at elevated pressure, within the vessel, to isolate the fuel flow rate from small fluctuations that in turn would cause large changes in the fuel flow rate. As discussed previously, using a plug flow exit velocity profile did cause some discrepancies between the results of this investigation and the results of others. However, as explained later in chapter 3, these discrepancies were studied and it was possible to show that the current experiments were in agreement with other researcher's experimental results when a parabolic fuel exit velocity profile was utilized, thus proving that the differences lye solely in the fuel exit velocity profile used for measurements. Since the current investigation set out to

compare atmospheric as well as elevated pressure results, and since the elevated pressure conditions required flow straightening of the fuel flow, the flow straightener in the fuel tube was necessary for the majority of the experiments, resulting in a plug fuel exit velocity profile. It should also be noted that the fuel and the diluent entered the burner through the fuel tube; however, they were introduced well in advance of the fuel exit plane and therefore were considered fully mixed.

The air co-flow portion of the burner had a combination of hollow glass spheres and ceramic honeycomb to instill uniform exit velocity profile. A quartz chimney was also utilized with the co-flow burner at both atmospheric and elevated pressure conditions. This chimney had an outside diameter of 71 mm, a 3 mm wall thickness, and a 40 cm overall height. This chimney, though slight modifications were necessary from experiment to experiment throughout this investigation (describe in detail in future sections), was necessary to combat air perturbations within the pressure vessel, caused by the geometry of the vessel.

## 2.2 Pressure Vessel and Ignition System

The vessel in which the co-flow burner is housed is a water cooled pressure vessel that is capable of continuous operation up to 30 atmospheres, although for this investigation it was not used at any greater pressure than 16 atmospheres. It was designed and originally built by Li (2001), shown in Figure 2.2. The vessel is one meter tall and has four flanges extended beyond its circular body. In three of these flanges there are glass windows, constructed of BK-7 (diameter of 7.6 and thickness of 2.5 cm), that allow for optical viewing and non-intrusive diagnostics. The fourth flange houses fittings for pressure readings and

holes for intrusive diagnostics. Because of the fuels used, and their sooting tendencies, the vessel has air ports on two of the windows to purge the area and prevent accumulation, of condensation and soot, on the window surface and thus allowing optical access. The co-flow burner housed inside the vessel is

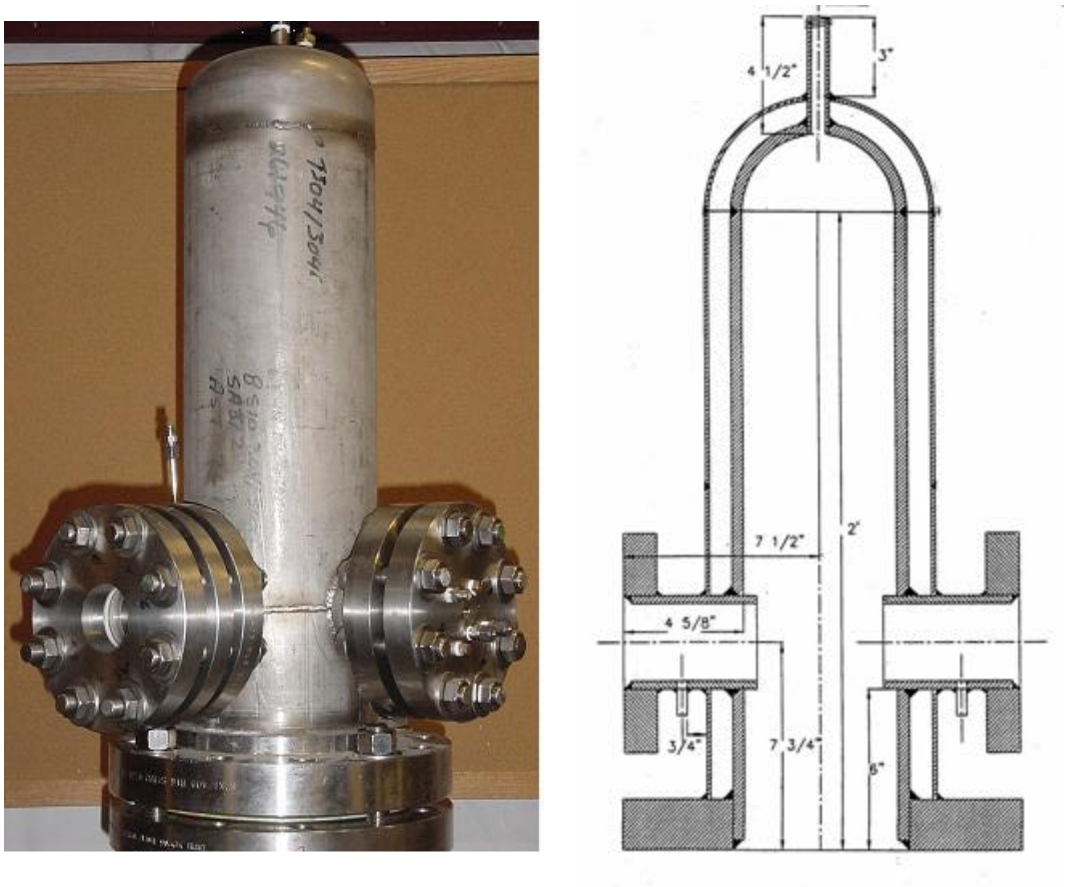


**Figure 2.2: High pressure vessel with dimensions**

capable of vertical translation, allowing for optical access to all portions of the flame. The pressure vessel was removed frequently between experiments for cleaning purposes.

The ignition system is of a very simple design, including a copper wire and a ceramic insulator. Even with the ceramic insulator surrounding the copper wire, to ensure the least

resistance to ground spark was not reached until it came into contact with the stainless steel fuel tube, several layers of electrical tape were applied to the outside of the ceramic.

The electrode was place inside the exhaust port of the pressure vessel and lowed through the open end of the quartz chimney, and then was place 3 to 5 mm from the fuel tube. Since the electrode passed through the exhaust port it was removed once ignition had occurred so the exhaust value could be replace on the exhaust port to meter the pressure in the vessel during experiments. As diagramed in Figure 2.3, the portion of the exposed copper wire that was outside of the pressure vessel was attached to an electrical cable that ran to a low-to-high voltage transformer, which was powered by a 12 volt deep cycle marine battery.

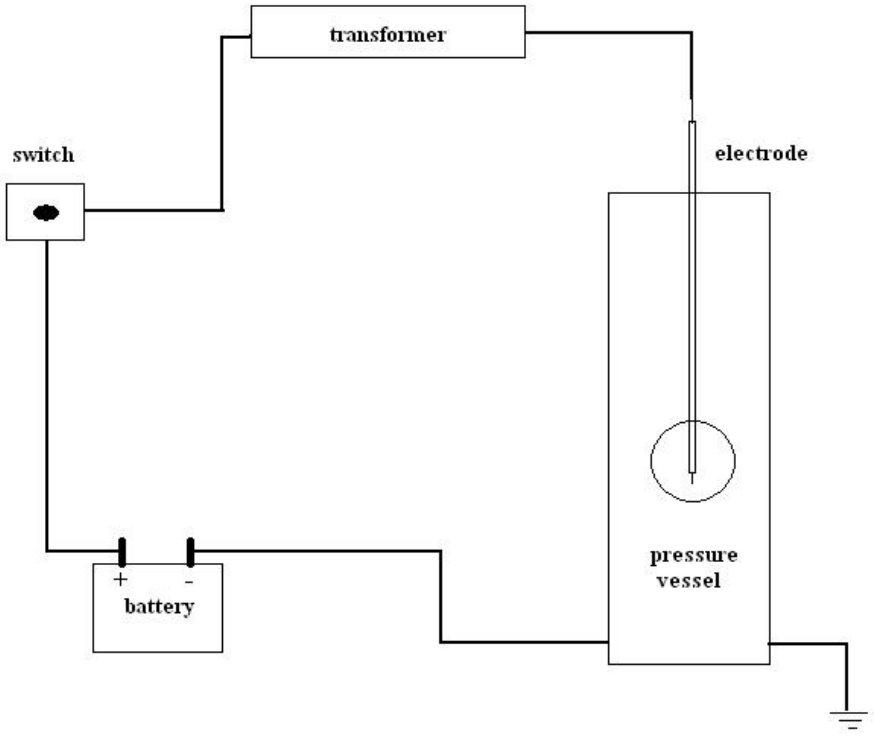


**Figure 2.3: Ignition system schematic**

A toggle switch between the battery and the transformer provided an electrical arc inside the pressure vessel from the copper wire to the fuel tube lip. This provided a very strong spark for the ignition of the flame within the vessel.

## 2.3 Pressure Metering

Elevating the pressure within the vessel is time consuming and very sensitive. The pressure is built in the vessel based on a simple concept of mass in versus mass out, such that the reactant and air come through the burner into the vessel and then the amount of products that are released from the vessel controls the pressure within the vessel. The air provided for combustion comes from compressed cylinders to ensure enough back pressure to sustain the pressure inside the vessel, the air is also ensured to by dry. A needle valve is attached to the exhaust port of the vessel and by opening and closing the needle valve the pressure can be metered. However, if at any time the needle valve closes completely the flame inside the vessel will be extinguished. The pressure inside the vessel is displayed on an external gauge and has a range of 0 to 1000 psig. The mass flux of co-flowing air is increased, while the needle valve is closed slowly to build pressure. It proves to be a taxing chore to maintain a velocity matched fuel to air ratio and building pressure within the vessel, while maintaining a flame that is not providing too much soot to the inside of the vessel. Window air is kept flowing (to prevent soot and condensation build-up on the windows), but with a very minimal flow rate, the air flow is considered negligible in the velocity matching calculations.

## 2.4 Fuel Flow Metering

In the base of the pressure vessel two ports exist, one for fuel and diluent inlet and the other for air co-flow inlet. Stainless steel fittings and plastic fuel lines carry the fuel, diluent, and air to the burner cup from the base of the vessel. On the outside of the pressure vessel, stainless steel fittings attach to stainless steel braided lines to carry the fuel, diluent, and air from the compressed cylinders, to the flow meters, and then on to the pressure vessel. As mentioned previously, two ports do exist on two of the optical flanges to provide air to the remove debris and condensation from the windows.

All of the air provided to the pressure vessel (both to the burner cup and to the window air) ran from the compressed cylinders to separate TeleDyne Hastings mass flow meters (Model 201). Each of these flow meters was calibrated with nitrogen for a range of 0 to 100 standard liters per minute (SLPM).

As for the fuel and the diluent, each was carried to individual TeleDyne Hastings mass flow meters (Model 200) that were calibrated with nitrogen for much slower flow rates, 1 to 1000 standard cubic centimeters (sccm). Each of the fuels (methane or ethylene) and diluents (helium, nitrogen, argon, or carbon dioxide) used were at least 99% pure and each mass flow meter was calibrated for the individual use of these gases.

Each of the four TeleDyne Hastings mass flow meters was powered by the same TeleDyne Hastings power supply (Model 40). This power supply not only provided power, but also provided a digital read-out of the flow rates for each meter. Since each of the flow meters was calibrated using nitrogen, it was necessary to input a correction factor, into the power supply for each fuel or diluent. These corrections are referred to as gas correction

factors and are provided by the manufacturer for air, ethylene, methane, argon, helium, and carbon dioxide with values of 0.998, 0.604, 0.770, 1.430, 1.430, and 0.73, respectively.

# 3 Smoke Point in Pure Ethylene and Methane Flames

## 3.1 Background

Although a large portion of the smoke point height measurements was accomplished while the author was seeking the degree of Master of Science, all of these measurements were repeated while the author was seeking the current degree of Doctor of Philosophy, and are essential to the fundamental understanding of the more recent research and therefore this experiment and its findings are included in this paper.

As mentioned previously, the smoke point of a fuel specific flame is a measure of the fuel's propensity to soot. It is the point at which the soot production and oxidation are directly offset and thus no visible smoke is emitted from the flame. For this experiment, pure ethylene and methane flames were tested up to 8 and 16 atmospheres, respectively to measure the smoke point height of each flame.

## 3.2 Experimental Apparatus

The most basic form of the current co-flow burner set-up was utilized for these smoke point height measurements. The burner, as stated previously, had a fuel tube diameter of 4.5 millimeters, a co-flow diameter of 65 millimeters, and a solid quartz chimney with an inside diameter of 65 millimeters. The fuel exit velocity profile, with stainless steel placed in the fuel tube, was plug.

Methane was chosen because it can be used to represent natural gas, which is commonly used in industry, and as it is the simplest hydrocarbon it has a low propensity to

soot. Ethylene was chosen as a representation of a complex hydrocarbon with a very high propensity to soot. A more commonly used fuel, propane, was considered for the experiments, but since propane has such a low saturation pressure at room temperature elevated pressure testing would have resulted in a liquid form of propane rather than a gaseous form.

The methane testing was completed over the pressure range of 2 to 16 atmospheres, while the ethylene pressure testing ranged from 1 to 8 atmospheres. Obtaining a pure laminar, steady, methane flame at atmospheric proved to be impossible in the current burner. However, other researchers have experienced the same problem with methane diffusion flames at atmospheric conditions (Kent, 1986). Each of the flames was tested at its smoke point and with fuel to air velocity ratios equal to unity.

To determine the smoke point height of each flame an iterative approach was used to adjust the fuel flow rate and air co-flow rate to unsure that the velocity ratio remained at unity. Fuel was increased until the flame emitted visible smoke and then the air co-flow was increased to the velocity matched ratio. If the visible smoke from the flame then ceased, more fuel was added to get to a smoking flame, and then the air increased, continuing this process until the velocity matched fuel to air ratio smoke point height of the flame was obtained. As the experiments were repeated several times, the iterative process improved to where roughly three iterations were required to obtain each smoke point height. Once the smoke point was reached, an image of the flame was taken with a digital camera and later analyzed using imaging software, determining a pixel per millimeter measure, and then a luminous height in millimeters.

As mentioned above, the current experiments were completed for the visible smoke point, and therefore the smoke point heights reported within should be understood to be luminous smoke point heights and not stoichiometric contour height measurements, which other researchers have investigated previously (Newman et al., 2004).

## 3.3 Results and Discussion

In order to determine the effects pressure has on the overall kinetics of the soot inception and oxidation portions of the soot formation process, smoke point height measurements were made. These smoke point heights were measured and then non-dimensionalized, by the fuel tube diameter (4.5 mm), for ease of comparison of results. Figure 3.1 shows the non-dimensionalized smoke point height of ethylene as a function of pressure from 1 to 8 atmospheres, and Figure 3.2 shows methane.

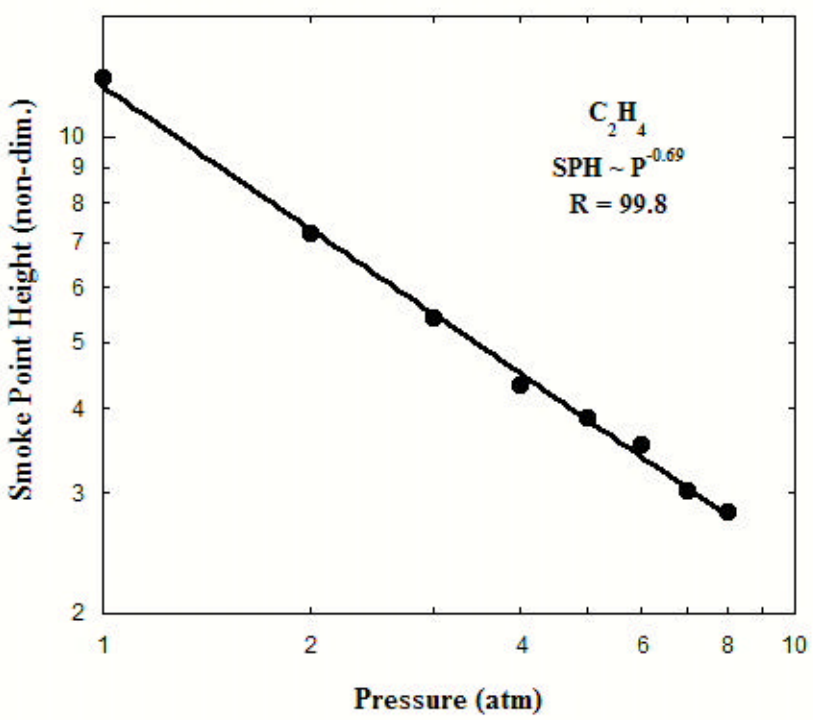


**Figure 3.1: Non-dimensionalized smoke point height of ethylene as a function of pressure**

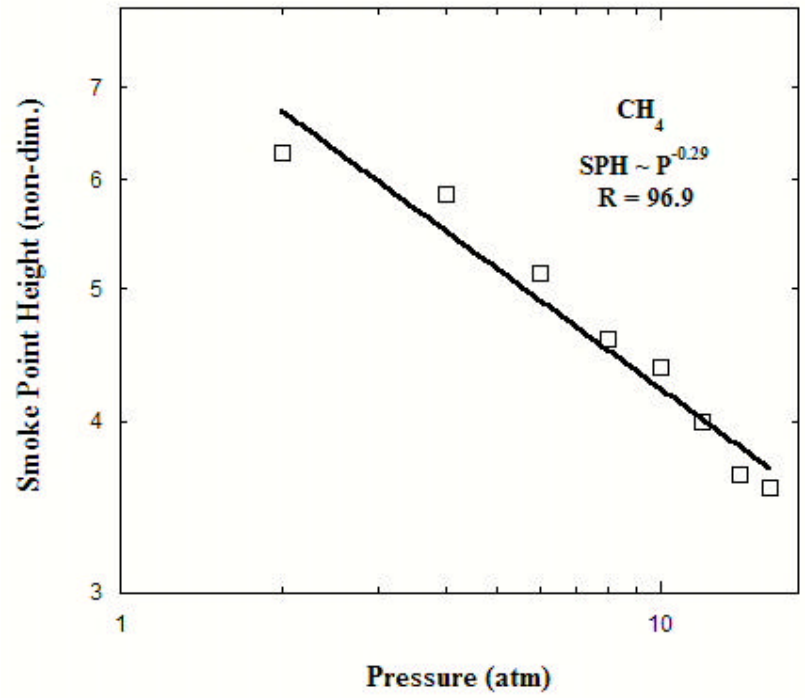


**Figure 3.2: Non-dimensionalized smoke point height of methane as a function of pressure**

The data in each of these figures is plotted in log-log space, and in this configuration the data fit to a power law where the smoke point height scales as a function of pressure to the -0.69 for ethylene and -0.29 for methane. In each case the smoke point height varied from the results of Schalla and co-workers (1954) in which they found the smoke point height to decrease nearly linearly with increasing pressure. These findings were the first that would later prompt the fuel exit velocity profile experiments (discussed in Chapter 4), as it was believed that these discrepancies were due to the plug fuel velocity exit profile used for this experiment.

The volumetric fuel flow rate (FFV) was also plotted as a function of pressure, for both ethylene (Figure 3.3) and methane (Figure 3.4), in order to determine if a functional dependence of FFV on pressure exists at the smoke point. In both instances, pure ethylene and pure methane, the best trend fit is available in log-linear space, yielding a logarithmic dependence from 2 to 8 atmospheres for ethylene and from 2 to 16 atmospheres for methane. From these plots it was possible to determine that the volumetric fuel flow scales as the exponential of 0.19 time pressure for ethylene and as the exponential of 0.10 times pressure for methane. The data point for pure ethylene at atmospheric conditions obviously does not fit the trend that exists for the ethylene date from 2 to 8 atmospheres.

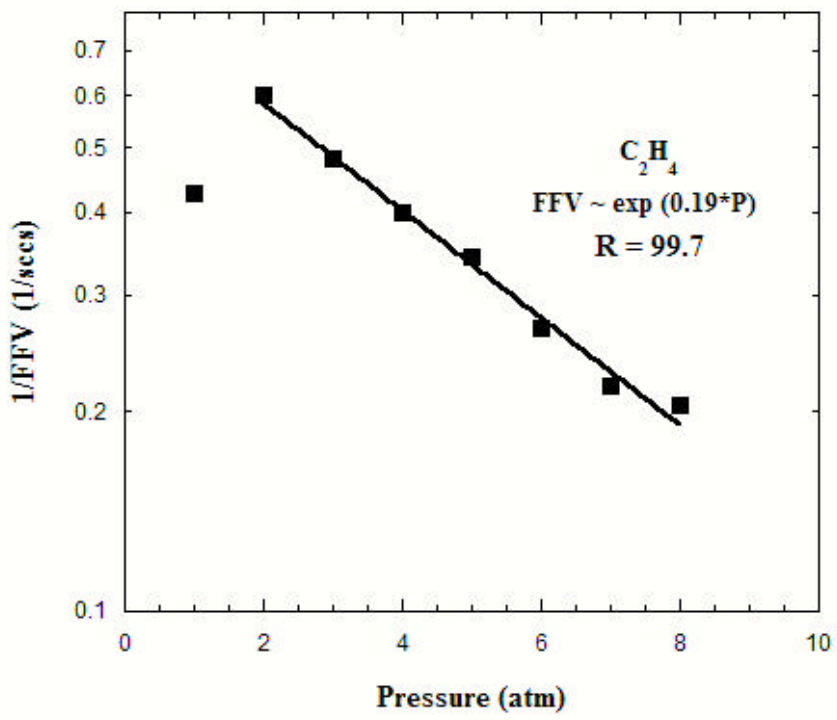


**Figure 3.3: Inverse volumetric fuel flow of pure ethylene as a function of pressure**

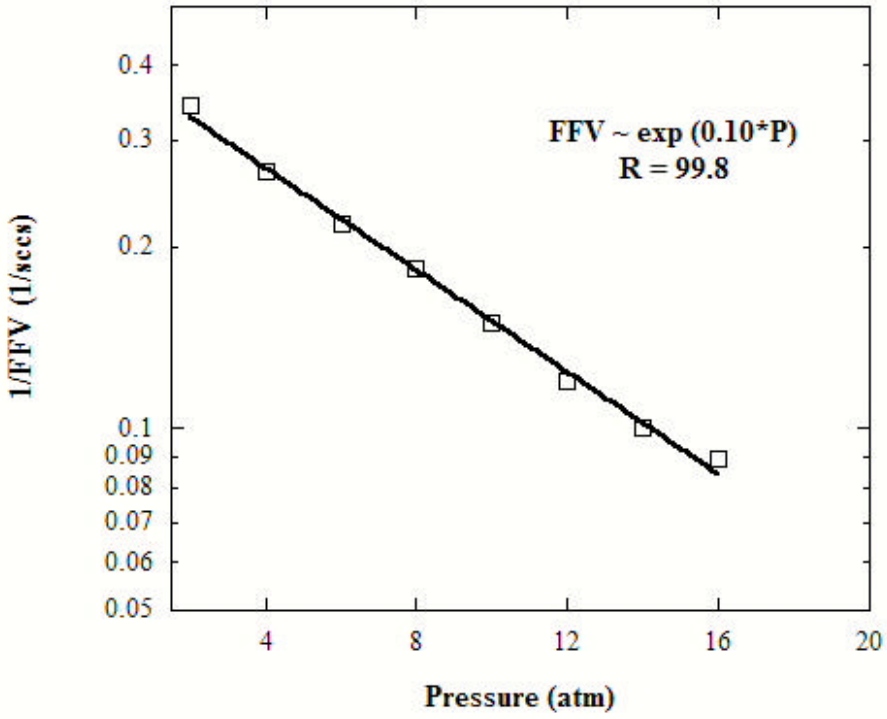


**Figure 3.4: Inverse volumetric fuel flow of pure methane as a function of pressure**

This difference in trend at atmospheric pressure is believed to be caused by residence time, but is not fully understood at this time. In each of these plots it should be noted that the pressure was non-dimensionalized and referenced to one atmosphere.

After analyzing the each of these figures, it was necessary to also look at a possible relationship between smoke point height and volumetric fuel flow rate because it was interesting to note that the inverse volumetric fuel flow rate and the flame height decrease as pressure increases. Therefore, in Figures 3.5 and 3.6 the inverse volumetric fuel flow rate was plotted as a function of the non-dimensionalized smoke point height for ethylene and methane, respectively. Each set of data was plotted in log-log space and clearly shows that in both instances, ethylene from 1 to 8 atmospheres and methane from 2 to 16 atmospheres, the relationship between volumetric fuel flow rate and smoke point height scales as pressure divided by the log of pressure, such that as pressure increases the slope increases.

## 3.4 Smoke Point Conclusions

This experiment was completed in order to gain more knowledge about the chemical kinetic processes and the emissions that result from them. As the process of soot formation at elevated pressures, where most practical devices operate, is not wholly understood, it is necessary to break apart and try to better understand the fundamental processes driving the formation and growth. This particular experiment focused on pure ethylene and methane and how pressure increases affect their smoke point. The conclusions obtained from this experiment are as follows:

1. As pressure increases, the flame height at the smoke point decreases. The behavior of ethylene and methane is quite different as the smoke point height scales as $P^{-0.69}$ for ethylene and as $P^{-0.29}$ for methane.

2. As pressure increases, the volumetric fuel flow rate at the smoke point also increases, but at a slower rate. For ethylene the inverse volumetric fuel flow rate scaled as exp(0.19*P) and for methane it scaled as exp(0.10*P).

3. The relationship between the inverse volumetric fuel flow rate and the smoke point height is not linear, but is obviously a function of pressure. The relationship, when plotted in log-log space, is nearly linear for methane due to its relatively weak pressure dependence, but the slope is much steeper for ethylene due to its much stronger pressure dependence.

# 4 Velocity Profile Effects with Dilution and Pressure

## 4.1 Background

As noted previously in Chapter 1, the experiments on velocity profile effects with dilution and pressure were not originally planned as a portion of this investigation. However, differences in results from the current study of smoke point height and the results of previous investigations into smoke point height prompted these experiments. With the addition of these experiments it was possible to show the results from the current smoke point height experiments as well as the results from other previous investigations (Schug et al., 1980; McLintock, 1968) were all correct. The differences in the results from each of these experiments were caused by the fuel exit velocity profile. As discussed in Chapter 1, for most instances in the current investigation, a plug fuel exit velocity profile was utilized (a necessary characteristic in order to take experimental data at elevated pressures with steady, laminar diffusion flames) where a parabolic fuel exit velocity profile was utilized by most other researchers.

For the current experiments discussed in this chapter, data was collected in three different configurations: in the co-flow burner discussed in §2.1 (with a plug fuel exit velocity profile) and in a larger co-flow burner with both a plug fuel exit velocity profile and a parabolic fuel exit velocity profile (detailed later in §4.2). By using both of these burners in several configurations, it is possible to replicate the current experimental data as well as the data of other researcher's investigations, and thus a comparison can be completed.

## 4.2 Experimental Apparatus

Given a sufficient length, the velocity profile from a constant area tube will be parabolic, often called fully developed. By adding flow obstructions, glass beads for this investigation, it is possible to cause a one dimensional exit velocity profile called a plug (or top-hat) flow velocity profile. In order to combat the dynamic pressure oscillations in the high pressure vessel, the fuel tube was filled with either stainless steel wool (burner 1) or glass beads (burner 2).

For this experiment two burners were employed to make measurements of smoke point height in steady, laminar diffusion flames at atmospheric and elevated pressures. One burner configuration that was utilized is the co-flow burner, chimney, and vessel described in detail in Chapter 2. As a reminder, this burner has a plug fuel exit velocity profile and is from here on referred to as burner 1.

In burner 1 the fuel and diluent (reactant) were mixed prior to entering the burner and an iterative approach was used to achieve and maintain the flames tested at their velocity matched smoke points. This particular burner and iterative approach were used to measure smoke point height with ethylene and methane diluted individually with four different diluents (He, $N_2$, Ar, and $CO_2$) at dilution levels ranging from 0% to 40% by volume.

The other burner utilized for these experiments (referred to from here as burner 2), used to better understand the discrepancies in the efficiency of suppressing soot between the previous results and those reported here, was also a co-flow burner but was larger than burner 1. Burner 2 has a fuel tube diameter of 11.9 millimeters and an air co-flow diameter of 101.6 millimeters. With a fuel to air velocity ratio of 1.39 (which is the largest velocity ratio

tested) the smoke point was reached with a volumetric fuel flow rate of 138 sccm and the corresponding air flow rate was 7100 sccm, which is more than three times larger than necessary to over-ventilate the flame. Therefore, although some of the experiments run with this burner are not fuel to air velocity matched, they are nonetheless highly over-ventilated.

In the cases where a plug fuel exit velocity profile was needed from burner 2, glass beads (3 millimeters in diameter) were packed into the fuel tube for 300 millimeters. For the parabolic fuel exit velocity profile cases, the beads were removed from the fuel tube. In both instances with burner 2, plug and parabolic, the air co-flow region had a combination of screens and ceramic honeycomb to ensure uniform air co-flow exit profile. Similar to burner 1, a quartz chimney (120 millimeter inside diameter) was incorporated to protect the flame from perturbations of the ambient air surrounding the burner (experiments in burner 2 were run at atmospheric pressure outside of the pressure vessel).

When testing with burner 2 occurred, ethylene was the only fuel used (since methane cannot yield a steady, laminar flame at its smoke point at 1 atmosphere), and it was diluted with either He or $CO_2$. For these measurements only two diluents were used because they represented the two diluents (out of the four previously used) that had the least (He) and greatest ($CO_2$) effect on the smoke point height of the flames.

## 4.3 Results and Discussion

Luminous smoke point heights were measured using burner 1 in diluted ethylene flames at 1, 4, and 8 atmospheres as well as in diluted methane flames at 4 and 8 atmospheres. As stated previously, all flames were stable, laminar, and non-flickering. The

fuel to air velocity ratio has a distinct effect on the smoke point, so in all cases, except where noted, an iterative approach was utilized to maintain velocity matched reactant (fuel plus diluent) to air conditions. Ethylene flames, diluted at atmospheric pressure, yielded the tallest flames, which in some cases were as tall as 130 millimeters. Since the diameter of the optical port of the pressure vessel was not as tall as some of the flames, the burner had to be translated vertically within the vessel to image the entire flame at its smoke point. Figure 4.1a-c show the effect of dilution level on the smoke point by plotting the inverse reactant volumetric flow rate as a function of the calculated inverse adiabatic temperature of ethylene and methane at increasing pressures. These plots are shown in log-linear space. This data was collected using burner 1, and it should be noted that from this point forward the ethylene data is represented by solid symbols and the methane by open symbols. The adiabatic flame temperatures are calculated using a standard chemical equilibrium calculator. Each flame is at its smoke point and therefore the soot loading, and thus the temperature decrease due to soot radiation, should be similar for each of the flames. It is clear from Figures 4.1b and 4.1c, at 4 and 8 atmospheres, that the smoke point for methane is higher than that of ethylene and both

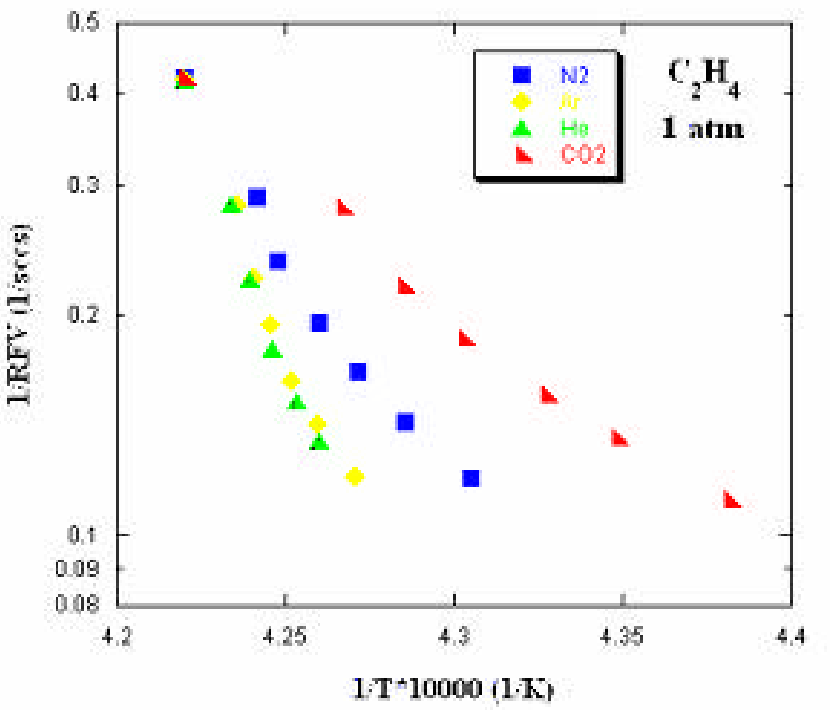
0.5
0.4
0.3
0.2
0.1
0.09
0.08
4.2
4.25
4.3
4.35
4.4
1/RFV (1/secs)
1/T*10000 (1/K)
N2
Ar
He
CO2
C2H4
1 atm

(a)

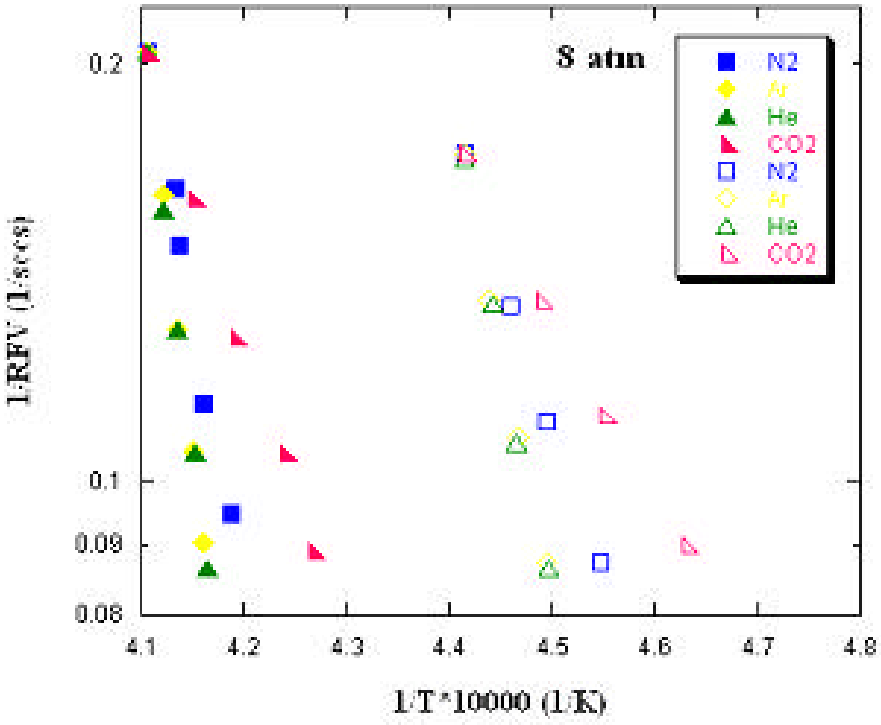
0.2
0.1
0.09
0.08
4.1
4.2
4.3
4.4
4.5
4.6
4.7
4.8
1/RFV (1/secs)
1/T*10000 (1/K)
8 atm
N2
Ar
He
CO2
N2
Ar
He
CO2

(b)

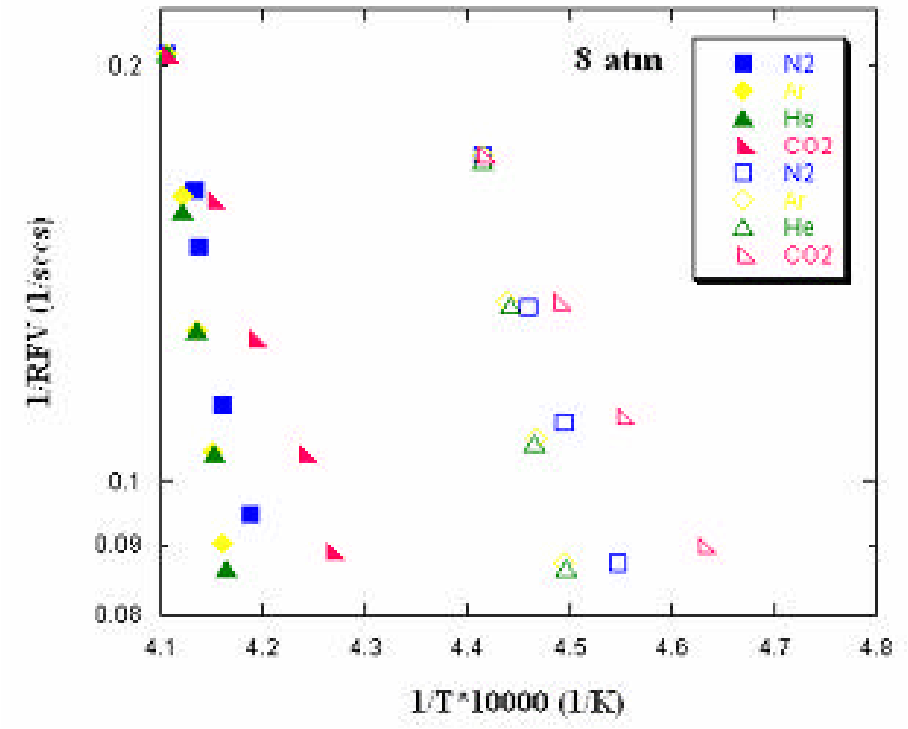


(c)

**Figure 4.1: Diluted ethylene and methane flames as a function of temperature at (a) 1, (b) 4, and (c) 8 atmospheres**

increase with dilution level as expected. There appears to be a linear dependence on temperature for the reactant flow rate at the smoke point, which is apparent with each of the diluents with a unique slope. It is very important that it be noted that the calculated temperatures plotted in these figures is the adiabatic temperature and not the soot nucleation temperature.

It has been shown by Glassman (1996) and others that had the soot nucleation temperature been plotted, there would not be a noticeable difference between the effects of each diluent at the smoke point of the flames. However, when plotting as a function of the adiabatic flame temperature, each diluent yields a different temperature at each individual

smoke point. It is also obvious from Figure 4.1 that the dilution effect is more important than the thermal effect. Figures 4.2 and 4.3 further emphasize this observation with each of the four diluents, where in Figure 4.2 the non-dimensionalized smoke point is plotted as a function of dilution level and in Figure 4.3 the volumetric fuel flow rate at the smoke point is plotted as a function of the volumetric diluent flow rate at 1, 4, and 8 atmospheres. In Figure 4.2 the atmospheric pressure, ethylene smoke point height increases significantly with increases in dilution level, but at elevated pressures the flame height at the smoke point becomes insensitive to the dilution level. It is also clear that in any of the three cases, the flame height is relatively insensitive to the particular diluent chosen.

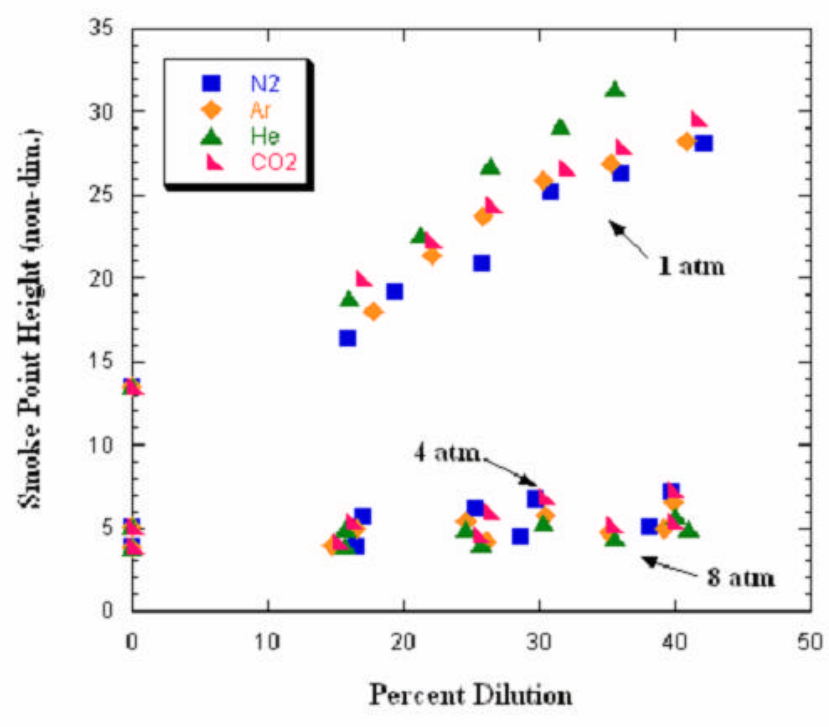


**Figure 4.2: Smoke point height as a function of percent dilution for a diluted ethylene flame at 1, 4, and 8 atmospheres**

Figures 4.3a, 4.3b, and 4.3c show how each diluent has relatively similar effects on the flame height, but the dilution level has an extremely pronounced effect of the flame height. Therefore, it becomes clear that from each figure (4.1, 4.2, and 4.3) the actual diluent is not as important as the dilution level. This however, disagrees from the findings previously reported by McLintock (1968) and Schug et al. (1980), where they observed a distinct difference between the diluents in atmospheric pressure flames, with the soot suppression ability scaling with the heat capacity, such that $CO_2$ was most effective and He was the least effective.

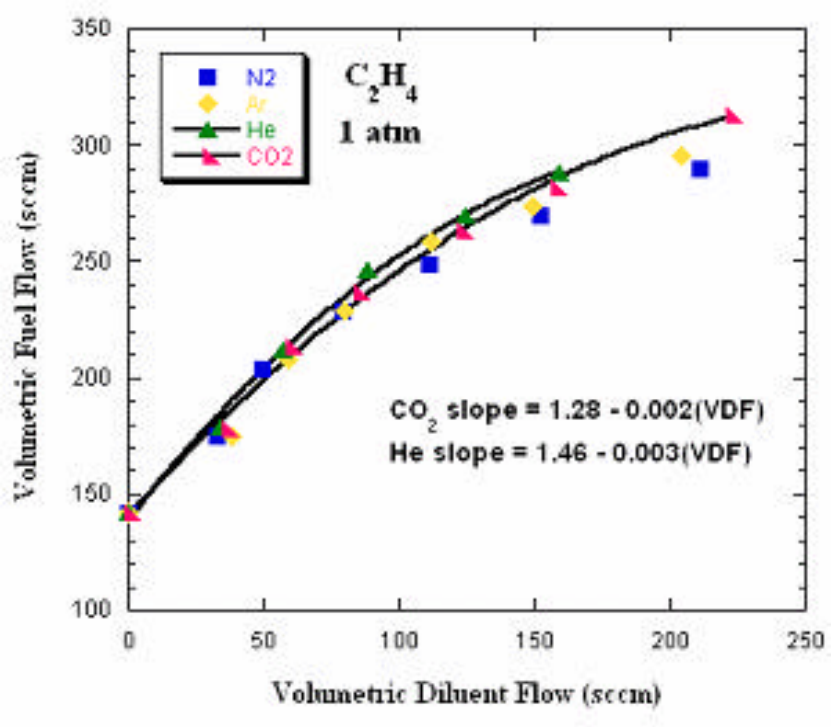
N2
Ar
He
CO2
C2H4
1 atm
CO2 slope = 1.28 - 0.002(VDF)
He slope = 1.46 - 0.003(VDF)
Volumetric Fuel Flow (sccm)
Volumetric Diluent Flow (sccm)
350
300
250
200
150
100
0
50
100
150
200
250

(a)

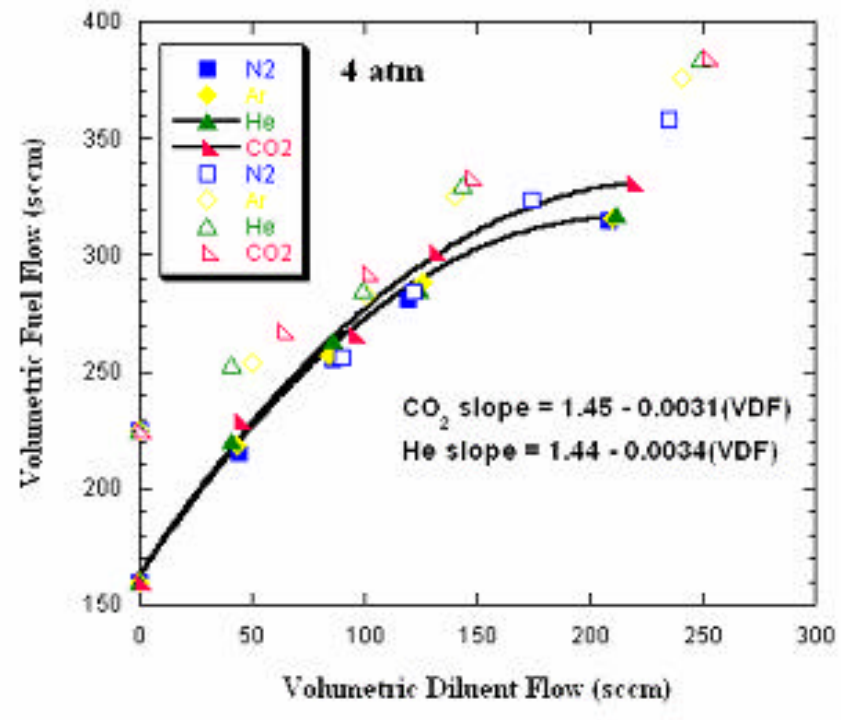
N2
Ar
He
CO2
N2
Ar
He
CO2
4 atm
CO2 slope = 1.45 - 0.0031(VDF)
He slope = 1.44 - 0.0034(VDF)
Volumetric Fuel Flow (sccm)
Volumetric Diluent Flow (sccm)
400
350
300
250
200
150
0
50
100
150
200
250
300

(b)

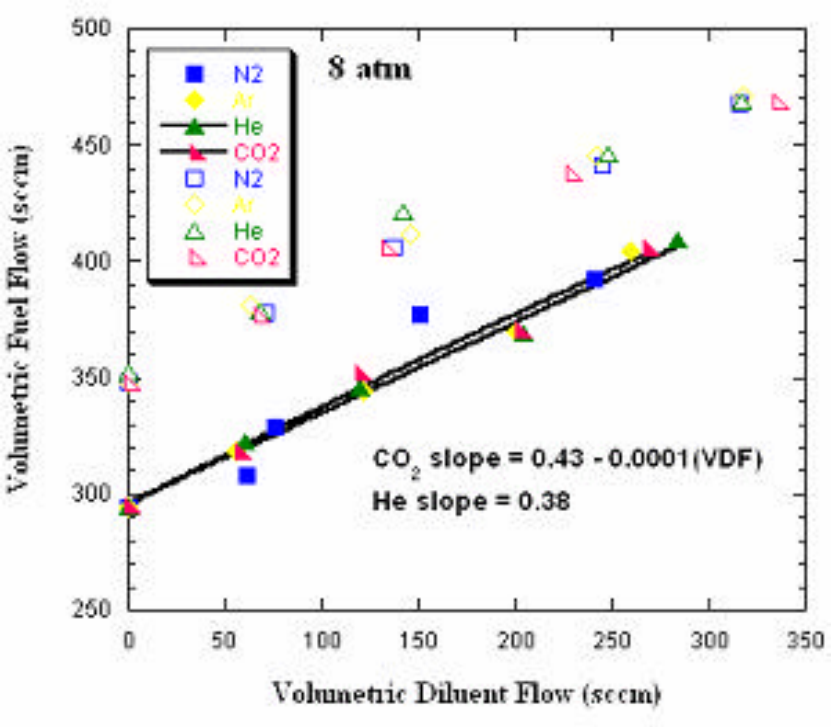


(c)

**Figure 4.3: Volumetric fuel flow rate versus diluent flow rate at (a) 1, (b) 4, and (c) 8 atmospheres with curve fits for $CO_2$ and He**

Glassman (1998) later showed that there is not only a thermal effect, but also a thermal diffusivity effect, such that $SO_2$ has a greater soot suppression effect than $CO_2$, while both have roughly the same heat capacity, and thus flame temperature. Although Ar and He are monotonic, have identical flame temperatures, He is not as capable of suppressing soot as Ar because of its much higher thermal diffusivity (recall Table 1.1 for the properties of the diluents at 20 degrees Celsius). The current experimental results suggest that there is also a viscosity effect, along with temperature and thermal diffusivity effects, as evidenced by the dependence on velocity ratio and exit velocity profile (plug versus parabolic). In Figures 4.4 and 4.5 these effects are shown in more detail, but first a discussion about the utilization of burner 2 for the data represented in these figures.

At atmospheric pressure in undiluted ethylene flames, the smoke point proves to be a strong function of the velocity ratio. For example, when the velocity ratio is unity, the fuel flow rate at the smoke point is 140 sccm, but at a fuel to air velocity ratio of 1.2, the fuel flow rate increases to 175 sccm, and at a fuel to air velocity ratio of 0.5 the fuel flow rate decreases to 105 sccm. In Table 4.1 the slopes of the fuel flow rate to diluent flow rate is shown (initial velocity ratio listed if it is know) for the current experiments as well as those completed by McLintock (1968) and Schug et al. (1980).

**Table 4.1: Slope of fuel flow rate versus diluent flow rate in ethylene flames at their smoke point for both $CO_2$ and He**

| Initial fuel to air velocity ratio | $CO_2$ slope | He slope | Reference |
|---|---|---|---|
| 1.38 | 0.75 | ~0 | McLintock |
| Unknown | 1.10 | 0.2 | Schug et al. |
| 1 | 1.28-0.002(VDF) | 1.46-0.003(VDF) | This work |
| 0.5 | 0.45 | 0.273 | This work |
| 1.2 | 0.33 | 0.36 | This work |

In this table the slope for the velocity matched case is given as a best fit second order polynomial, while the other entries are for fixed air co-flow rates. It is clear from this table that the velocity ratio is of primary importance in determining the ability of the diluent to suppress soot formation.

Smoke point measurements were made in burner 2 at atmospheric pressure with only ethylene flames diluted with either $CO_2$ or He. In Figure 4.4, the results of these measurements are shown, where the smoke point volumetric fuel flow rate (non-

dimensionalized by the undiluted volumetric fuel flow rate) is plotted as a function of volumetric diluent flow rate.

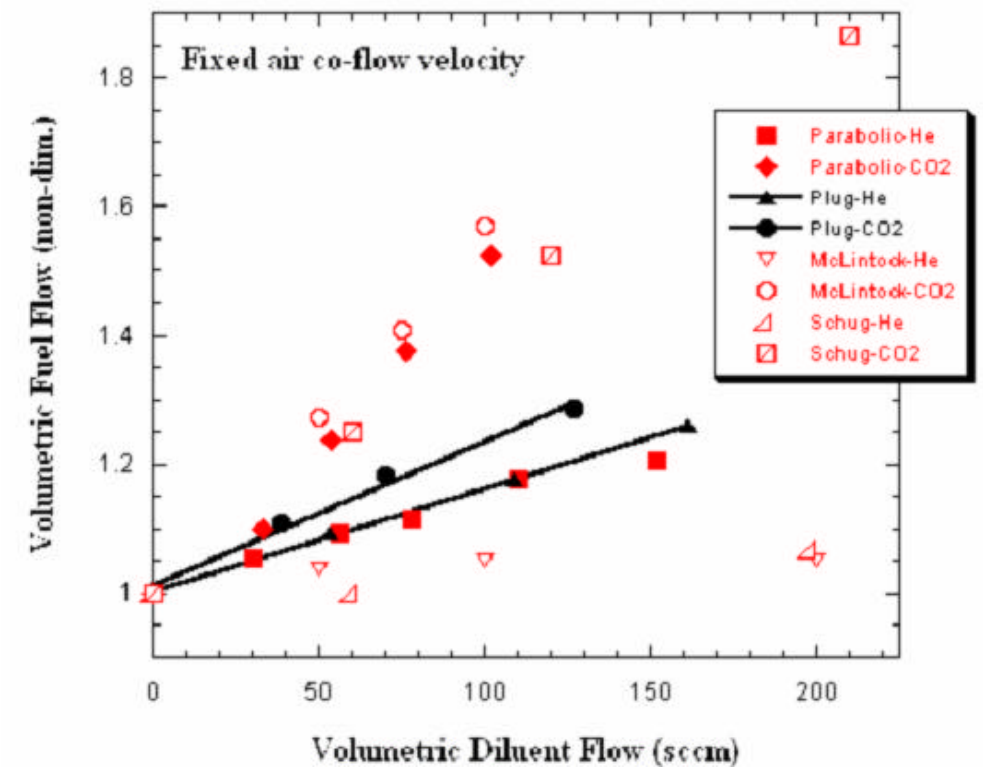


**Figure 4.4: Volumetric fuel flow as a function of volumetric diluent flow for a plug and parabolic exit velocity profile along with previous researcher's findings**

These measurements were all made with a fixed air co-flow velocity to better simulate the work preformed in previous investigations by other researchers. From this figure it is apparent that the effect of $CO_2$ addition on the smoke point depends strongly on whether the fuel exit velocity profile is parabolic or plug.

The parabolic exit velocity measurements, taken in the current experiment, agree quite well with the measurements from McLintock and Schug's experiments. However, the current measurements made with the plug fuel exit velocity profile shows the effect of $CO_2$

on smoke point to be much less. In contrast, the effect of He addition on smoke point is very insensitive to fuel exit velocity profile, and neither case is dramatically different from the results reported by McLintock or Schug and co-workers. As seen in this figure, when the plug fuel exit velocity profile is tested, there is little difference between the effects of $CO_2$ and He.

The volumetric fuel flow for pure ethylene flames plotted as a function of velocity ratio for the two different exit profiles is shown in Figure 4.5. It is interesting to note that the volumetric fuel flow and the smoke point height are both approximately parabolic with velocity ratio, both peaking near a velocity ratio of unity for the plug flow exit velocity profile, whereas the flow rate and flame height both decrease nearly linearly with increasing velocity ratio for the parabolic velocity profile.

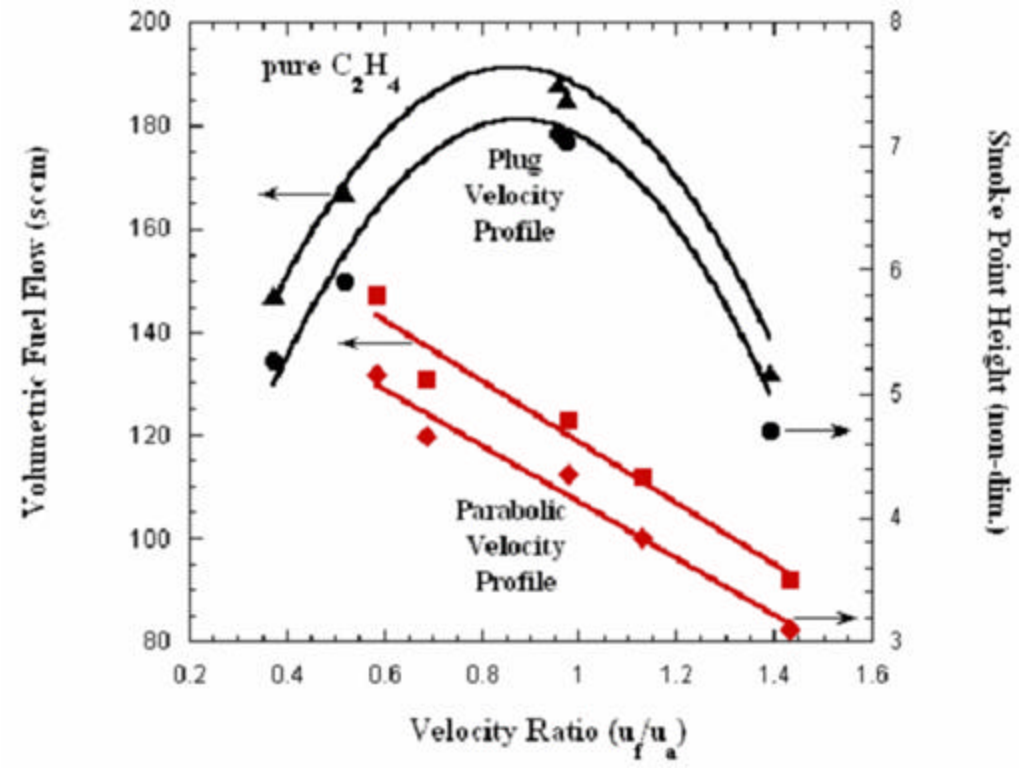


**Figure 4.5: Volumetric fuel flow and smoke point as a function of fuel to air velocity ratio for undiluted ethylene in two different burner configurations**

## 4.4 Velocity Profile Conclusions

For this portion of the overall investigation the smoke point was measured in both pure and diluted ethylene-air and methane-air laminar jet diffusion flames at atmospheric and elevated pressures. To gain a better understanding of the driving conditions behind these flames, the smoke point was measured as a function of volumetric fuel flow rate, diluent, dilution level, and fuel exit velocity profile. Four diluents were employed for these measurements (He, $N_2$, Ar, $CO_2$) in order to cover a wide range of heat capacity, thermal conductivity, diffusivity, and kinematic viscosity. Two different fuel exit velocity profiles

(plug and parabolic) and a range of reactant to air velocity ratios were utilized to investigate entrainment and shear layer effects. The following conclusions can be drawn:

1. Plotting reactant flow rate versus calculated equilibrium temperature for the four diluents at elevated pressure shows that the dilution effect is more important than the thermal effect on soot production and oxidation. This result holds true for both fuels tested using a plug fuel exit velocity profile.

2. The smoke point height increases significantly with dilution at atmospheric pressure (for ethylene), but at elevated pressure the flame height at the smoke point becomes insensitive to dilution level for both methane and ethylene flames.

3. For fuel to air velocity matched flow rates, with a plug fuel exit velocity profile, there is very little difference in smoke point with the four diluents tested. However, when a parabolic fuel exit velocity profile is used, $CO_2$ and He have very pronounced differences in their effectiveness at increasing the smoke point with dilution, which is in agreement with previous research by McLintock and Schug et al.

4. The differences observed between $CO_2$ and He with parabolic fuel exit velocity profile is likely due to differences in entrainment and mixing, from large differences in kinematic viscosity, rather than heat capacity or chemical kinetic effects.

5. The most effective fuel to air velocity ratio for increasing smoke point near is unity for plug flow exit velocity profiles and continuously decreasing with increasing fuel to air velocity ratio for parabolic flow exit velocity profile, which yields a lower smoke point height overall.

# 5 Soot Surface Temperature

## 5.1 Background

Two-dimensional temperature profiles of ethylene diluted with four diluents (He, $N_2$, Ar, and $CO_2$) were measured at atmospheric and elevated pressures. These temperature profiles of diffusion flames are necessary for a better understanding of the structure of flames, since the temperature can effect the concentrations of species products within the flame, and for comparison to other experiments within the current investigation (i.e. major hydrocarbon species concentration measurements and soot volume fraction). The measurements proved to be in agreement to recent measurements of pure fuel flames at increasing pressures. In each of these flames it was possible to measure the overall peak temperature as well as the peak temperature at 65% of the flame's height. It was possible to see a consistent trend where the overall temperature decreases with increasing pressure.

Also, a previous investigation by McCrain and Roberts (2005) measured soot volume fraction of pure ethylene flames at elevated pressures using laser induced incandescence. Since their measurements were made with the same burner configuration, these values of soot volume fraction have been used for comparison and a quantification of the radiative heat losses.

## 5.2 Experimental Apparatus

Pure and diluted ethylene-air flames were investigated in a high pressure vessel in order to image each flame's soot surface temperature. As with previous experiments within

the current investigation an iterative approach was used to maintain a fuel to air velocity ratio of unity in most cases (except where noted). However, in order to compare the current results with those of the previous work by McCrain and Roberts (2005), a few cases the fuel flow rate was held constant. The burner, chimney and pressure vessel that is described in detail in Chapter 2 was used for these measurements. The fuel exit velocity profile throughout these measurements was uniform (plug).

The current experiments are conducted through a technique of deconvolution of spectral radiation intensities, also known as soot pyrometry. Two images were acquired of the same flame but with two different color filters, 632 nm and 766 nm. These images were manipulated, through use of imaging software, and a ratio of the intensities present with each color filter was determined. Planks's equation was used to calculate a ratio value between Planck's equation solved for using wavelengths equal to 632 nanometers and 766 nanometers. This ratio of values, over a range of temperatures, yielded a fourth-order polynomial equation (Eq. 5.1),

$$T = -8551.5R^4 + 13789R^3 - 8097.9R^2 + 4885.3R + 802.85 \qquad \textbf{(5.1)}$$

where R is the ratio of intensities. Then a black body calibrator was employed to determine a correction factor based on the ratio between the black body intensity at 632 and 766 nanometers, and the correction was multiplied by the temperature ratio in the MATLAB program. With the use of a MATLAB program (Appendix 11.1), the ratio of images, the calibration, and the fourth order polynomial equation were used to create a temperature

profile of each flame. Another major difference between the current experiment and those of previous researchers is that the current measurements were taken at the flame's smoke point.

Soot pyrometry has been shown to be a very powerful non-intrusive technique for determining the soot surface temperature in flames. However, several factors must be taken into consideration in order to produce quantitative data, such as calibration of the measurements using a black body and wavelength selection to avoid false signals due to spectral emission from hot species (i.e. water).

### 5.2.1 Camera Specifications

The camera used (shown Figure 5.1) was a WATEC 902 Ulitmate monochrome CCD camera (8 bit, 640 x 480) with a quantum efficiency peaking around 900 nanometers. With this camera it was possible to control the shutter speed and gain control, which both proved to be very necessary to the current experiment. The camera was fitted with a Nikon lens with the focal length set to 50 millimeters and the f-stop number of 5.6 was utilized. All of these settings were held constant throughout the measurements and throughout the calibration of the black body, leaving the color filters and the neutral density filters as the only variables in imaging. Two near infrared (IR) color filters, centered about 632 and 766 nanometers, were used in combination with neutral density filters. The neutral density filters were only necessary to avoid over-saturation of the 8-bit detector of the camera over the wide range of soot densities and temperatures.

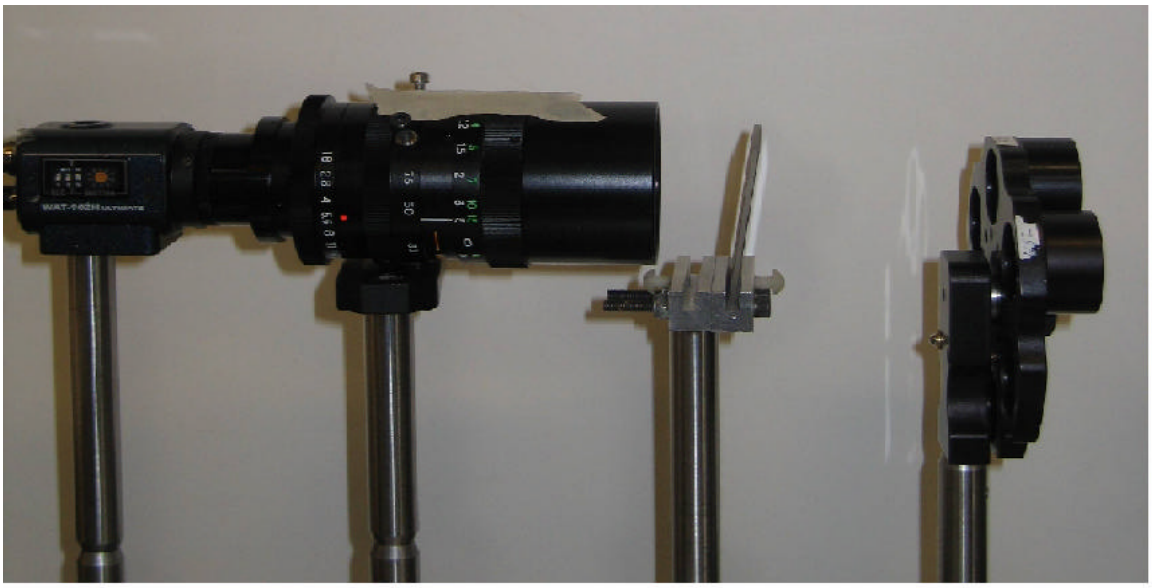

**Figure 5.1:Watec 902 Ultimate monochrome CCD camera with ND filter and color filter wheel**

### 5.2.2 Black Body Calibrator

An IR black body calibrator (shown in Figure 5.2), made by Infrared Systems Development Corporation was employed to make a temperature look-up table for the dual image data reduction based on the ratio of the spectral emissions of the flame at two different wavelengths. The calibrator was capable of accurate operation up to 1050 degrees Celsius and higher temperatures required extrapolation. Once the two images of the flame (one with each color filter) were taken, nearly simultaneously, the images were imported into a MATLAB program, shown in Appendix 11.1. The MATLAB program then divided the 632 nanometer image by the 766 nanometer images and then used the temperature correlation equation, developed by the calibration with the black body calibrator, to generate the temperature profile for entire soot surface region of the flame. In the early stages of the experiment, a third near IR color filter was incorporated, 905

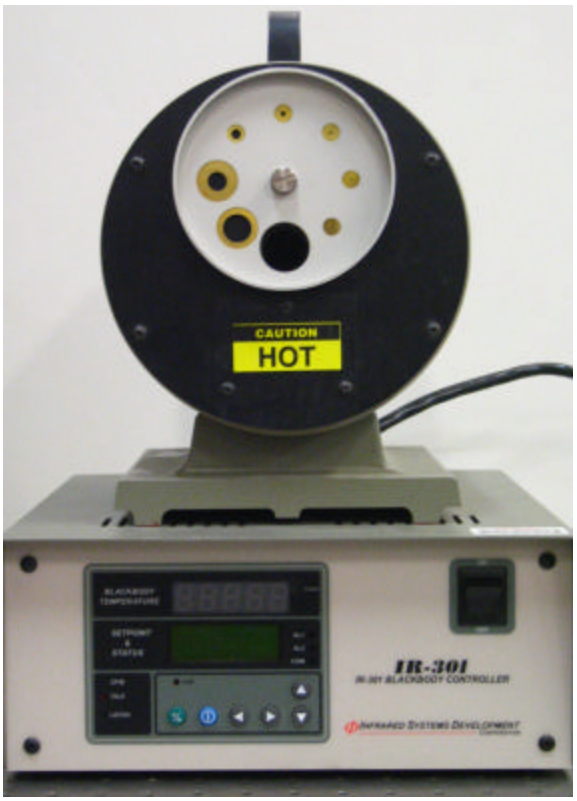


**Figure 5.2: Black body calibrator**

nanometers, but soon it was found to pollute the signal with spectral emission of hot water, and thus it was found to be unusable.

## 5.3 Results and Discussion

Soot surface temperature measurements were taken in ethylene-air flames, both pure and diluted, at their smoke points (and at 80% of the volumetric fuel flow rate at their smoke point) at 1, 2, 4, and 8 atmospheres. Also, some measurements were made with a constant fuel flow rate to evaluate the effects of pressure and to compare to a previous investigation into soot volume fraction.

Figure 5.3 shows the temperature contours of the velocity-matched, undiluted ethylene flames taken at their respective smoke point heights with increasing pressure. Although the fuel flow rate more than doubles with pressure increases from 1 to 8 atmospheres, it should be recalled that each of the undiluted flames are at their smoke point.

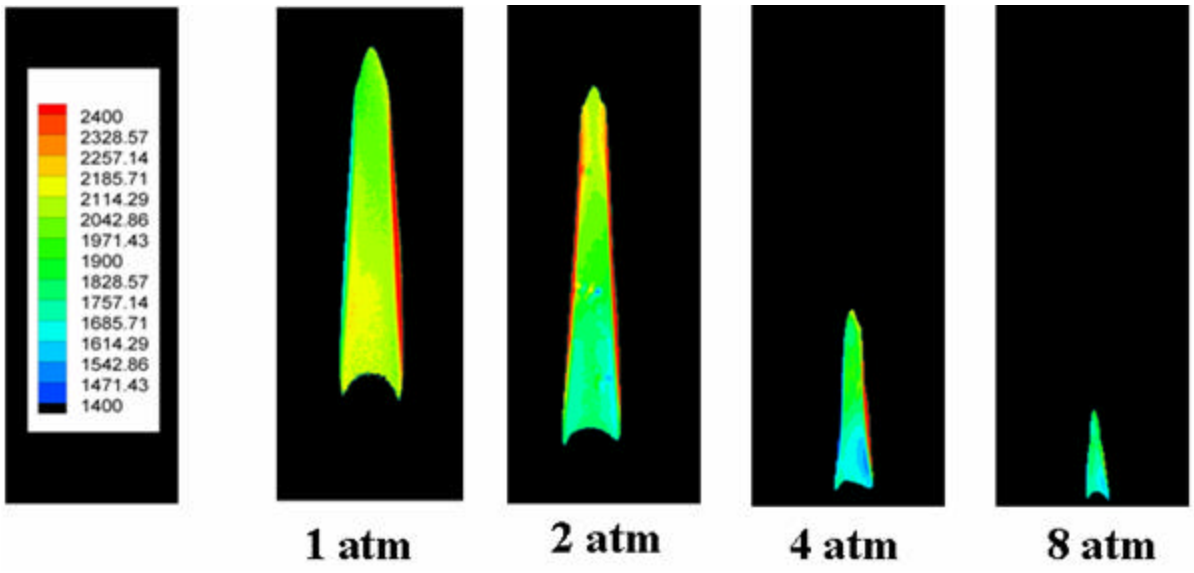


**Figure 5.3: Pure ethylene soot surface temperature profiles as a function of pressure**

These undiluted ethylene flames at 1, 2, 4, and 8 atmospheres had fuel flow rates of 142 sccm, 202 sccm, 260 sccm, and 294 sccm, respectively. It should be noted that each of these images were taken at the same burner height; however, as pressure increases the soot free (blue) region is eliminated, and thus the flame sits closer to the burner lip. Two effects became apparent as the pressure increased from 1 to 8 atmospheres. The flame became cooer and, as expected, shorter with increased pressure. As the pressure increased, the flame height shortens and the base of the flame moves closer to the fuel tube lip, which causes a cooling at the flame base. Gulder and co-workers (2006) investigated the effects of material of which

the fuel tubes were constructed, finding that stainless steel fuel tubes cause more cooling at the flame base. Very similar trends occurred in the measurements made at 80% volumetric fuel flow rate.

Similar to the undiluted soot surface temperature measurements, flames diluted individually with He, $N_2$, Ar, or $CO_2$ were imaged to provide temperature profiles over the same pressure range, 1 to 8 atmospheres. These flames were also at their velocity-matched smoke point heights, which changed with each diluent, dilution level (0% to 40% by volume), and pressure. The primary effect of dilution on these flames was a reduction in soot surface temperature but not nearly as large a reduction as predicted from non-sooting and non-radiating equilibrium calculations. For example, at four atmospheres the overall peak temperature in the undiluted ethylene flame was measured to by 2010 K whereas equilibrium calculations using CET, which does not take into account radiative losses from the soot, calculated the overall peak temperature of the flame to be 2420 K. With nitrogen dilution, the calculated temperature change was small, approximately 50 K, but the measured change in peak temperature was larger, 100 K at 1 atmosphere and 170 K at 4 atmospheres. Additionally, with pressure, the calculated equilibrium temperature increases by almost 50 K due to a reduction in dissociation, but the measured temperatures show a decrease; 140 K in the undiluted flame and more than 200 K in the nitrogen diluted flame at 8 atmospheres.

A second effect of the dilution is an overall lengthening of the flame. For instance, in the ethylene flame mentioned above at four atmospheres, the flame height grows from 20 millimeters, to 24 millimeters, to 29 millimeters for 0%, 20%, and 40% dilution, respectively. There is some effect of the specific diluent on the flame height, with helium

yielding the shortest flame while carbon dioxide yields the tallest. The helium diluted flame being shorter was expected, as helium has a much higher (approximately three times higher) molecular diffusivity than carbon dioxide.

As with the undiluted flames, the soot gets cooer as it moves closer to the fuel tube exit, which occurs as pressure increases. Figure 5.4 shows temperature profiles at 40% dilution at four atmospheres of pressure with each other four different diluents. Similar results were observed at 20% dilution and at other pressures.

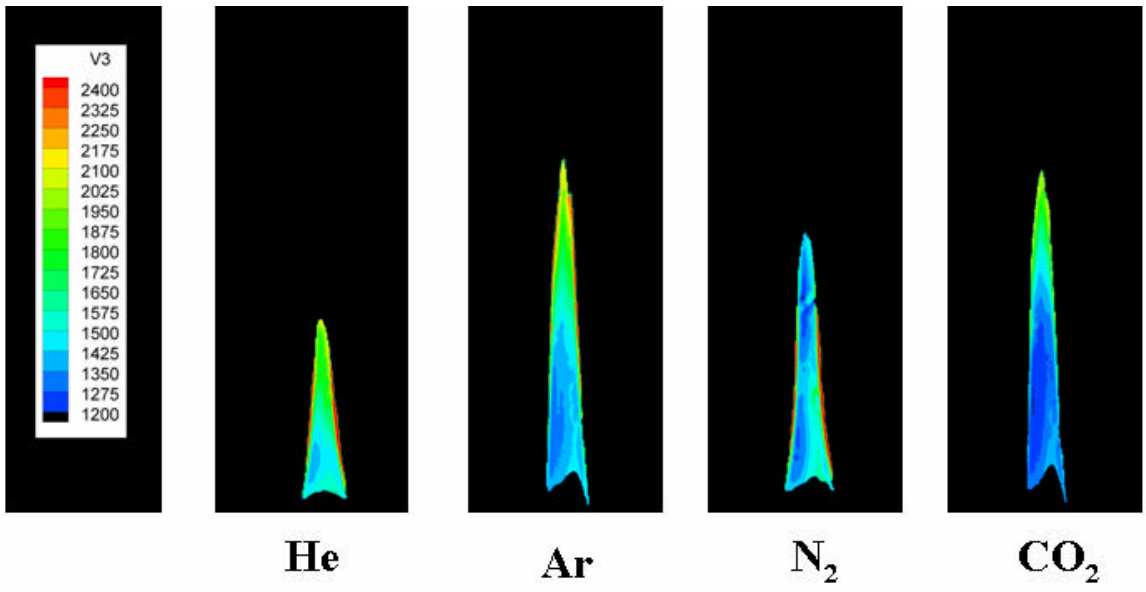


**Figure 5.4: Soot surface temperature profiles of ethylene flames diluted 40% by volume**

For each of the diluted flames to be velocity-matched and at their smoke points, at 4 atmospheres, the following fuel flow rates of 317 sccm, 316 sccm, 315 sccm, and 331 sccm were used for the He, Ar, $N_2$, and $CO_2$, respectively. Several observations should be noted about these flames. The He diluted flame is the shortest of the four flames shown, and is

roughly the same height as the undiluted ethylene flame at four atmospheres. The Ar and $CO_2$ diluted flames are the tallest and similar in height, while the $N_2$ flame is at an intermediate height. This is because the flame height scales inversely with molecular diffusivity and therefore scales directly with molecular weight. Furthermore, in diluting the flame from 0% to 40%, the fuel flow rate had to be increased approximately 20% for He, Ar, and $N_2$ to reach the smoke point. However, for the $CO_2$ flame to reach the smoke point the fuel flow rate had to be increased 27%, indicating that $CO_2$ is better at suppressing soot, which is in agreement with previous research conducted by Glassman (1981). It is also interesting to note that the soot temperature is much more uniform with He dilution compared with the other diluents. As expected, the $CO_2$ yields the coolest soot due to both its high heat capacity and its ability to be an efficient radiator.

Soot surface temperatures of undiluted and diluted ethylene flames are plotted as a function of pressure in Figures 5.5a and 5.5b. The peak soot surfaces temperatures were measured as an overall peak temperature as well as peak temperature at 65% of the flame height as a function of pressure. The soot temperatures were measured for peak temperatures at 65% of the flame height in order to compare to the soot volume fraction findings of McCrain and Roberts (2005). It has been shown, by Santoro (1983) that for undiluted flames at atmospheric pressure, 65% of the flame height corresponds to the location of peak soot volume fraction, and therefore, peak temperatures at this flame height were of interest for comparisons to peak soot volume fractions.

In each of the cases, both pure and diluted flames, the soot temperature at 65% of the flame height is cooler than the measured overall peak soot temperature. This was expected at

atmospheric pressure due to radiation losses from the high soot loading. As the pressure increases the location of maximum soot temperature moves towards the tip of the flame. It is interesting to note that the relative ratio of overall peak to peak at 65% does not vary significantly. It should also be noted that as the pressure increases, overall flame temperature decreases due to heat losses from radiation and to the fuel tube.

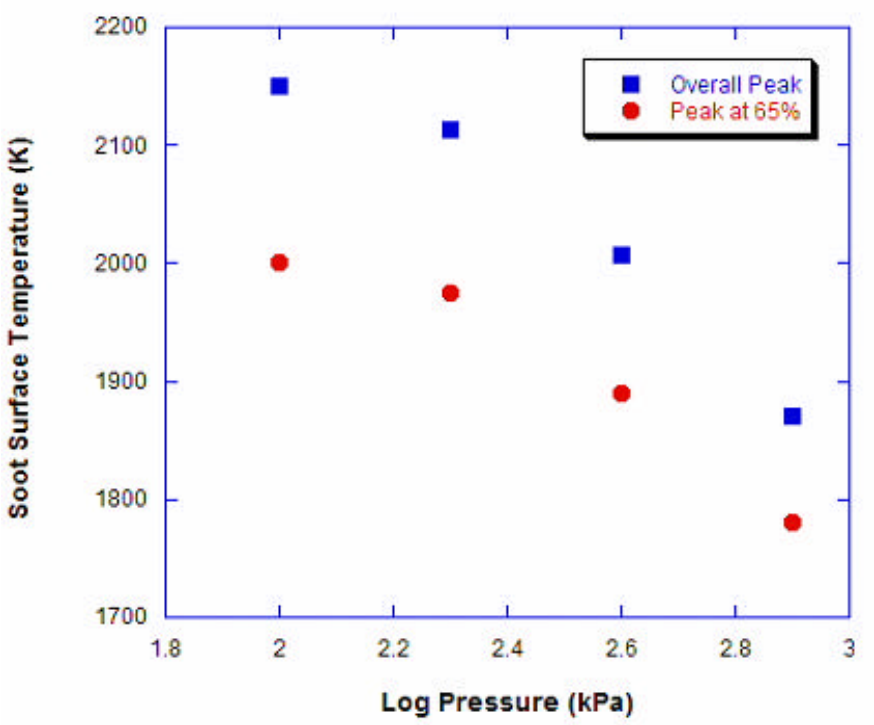


(a)

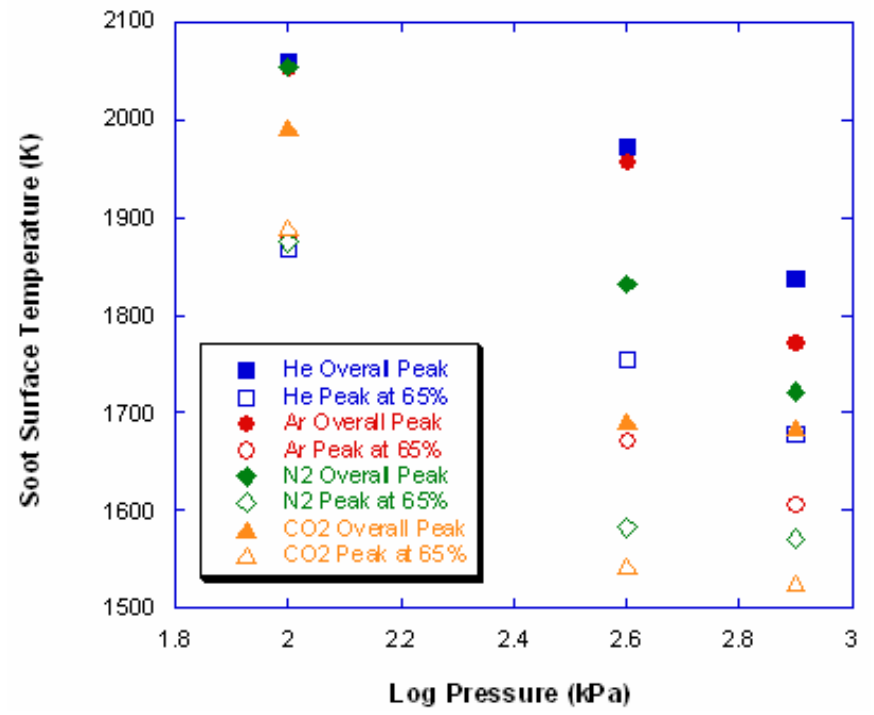


(b)

**Figure 5.5: Maximum soot surface temperatures for (a) undiluted ethylene and (b) ethylene with 40% dilution**

For both plots (Figures 5.5a and 5.5b) the "Overall Peak" temperature is determined from the entire soot surface of the flame, whereas the "Peak at 65%" temperature refers to the maximum temperature at 65% of the flame height.

In order to compare with the previous soot volume fraction measurements of McCrain and Roberts (2005), soot surface temperature measurements were made in undiluted ethylene flames with a constant fuel mass flux. Therefore, for the data shown in Figures 5.6a and 5.6b, the flames measured are not velocity-matched, and are not at their respective smoke points. Therefore, with constant fuel mass flux the flames were above their smoke points at low pressures and were below their smoke points at high pressures. The comparison between soot volume fraction and soot surface temperature is discussed in more detail in Figures 5.6a and 5.6b.

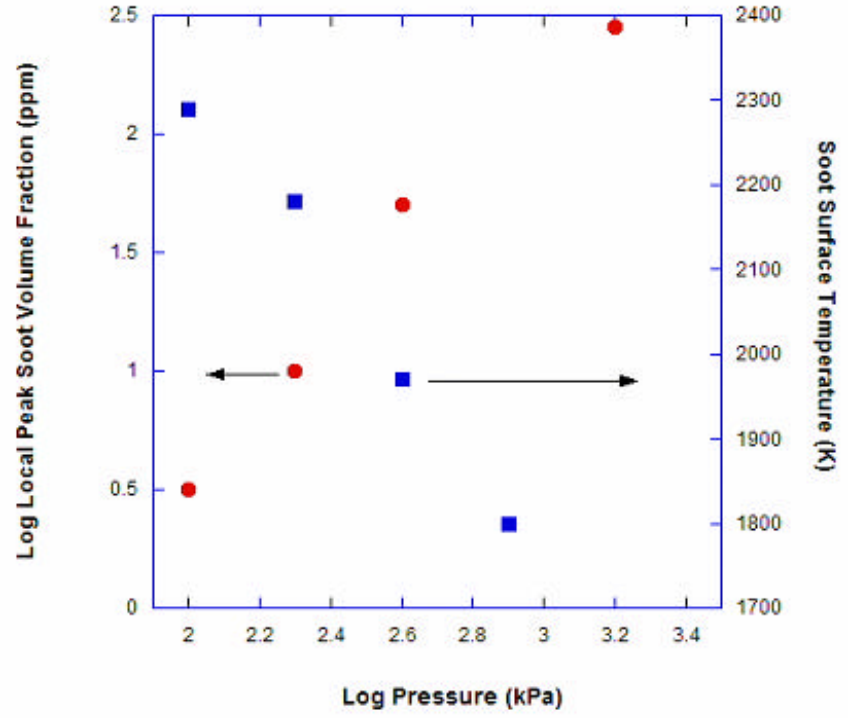


(a)

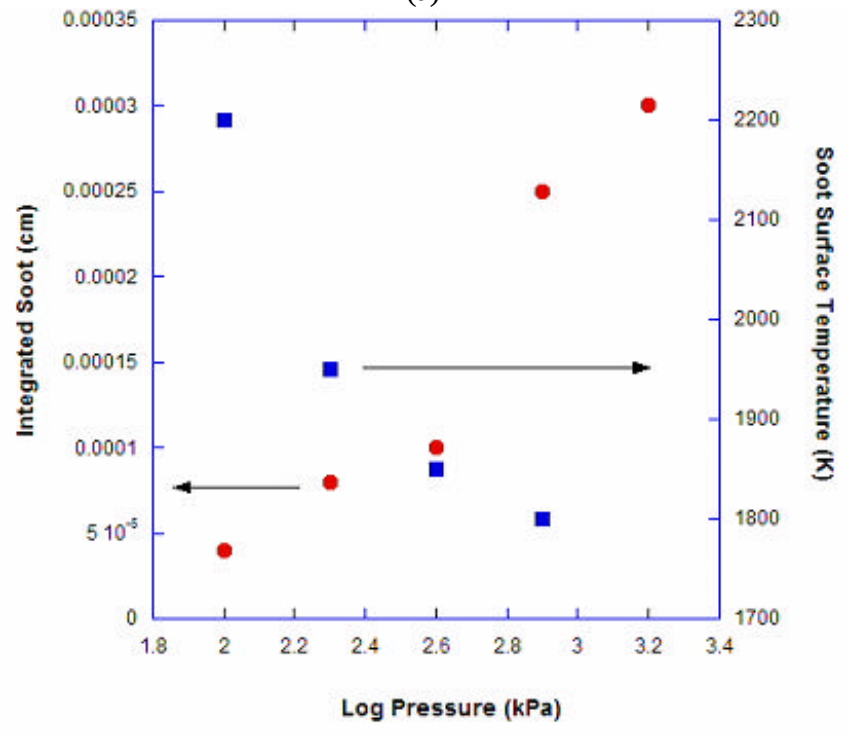


(b)

**Figure 5.6: Soot volume fraction and soot surface temperatures as a function of pressure for undiluted, constant fuel mass flux ethylene flames**

Soot volume fraction measurements were taken using a laser induced incandescence technique in a similar burner as used for the current experiment by McCrain and Roberts (2005). In Figure 5.6a the local peak soot volume fraction is compared to the peak flame temperature found at 65% of the flame's height, as this is where peak soot volume fraction has been shown to exist in undiluted, atmospheric conditions. However, in Figure 4.6b the integrated soot volume is compared to the overall peak flame temperature. From these plots it is clear that as the pressure increases, the local peak soot volume fraction, taken at 65% of the flame's height, and the integrated soot volume fraction, taken from the overall flame, increase in value while the soot surface temperature in each case decreases. As expected, the increase in soot volume fraction with pressure leads directly to a decrease in soot surface temperature. As the pressure increases, the soot-free (blue) region of the flame is eliminated and more soot is produced (since flames are at or below the smoke point, the soot is oxidized) which eventually leads to an overall cooling of the flame.

The soot surface temperature at constant fuel mass flux decreased with pressure. The soot volume fraction increases with pressure and therefore so does the losses from soot radiation. To determine if the reduction in soot surface temperature could be attributed completely to the increased radiation losses, a simple calculation was performed. By knowing the soot volume fraction and the flame's cross-sectional area at 65% of the flame height, and assuming a constant soot spherule diameter and emissivity, a temperature can be calculated.

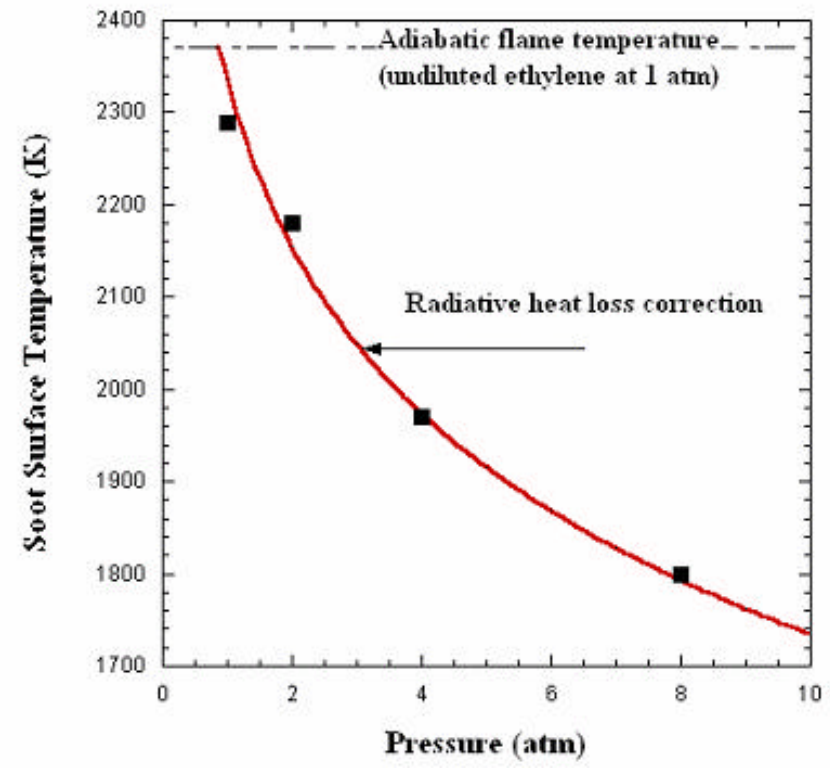


**Figure 5.7: Measured soot surface temperature with radiative losses represented**

This calculated temperature is plotted in Figure 5.7 with the actual soot temperature measurements at 65% of the flame height at constant fuel mass flux. In the undiluted ethylene flames evaluated as a function of increasing pressure, the measured soot surface temperatures (averaged radially at 65% of the flame height) are shown in square symbols while the model accounting for radiative losses from soot is shown as a line. From Figure 5.7 it is possible to see that the measured reduction in soot surface temperature can be attributed completely to the increased radiation losses due to increased soot loading.

## 5.4 Thermometry Conclusions

Soot surface temperatures were measured in both pure and diluted ethylene flames from 1 to 8 atmospheres. Four diluents were utilized, covering a wide range of heat capacities, thermal conductivity, diffusivity, and radiative emissions. These diluents were added to the ethylene fuel stream individually at 20% and 40% by volume. The findings from this experiment are as follows:

1. The flame height decreases, with increasing pressure, increasing the rate of heat transfer to the fuel tube and causing a cooling at the base of the flame.

2. The addition of a diluent cools the soot surface, as expected. With the addition of diluent, the soot at the tip of the flame remains hotter than soot lower in the flame. This effect becomes more pronounced with increased dilution (up to 40% by volume). Overall, the He diluted flames are the warmest and the $CO_2$ flames are the coolest. This is not only a heat capacity effect, but also a small contribution comes from radiative heat loss with the use of $CO_2$.

3. The measured temperature changes with both pressure and dilution, and these changes were larger than calculated based on chemical equilibrium. With pressure, equilibrium calculations predict an increase in flame temperature, while the measurements indicate a reduction in soot temperature on the order of 10%. However, the equilibrium calculations do not account for radiation. The measured temperatures decrease more dramatically with dilution than predicted from equilibrium calculations, at all pressures, despite the similar soot loading between flames, with each flame being at its smoke point.

4. The overall peak temperature of flames at 0%, 20%, and 40% dilution, with increasing pressure, is consistently higher than the temperatures recorded at 65% of the flame height and both the peak and the 65% flame height temperature continue to decrease with increasing dilution levels.

5. There is a chemical effect on overall soot production in flames diluted with $CO_2$, in agreement with previous studies conducted by Glassman (1981), such that higher fuel flow rates are required to reach the smoke point. Flame height scales directly with the molecular weight of the diluent, as expected. The He diluted flame looks very similar to the undiluted ethylene flame in both height and temperature uniformity.

6. With increased pressure in the undiluted flame it was previously reported that the soot volume fraction at 65% of the flame height, as well as the integrated soot, increase. The current experiments show that the overall peak temperature of the undiluted flames decrease with pressure from approximately 2300 K (1 atm) to approximately 1800 K (8 atm). This reduction in soot surface temperature can be fully explained by increased soot radiation, due to higher soot loading with pressure.

# 6 Hydrocarbon Species Concentrations

## 6.1 Background

Hydrocarbon species concentrations were measured in a laminar jet diffusion flame at atmospheric and elevated pressures. These measurements were made to aid in the analysis and understanding of soot production and oxidation, leading to possible methods for reducing or eliminating soot emissions from common combustion devices. Focusing on major hydrocarbon species that exist in ethylene flames, diluted 80% by volume with either He or $CO_2$, gas samples were drawn from the flame's centerline as well as from its luminous surface. In all cases, each flame was investigated at highly over-ventilated, laminar, stable conditions. These flames also had a fuel to air velocity ratio of unity, such that the air had the same exit velocity as the reactant (fuel plus diluent) exit velocity. Another important factor in these measurements was that the fuel mass flux was held constant at all pressures.

## 6.2 Experimental Apparatus

A microprobe was designed and constructed to extract gas samples and is described below. A method of sample extraction at elevated pressures was also developed. All stable hydrocarbon species with a molecular weight up to 150 grams per mol were measured. However, only data for eleven hydrocarbon species was analyzed and reported here. The major hydrocarbon species reported in this experiment are listed below in Table 6.1 in order from lightest to heaviest.

**Table 6.1: Major hydrocarbon species measured**

| Chemical Formula | Name | Molecular Weight (g/mol) |
|---|---|---|
| $C_2H_2$ | acetylene | 26 |
| $C_2H_4$ | ethylene | 28 |
| $C_2H_6$ | ethane | 30 |
| $C_3H_8$ | propane | 44 |
| $C_4H_6$ | 1,3 butadiene | 54 |
| $C_4H_8$ | butene | 56 |
| $C_5H_{10}$ | cyclopentane | 70 |
| $C_6H_6$ | benzene | 78 |
| $C_6H_{14}$ | hexane | 86 |
| $C_7H_8$ | toluene | 92 |
| $C_{10}H_8$ | naphthalene | 128 |

The current research findings were in relative agreement with previous research findings taken from the centerline of the flames at atmospheric pressure. However, the current experiment was expected to yield somewhat different results from those of previous researchers because while other researchers described their flames as "highly over-ventilated," this work used flames that were both highly over-ventilated and velocity matched. As discussed in Chapter 4, the velocity ratio has a strong effect on flame structure and therefore species concentrations. As mentioned previously, maintaining a velocity matched profile ensured that the current experiment's samples were taken from a buoyancy dominated flame with negligible shear layer effects, thus the flames are driven by the choice of diluents which in this case were He and $CO_2$.

The original intent of this research was to measure hydrocarbon species concentrations in each flame where the soot surface temperature was measured, allowing comparison of species concentrations and flame temperatures. However, through many

iterations of the microprobe gas sampling device, it was determined that samples could only be successfully acquired in low soot regions of the flames. This limitation prevented sampling of undiluted flames at elevated pressure. Therefore, flames diluted 80% by volume, with either He or $CO_2$, were utilized for these species concentration measurements where the peak soot volume fraction was low enough to allow sampling.

The gas samples were pulled through the microprobe, utilizing a pressure drop between the vessel and the ambient laboratory environment, and into an evacuated Tedlar bag. The samples were then transported to the EPA for analysis using a gas chromatograph with a flame ionization detector (GC-FID) system, which is discussed later in §6.2.3.

### 6.2.1 Burner and Chimney Modifications

The same pressure vessel and burner that have been used throughout the investigation were utilized for these measurements. However, extensive modifications to the quartz chimney were necessary to permit gas samples to be drawn, as well as slight modification to the vessel.

The quartz chimney still remained the same size, but a channel had to be laser cut to allow the probe to enter the flame for gas sample extraction. This channel allowed the burner to be translated vertically while the probe remained stationary. The channel (Appendix 11.3) was 130 millimeters long and 6.4 millimeters wide. This channel in the quartz chimney enabled the 6.35 millimeter diameter probe to move axially along the entire height of each of the flames tested.

To avoid flame perturbations from entrainment and vortices caused by the optical arms, the portion of the channel in the chimney that was not being used during samples

collection needed to be covered. Therefore a sleeve (Appendix 11.4) was designed to move with the probe and to keep the portion of the open chimney sealed from air perturbations within the vessel. The sleeve had an inside diameter equal to the outside diameter of the quartz chimney and a 3 millimeter thickness. A hole, 6.4 millimeters in diameter, was laser cut into the sleeve to allow the microprobe access to the flame for sampling.

### 6.2.2 Probe Design

The microprobe design proved to be very specific, requiring a probe tip that would not perturb the flame, would aerodynamically quench the sample to avoid chemical reactions within the probe, and maintain an unclogged, soot-free nozzle, probe tip, and probe.

The microprobe went through five design iterations prior to arriving at the final microprobe design. A study by Drake and co-workers (1987) tested four microprobes (cooled stainless steel, uncooled stainless steel, cooled quartz, and uncooled quartz) and saw very little change in their species concentrations due to probe material or thermal environment. Therefore, the current investigation first used an uncooled stainless steel microprobe due to ease of probe fabrication. Two of the iterations of the microprobe were constructed of stainless steel, with varying nozzle and tip configurations. However, after sampling and analyzing species concentrations, it became apparent that the nickel in the stainless steel was catalytically reacting with several of the hydrocarbon species and eliminating all of the higher molecular weight species.

After conferring with several researchers who had previously extracted samples from flames at atmospheric pressure (McEnally & Pfefferle, 1999, Kennedy et al., 1996), it was decided that the microprobe should be made from quartz to avoid chemical reactions within

the probe. Also, it was determined that the tip of the probe needed to act as a "hole in a plate" where the sample could expand as rapidly as possible in the probe to aerodynamically quench the sample, preventing chemical reaction in the probe. Therefore, several sizes of probe tips, constructed of quartz, were tested. Up to this point, the probes had all been straight tubes with a decreasing radius nozzle at the flame side of the probe. The probe tips that were tested had orifices ranging in diameters of 200, 450, and 700 microns. It was found that the 200 micron orifice provided sufficient aerodynamic quenching of samples and allowed for samples to be pulled through the probe and into the Tedlar bags.

In flames or portions of flames with a large soot volume fraction, the probe tip would become surrounded by soot build-up and eventually the tip would clog completely. The first sample drawn would show good results, but the results were not repeatable until the probe was removed from the vessel and cleaned, which clearly is not a viable procedure or technique. The probe clogging problem was solved by adding a sapphire rod down the length of the probe and vibrating this sapphire rod using a dc motor, a suggestion from Robert Santoro, Ph.D. based on his previous research with Rapp (1996). The sapphire rod had a diameter of 125 microns and a length of roughly 35 centimeters. With this sapphire rod placed inside the microprobe, and vibrating constantly, it was possible to keep the probe tip, orifice, and the full length of the probe free from soot build-up. However, the microprobe required one last modification before it was ready for use. The probe was changed from a straight tube to a 'Y' shape (shown Figure 6.1). With the 'Y' shape, it was possible to constantly vibrate the sapphire rod (via the dc motor) and extract the sample through the other arm of the probe.

**Figure 6.1: Final quartz microprobe design**

In order to use the probe at elevated pressure, the final probe design required the addition of a stainless steel threaded rod (Appendix 11.5), which can be seen in place and sealed to the microprobe in Figure 6.1. This addition was necessary to mount the probe into the vessel, providing a sealed fit for elevated pressure testing, and the ability to translate the probe horizontally throughout the flame. With the flame being axisymmetric and the ability to translate the probe horizontally, it was possible to sample radially through the entire flame.

### 6.2.3 GC-FID

Two GC-FID systems were utilized for the current species concentration experiments. One of the GC-FID systems focused on separating lower, similar molecular weight species (from here forth referred to as GC-FID #1) and the other system focused on the slightly heavier, more easily distinguished, hydrocarbon species (from here forth referred to as GC-FID #2). In both systems, the gas chromatograph was made by Hewlett Packard, model number 5890. Also with each GC-FID system the software used to sample analysis was developed by Agilent Software, ChemStation version B.01.03. Each GC-FID was calibrated by NIST standard propane in air standard reference material (SRM), and GC-FID #2 was

also calibrated using a NIST benzene in nitrogen SRM that was able to confirm the benzene response.

Originally, an attempt was made to use a gas chromatograph with a mass spectrometer (GC-MS) for the hydrocarbon species measurements. However, problems with using the GC-MS presented themselves, such that distinction between species could not be reliably established. It proved to be difficult to separate the acetylene ($M$=26 g/mol), ethylene ($M$=28 g/mol), and nitrogen ($M$=28 g/mol) especially since the concentration of nitrogen is many orders of magnitude greater than the concentration of either of the hydrocarbons. Ultimately, the GC-FID proved necessary for the measurements because it only has the capability to measure hydrocarbon species and thus does not respond to nitrogen.

GC-FID #1 was the shorter of the two columns (GSQ) being half the length of column used in GC-FID #2, or 30 meters long. The column had an inside diameter of 0.53 millimeters, and was constructed of a porous polymer with GSQ particles coating the walls of the open tubular column. A 250 microliter sample was injected for analysis on a column that started at 50º C, held for 5 minutes, and then incremented 20º C per minute up to 150º C.

GC-FID #2 had a longer column (DB-1) that was non-polar liquid phase. The column was 60 meters long and coiled inside the gas chromatograph's oven. The column had an inside diameter of 0.32 millimeters. The column walls were coated in a viscous liquid with a thickness of 1 micron. A sample size volume of 2 milliliters was injected for each analysis. The column temperature program was set to begin (cryogenically cooled with

liquid nitrogen) at -50º C, held for 2 minutes, and then increment 8º C every minute up to 280º C.

## 6.3 Results and Discussion

Major hydrocarbon species concentrations were measured in ethylene flames diluted with either He or $CO_2$ (80% by volume) at 1, 2, 4, and 8 atmospheres. Of the many species that were measured, having molecular weights up to 150 g/mol, eleven of the most prevalent species studied along the axial centerline of the flame were analyzed in more detail and are reported within this chapter. Samples were drawn and measurements were made not only along the axial centerline, but also at the surface of the luminous flame. However, after analyzing the samples, very few hydrocarbons were found at the surface of the flame as expected (virtually negligible compared to the concentrations along the centerline), and thus they are not reported here. For comparison, each flame was investigated at roughly 25%, 33%, 40%, 55%, and 69% of the overall flame height. This was the best means of comparison since each of the flames is slightly different in height and width. It was expected, from the findings of previous researchers that the width should change like $P^{0.5}$, while the height should remain relatively constant.

Table 6.2 shows the peak concentration for each of the eleven major hydrocarbon species analyzed from the samples extracted, as well as the height (a percentage of the height of the flame) and the pressure at which the peak concentration occurred in both the He and $CO_2$ diluted flames.

**Table 6.2: Peak concentrations of major hydrocarbon species**

| Species | Carbon Dioxide Concentration | | | Helium Concentration | | |
|---|---|---|---|---|---|---|
| | Peak (ppm) | % Flame Height | Pressure (atm) | Peak (ppm) | % Flame Height | Pressure (atm) |
| | | | | | | |
| acetylene (C2H2) | 6220.0 | 69 | 4 | 12100.0 | 69 | 8 |
| ethylene (C2H4) | 169800.0 | 25 | 1 | 172000.0 | 33 | 8 |
| ethane (C2H6) | 120.9 | 33 | 2 | 507.0 | 69 | 8 |
| propane (C3H8) | 93.3 | 55 | 2 | 342.9 | 69 | 8 |
| 1,3 butadiene (C4H6) | 1.9 | 55 | 2 | 6.1 | 69 | 8 |
| butene (C4H8) | 41.4 | 69 | 4 | 65.8 | 40 | 8 |
| cyclopentane (C5H10) | 0.5 | 69 | 4 | 6.4 | 69 | 8 |
| benzene (C6H6) | 94.4 | 69 | 8 | 334.7 | 69 | 8 |
| hexane (C6H14) | 0.3 | 69 | 8 | 2.9 | 69 | 8 |
| toluene (C7H8) | 5.8 | 69 | 8 | 22.6 | 69 | 8 |
| naphthalene (C10H8) | 0.6 | 69 | 8 | 1.81 | 69 | 8 |

From this table it is observed that the majority of the species had their peak concentration at roughly 69% of the flame height, which was the highest position measured. This was true in most cases regardless of the pressure at which the peak concentration occurred. In the He diluted flame, the peak concentrations occurred at 8 atmospheres for all measured species, and helps to further emphasize that He has a limited ability (as a diluent) to suppress the production of soot precursors and thus soot is formed especially at elevated pressures. It is expected that soot production increases at elevated pressures because of the increase in chemical reaction rates. The $CO_2$ diluted flames showed substantially lower species concentrations for each of the measured species than the He diluted flames. Furthermore, several of the peak species concentrations in the $CO_2$ diluted flames occurred at 1, 2, and 4 atmospheres.

Of the eleven major species measured, four of them were of most interest and will be discussed in further detail here. Acetylene ($C_2H_2$), ethylene ($C_2H_4$), and benzene ($C_6H_6$)

were of greatest interest as they give the most insight to the inception, growth, and oxidation processes of soot formation. Naphthalene ($C_{10}H_8$) was of interest to the current experiment after seeing strong pressure effects on its concentration.

Acetylene is the first step in the soot formation process, and a fuel with a high propensity to soot (such as ethylene) has a favorable thermal decomposition pathway into acetylene. Figures 6.2a and 6.2b show the concentration of $C_2H_2$ in the He and $CO_2$ diluted flames (respectively) as a function of flame height at various pressures.

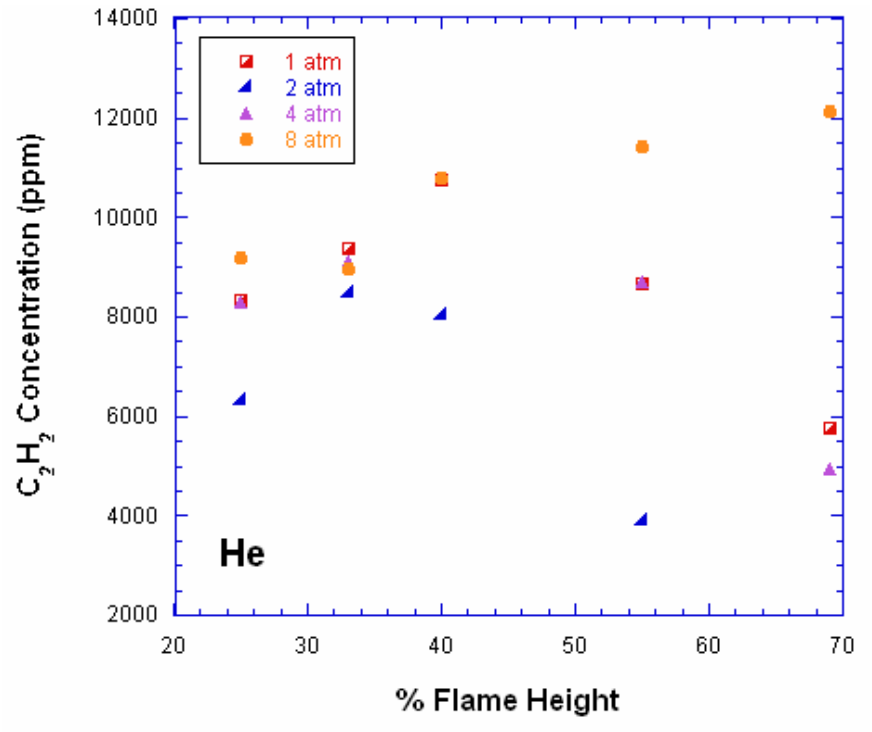


(a)

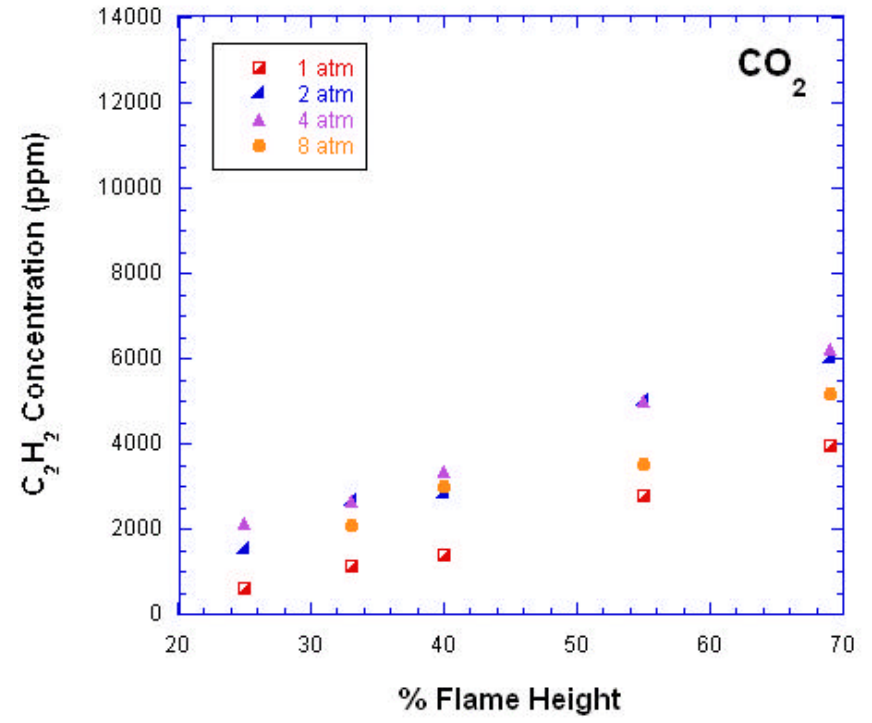


(b)

**Figure 6.2: $C_2H_2$ concentration in (a) helium and (b) carbon dioxide diluted flames**

The concentration of $C_2H_2$ increases with increasing pressure from 1 to 4 atmospheres in the $CO_2$ diluted flames (though slightly dropping from 4 to 8 atmospheres) and the concentration also increases nearly linearly from the base to the tip. However, in the He diluted flame, the concentration of acetylene does increase with increasing pressure (except for the 2 atmosphere case) but not in a uniform manner. There is a slight increase in concentration starting at the base of the flame, but then an overall decrease in acetylene concentration from base to tip in a non-monotonic trend in the He diluted flame. From 1 to 8 atmospheres the overall concentration increased roughly 55% and 25% in the He and $CO_2$ diluted flames, respectively. It should be noted that the concentration of $C_2H_2$ in the He diluted flame is more than double that of the $CO_2$ diluted flame.

Figures 6.3a and 6.3b show the concentration of $C_2H_4$ as a function of flame height and pressure from 1 to 8 atmospheres.

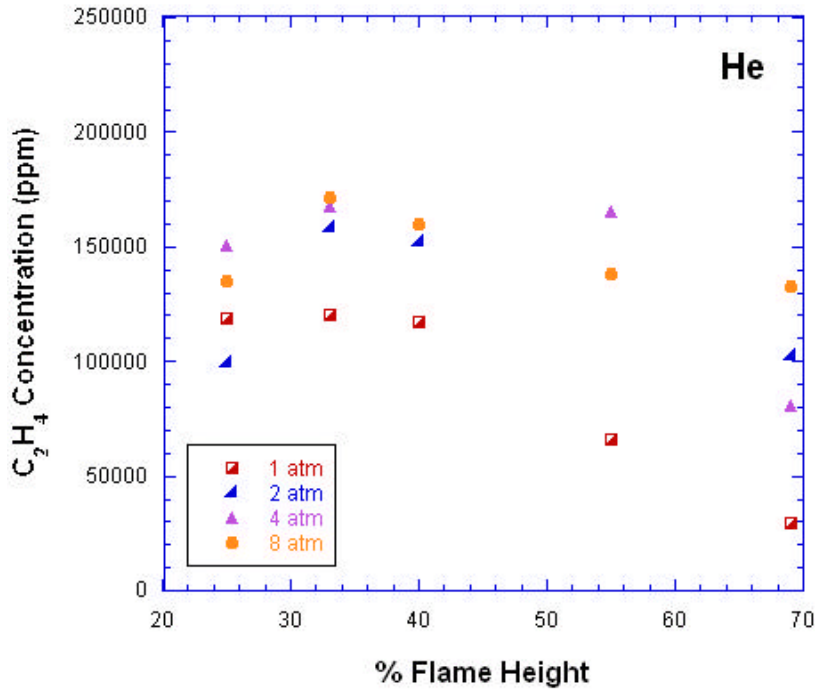


(a)

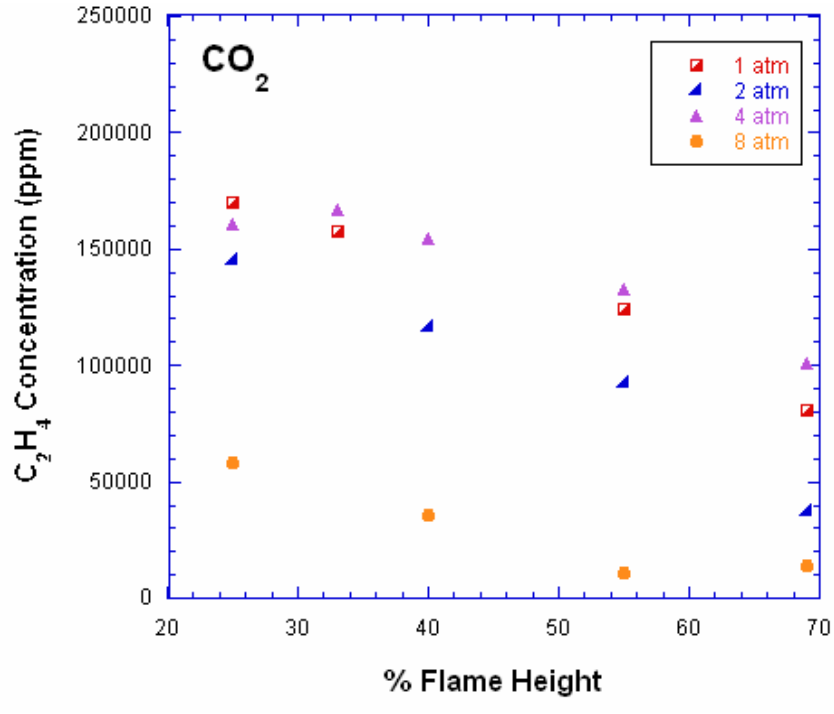


(b)

**Figure 6.3: $C_2H_4$ concentration in (a) helium and (b) carbon dioxide diluted flames**

As expected, the concentration of $C_2H_4$ decreases, from the base to the tip, along the axial centerline, with the peak value of 172,000 ppm for the He diluted flame and 169,800 ppm for the peak concentration in the $CO_2$ diluted flame. For the He diluted flame the concentration of $C_2H_4$, while decreasing with axial flame height, increased with pressure from 1 to 8 atmospheres, whereas the concentration of $C_2H_4$ in the $CO_2$ diluted flame decreased, not only with axial flame height, but also with pressure. Furthermore, the He diluted flame concentrations of $C_2H_4$ initially increase; reaching a maximum near the center point of the flame, but this is not seen in the $CO_2$ diluted flame. The observation can be made from these trends that $C_2H_4$ has high concentrations in heavily diluted flames at the base where little to no thermal decomposition to acetylene occurs. These observations are yet another example of $CO_2$ being a better diluent than He to increase fuel efficiency because more of the ethylene is being used, rather than staying unburned, as pressure increases, and less soot precursor is being formed.

Kim et al. (2008) measured hydrocarbon concentrations in co-flowing diffusion flames at one atmosphere and reported similar findings as the current experiment. However, their measurements were slightly different as they used He dilution in both the fuel and oxidizer stream (which was $O_2$ rather than air). They reported peak concentrations of roughly 100,000 ppm of $C_2H_4$ (low in the flame) and roughly 15,000 ppm of $C_2H_2$. The current experiment observed peak concentrations of approximately 120,000 ppm of $C_2H_4$ and 11,000 ppm of $C_2H_2$ at 1 atmosphere.

Next, benzene concentration in these He and $CO_2$ diluted flames was analyzed. The concentration of benzene, as mentioned previously, is of interest because the $C_6H_6$ rings

combine to form polycyclic aromatic hydrocarbons which are the building blocks of soot primary spherules. Figures 6.5a and 6.5b are plots of the $C_6H_6$ concentration, in He and $CO_2$ diluted flames, as a function of axial flame height and pressure.

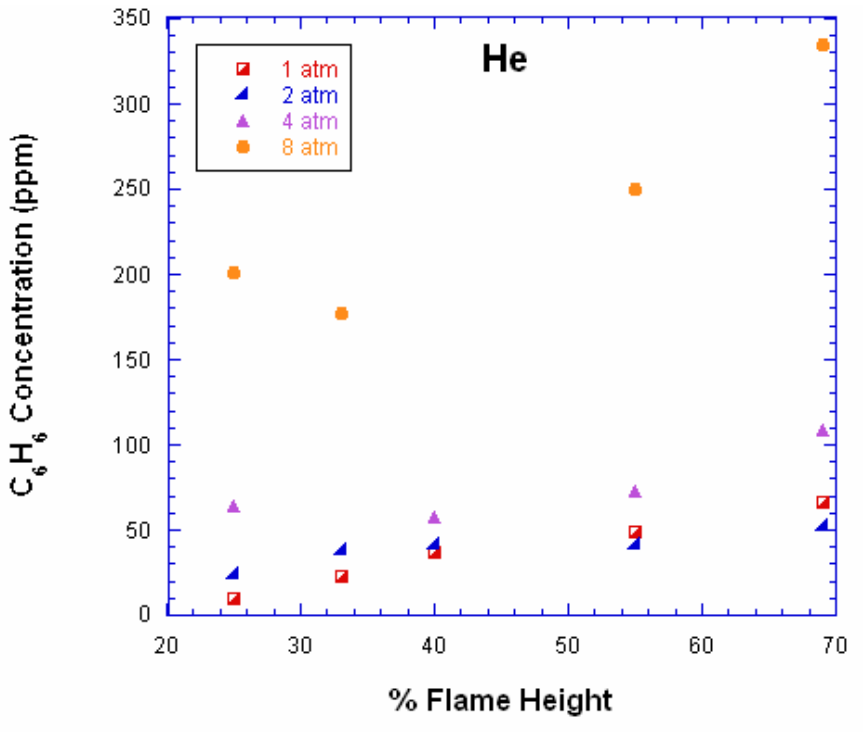


(a)

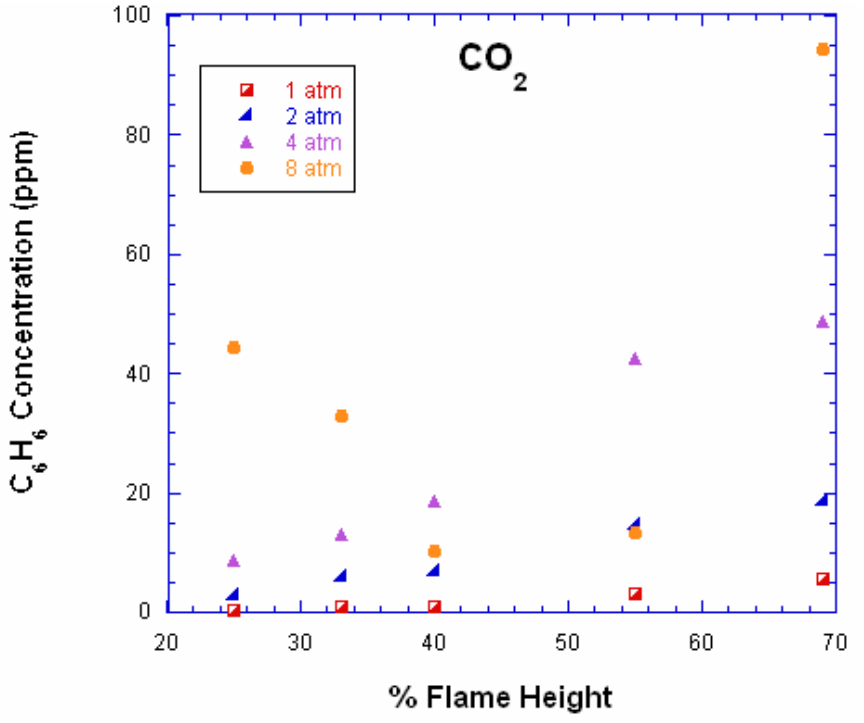


(b)

**Figure 6.4: $C_6H_6$ concentration for (a) helium and (b) carbon dioxide diluted flames**

In each of the flames (He and $CO_2$ diluted) the concentration of $C_6H_6$ increases overall from the base of the flame moving toward the tip of the flame; however, the increase in concentration is relatively linear for cases from 1 to 4 atmospheres and then non-monotonic at 8 atmospheres (particularly for the 8 atmosphere $CO_2$ diluted flame where the concentration of $C_6H_6$ is observed to drop by a factor of three before increasing again). Also in both flames the concentration of $C_6H_6$ increases with pressure, as expected. It is interesting to note that the concentration of $C_6H_6$ in the He flame is substantially greater than those in the $CO_2$ diluted flame, with the peak value in the He flame of 334.7 ppm and the peak value of 94.4 ppm in the $CO_2$ flame. Furthermore, at 1 atmosphere at 20% flame height the concentration of benzene is ten times higher in the He diluted flame than the $CO_2$ diluted flame. Therefore roughly 70% more $C_6H_6$ exists in the He diluted flame at 8 atmospheres. Again, it is clear that $CO_2$ dilution is better at suppressing soot production than He dilution, even at elevated pressures.

While McEnally and Pfefferle (1999) report hydrocarbon species concentrations (from ethylene diluted 80% by volume with nitrogen co-flowing diffusion flames) that are slightly greater than the current $CO_2$ and He diluted flame concentrations, it is interesting to note that in both experimental works the peak benzene concentration at 1 atmosphere is roughly 1% of the peak acetylene concentration. Furthermore, McEnally and Pfefferle found that their peak concentration values, in nearly all species reported, occurred at 2/3 of the flame height, which is consistent with the current experimental findings.

The last major species that warranted more analysis is naphthalene. $C_{10}H_8$ is a complex molecule and was one of the largest measurable hydrocarbon species possible with

the current GC-FID apparatus, with a molecular weight of 128 g/mol. The concentration of $C_{10}H_8$ in the diluted flames was very low, i.e., a few parts per million. However, it was of interest because of the substantial pressure dependence. Figures 6.6a and 6.6b show naphthalene concentrations for both He and $CO_2$ diluted flames as a function of flame height and pressure. Similarly to other species of interest, the $C_{10}H_8$ concentration in both the He and the $CO_2$ diluted flames increases with increasing pressure from 1 to 8 atmospheres, nearly linearly from 1 to 4 atmospheres and non-monotonically at 8 atmospheres. Also, the concentration of $C_{10}H_8$ increases moving upward along the axial centerline from base to tip. In both diluted flames, the concentration of $C_{10}H_8$ increased roughly 90% when increasing from 1 to 8 atmospheres, and was one of the most sensitive species to this pressure change.

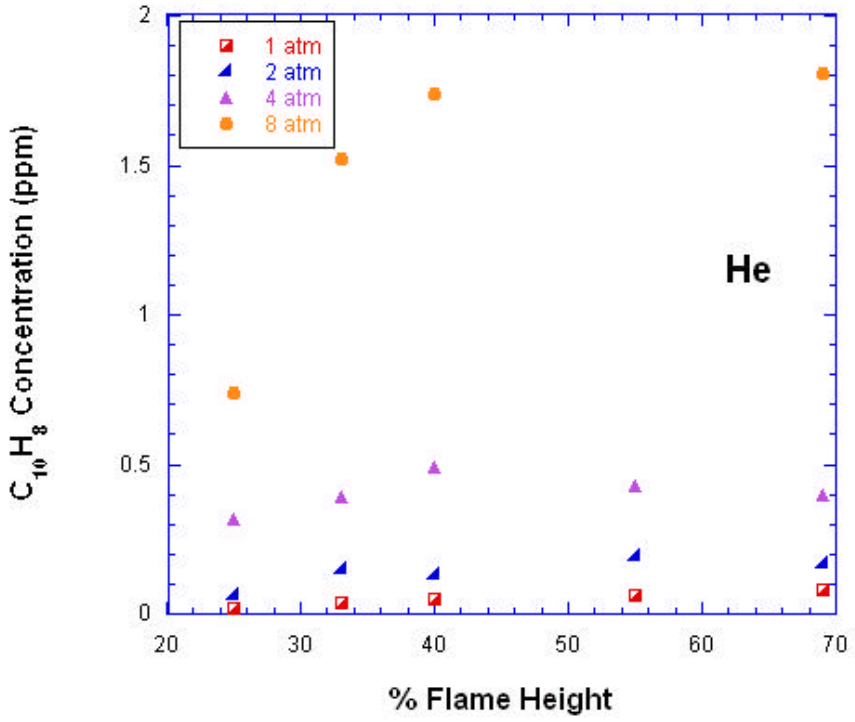


(a)

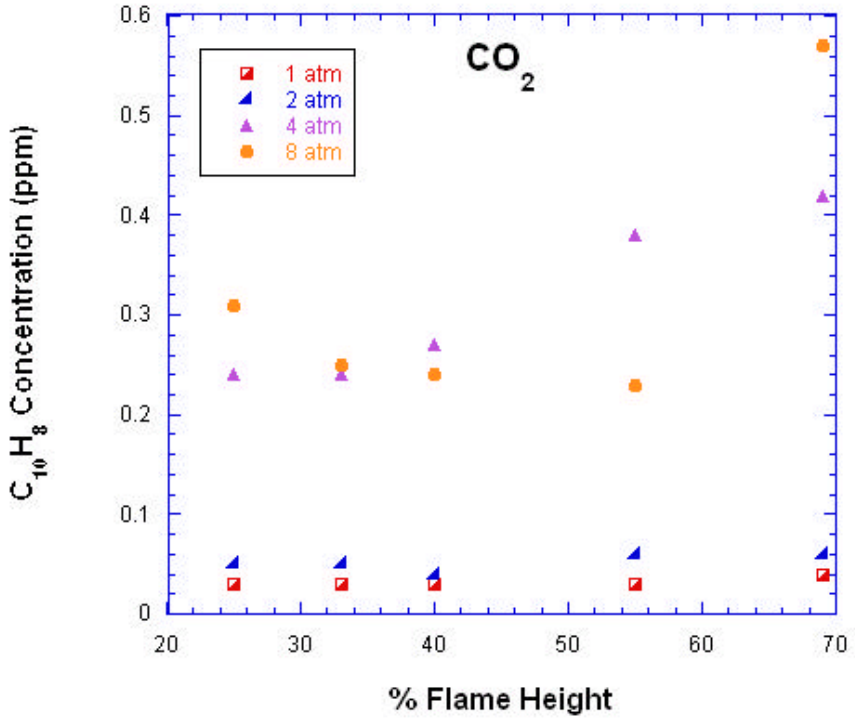


(b)

**Figure 6.5: $C_{10}H_8$ concentration in (a) helium and (b) carbon dioxide diluted flames**

## 6.4 Hydrocarbon Species Conclusions

Measurements of major hydrocarbon species were measured from 1 to 8 atmospheres, utilizing a co-flow laminar jet diffusion flame with ethylene diluted 80% (by volume) with He and $CO_2$ individually. The concentrations of hydrocarbons with molecular weights up to 150 g/mol were measured. Species most able to provide information about soot production, acetylene and benzene, were of particular interest. The following conclusions can be drawn from the current measurements:

1. In nearly every instance (other than $C_2H_4$), overall concentration increases with pressure. This is expected as the chemical reaction and kinetic rates increase substantially with increasing pressure.

2. It is known that the soot produced by a $CO_2$ diluted flame is less than that produced by a He diluted flame (since $CO_2$ is a better soot suppressant), and the current measurements confirm this. In the case of $C_2H_2$ and $C_6H_6$ concentrations, which the presence of each would suggest precursor formation and growth, the flames diluted with He have much higher concentrations of both species than the $CO_2$ flames. At 8 atmospheres the peak $C_2H_2$ concentration for He and $CO_2$ diluted flames were 12100 ppm and 5170 ppm (approximately 55% more $C_2H_2$ in the He flames), respectively. Also at 8 atmospheres, the peak $C_6H_6$ concentrations were 334.7 ppm and 94.4 ppm for He and $CO_2$ (approximately 70% more $C_6H_6$ in the He flames), respectively.

3. In every case the peak concentrations of hydrocarbons in the He diluted flames occurred at 8 atmospheres while in the $CO_2$ diluted flames only the peak concentrations of the heavier hydrocarbons occurred at 8 atmosphere with other species peaking at 1

(ethylene), 2 (ethane), and 4 (acetylene) atmospheres. This can be explained completely by a diffusion effect where He (being light weight) diffuses away fastest and in the $CO_2$ diluted flame the species lighter in weight than $CO_2$ diffuse away faster.

4. As expected virtually no species concentrations existed at the flame surface, and any concentration that did exist was completely negligible when compared to the centerline concentrations. It is expected that large concentrations of non-hydrocarbon species, such as $N_2$, $H_2O$, CO, $CO_2$, etc., exist at the surface of the flame, but GC-FID can only be utilized for measuring hydrocarbon species. It should also be noted that along the centerline, in the majority of instances with both diluents, the peak values occurred at 69% of the flame height.

5. Although peak concentrations occurred at varying pressures, the He diluted flame had peak concentrations over three times higher than the $CO_2$ diluted flame for $C_2H_6$, $C_3H_8$, $C_4H_6$, $C_6H_6$, $C_7H_8$, and $C_{10}H_8$, and two times higher for $C_2H_2$.

# 7 Soot Volume Fraction

## 7.1 Background

Soot volume fraction was measured in undiluted and diluted ethylene-air co-flowing diffusion flames at atmospheric and elevated pressures. Soot in ethylene flames diluted with either He or $CO_2$ was measured at 1, 2, 4, and 8 atmospheres (undiluted ethylene flame only measured at atmospheric pressure), for a total of nine flames coming under investigation.

The current measurements of soot volume fraction are reported utilizing two different experimental methods. One technique used a two-color emission technique, or pyrometry (similar to the soot surface temperature measurements discussed in Chapter 5), to measure the temperature of the flame and soot volume fraction. The other technique used laser extinction and a tomographic inversion to provide the deconvolved soot volume fraction.

Each of these techniques provided a measure of soot volume fraction, while the two-color pyrometry technique also provided a temperature field for each of the nine flames investigated. Each of these techniques, as well as the results obtained from the measurements, is discussed in detail within this chapter.

## 7.2 Experimental Apparatus

For these experiments, measuring soot volume fraction and the temperature field, ethylene was the only fuel used. Ethylene was not only used in its pure form, it was also used diluted 80% (by volume) with either He or $CO_2$, while air was the co-flow. In all cases, the flames had a velocity ratio of reactant (fuel plus diluent) to air equal to unity. However,

differing from some previous measurements within this investigation, the flames used for these experimental measurements were not at their smoke point. These measurements were intended for comparison with the species concentration measurements, and thus the same conditions were used for these experiments. In all instances the fuel flow rate, diluent flow rate, and air co-flow rate remained constant at 125 sccm, 475 sccm, and 127 SLPM, respectively. Therefore, the only changes within each flame were due to pressure effects. For the most part, each of the flames stayed below their luminous smoke point. However, in the 8 atmosphere He diluted flame there was visible smoke emitting from the flame while these measurements were conducted. The heights of these diluted flames were not effected by increases in pressure, differing from the flames at their smoke point considered for the previous experiments on soot surface temperature measurements (Chapter 5); however, the widths decreased with increases in pressure, as expected.

For all of the measurements the same co-flow burner and high pressure vessel, discussed in Chapter 2, were utilized. However, the quartz chimney had to again be modified for these measurements. It was necessary to modify the quartz chimney for better resolution of imaging (for the pyrometry technique) and for minimizing the amount of reflection from the laser beam (for the extinction technique). These modifications included cutting two rectangular sections from the cylindrical chimney (shown in Appendix 11.6) and replacing the sections with anti-reflective coated, optically polished, flat quartz plates. The quartz plates, which were glued onto the openings left by the cuts in the quartz chimney, were 125 millimeters long, 28 millimeters wide, and 3 millimeters thick.

### 7.2.1 Pyrometry

The pyrometry technique used for the soot volume fraction measurements discussed here was very similar to the two-color pyrometry technique used for the soot surface temperature measurements (discussed in detail Chapter 5). Again a monochrome CCD camera was utilized for imaging of each of the flames twice, once with a 632 nanometer color filter and once with a 766 nanometer color filter. The camera was set to an f-stop number of 1.4 to provide for the narrowest field of view, and was focused to the axial centerline of the flames. Neutral density filters were also employed to avoid saturation of the camera. Each image was acquired and saved to a desktop computer. Using ImageJ software it was possible to take live images of the each flame, averaging ten images of the flame with each color filter. The images that required averaging were mostly at elevated pressures where the flames, although stable, on occasion would "flicker". The images saved to the desktop were then imported into a MATLAB program for analysis (shown in Appendix 11.2).

The MATLAB program took the ratio of the two images, corrected the ratio for the camera settings using a calibration performed with a black body calibrator, and then calculated a temperature profile based on Planck's equation (Equation 5.1). The calibration performed with the black body calibrator was slightly more specific for these soot volume fraction measurements than for the soot surface temperature measurements discussed in Chapter 5, such that the ratio of intensities (from the images) was multiplied by a linear function (0.2324*[ratio] + 0.0378) rather than just multiplying by a factor of 0.4319 (calibration factor used for soot surface temperature measurements). By using a linear

function for correction it was possible to obtain more accurate calibration for the temperature field.

Once the temperature field was determined, the program then used two similar equations for deriving soot volume fraction profiles. The relationship between measured spectral emission, temperature, and soot volume fraction is given by DeIllius, Cignoli, and co-workers (1998 and 2001). The equations used to solve for soot volume fraction are discussed in detail in §1.7.2, including detail of which variables are measured and which are calculated. The soot volume fraction profiles differed from the temperature field because it was possible to calculate a soot volume fraction for each of the images (one for 632 nanometers and one for 766 nanometers), where a ratio of the two images was needed to calculate the temperature field. The soot volume fraction equation called for a measured value of soot temperature (from the ratio of the images at each wavelength), but then only an image of the flame at one wavelength for the soot volume fraction. Therefore, with two wavelengths it was possible to calculate two soot volume fraction profiles with one temperature field, which gave a redundant profile to ensure that the soot volume fraction was being calculated correctly.

### 7.2.2 Extinction

The extinction technique utilized in the current investigation has been used for decades in laboratory settings (D'Alessio et al., 1972). Recently, this technique of extinction measurements has been used by McCrain and Roberts (2005) in the same pressure vessel and with a similar burner configuration as the current investigation. For this technique a Helium-Neon laser is used (632 nanometer), the beam is split and the two consequent beams

(attenuated and reference) pass through and below the soot incandescence region of the flame while in the pressure vessel. The intensities of the beams are then measured by photo diodes whose output is measured on an oscilloscope. A rough schematic of the apparatus is shown in Figure 7.1.

The beam splitter provided two beams from one, with one of the beams having a much weaker signal than the other. The weaker of the two beams passes through the soot free (blue) region of the flame (reference beam), whereas the stronger signal beam passes through the soot region and becomes attenuated.

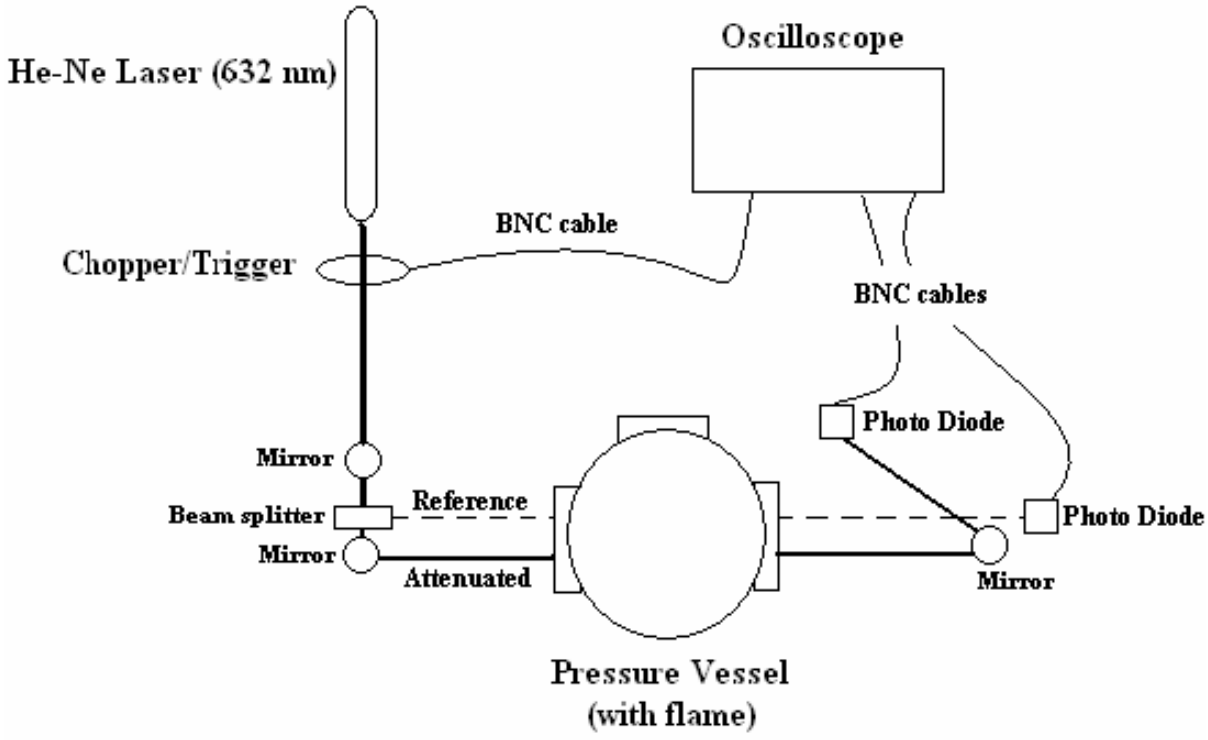


**Figure 7.1: Extinction measurement schematic**

First, the intensity of a beam passing through the pressure vessel, without a flame, was measured to give the unattenuated signal ($I_0$) for calculating soot volume fraction. The reference beam was used to correct the attenuated and the unattenuated signals for any soot that existed in the pressure vessel or on the optical ports of the vessel. The signal values from the oscilloscope were then recorded into an Excel spreadsheet that calculated the line of sight average soot volume fraction (at one location) based on D'Alessio's soot volume fraction calculations (Equation 1.2). The extinction measurements were made at one axial height in each flame, at approximately 65% of the flame height, which has been shown to correspond to the peak soot volume fraction of undiluted ethylene flames at one atmosphere. However, all of the optics, photo diodes, and the He-Ne laser were mounted on optical arms attached to precision translation mounts. Therefore, optics on either side of the pressure vessel (once properly aligned) were capable of precise movement radially within the flame. Several measurements, still at one axial height, were made at different radial locations in each of the flames. This was necessary for the soot volume fraction measurements since they were line of sight measurements in order to deconcolve the flame. The path lengths needed for the calculations to deconvolve the flame and determine soot volume fraction were measured from images taken of the flames. The soot volume fraction measurements were expected to be low when passing through the radial center of the flame and high when passing through the wings of the flame. Since the high soot regions exist on the wings of the flame and the beam is essentially passing through "both" sides of the flame, more soot attenuates the beam that passes through the flame near the surface (or edge) of the flame. Therefore it was necessary to "correct" the soot volume fraction values obtained through the

extinction measurements. A tomographic inversion was used to deconvolve the soot field and then calculate more accurate soot volume fraction values, taking into account the flame being axisymmetric rather than a flat plate.

## 7.3 Results and Discussion

Measurements of soot volume fraction were taken with an undiluted ethylene laminar diffusion flame at 1 atmosphere as well as diluted flames (either He or $CO_2$ at 80% by volume) at 1, 2, 4, and 8 atmospheres. The data collected from the experiments (both pyrometry and extinction) are discussed below as a comparison between the two techniques and the results were also examined for trends present from the effects of pressure and dilution on soot volume fraction.

In order to have confidence in the results determined by the current experiment it was necessary to first compare a portion of the data to another set of well referenced data on soot volume fraction (Quay et al., 1994). However, the data taken by these researchers was only at atmospheric pressure in an undiluted ethylene flame. In Figure 7.2 it is observed that the two current techniques agree rather well with the extinction measurements of Quay and co-workers (1994). Although Quay (1994) uses a larger burner than the current investigation, the soot volume fraction values were compared at approximately 65% of either flame's height, at which height Quay's flame was nearly the same as the current flame.

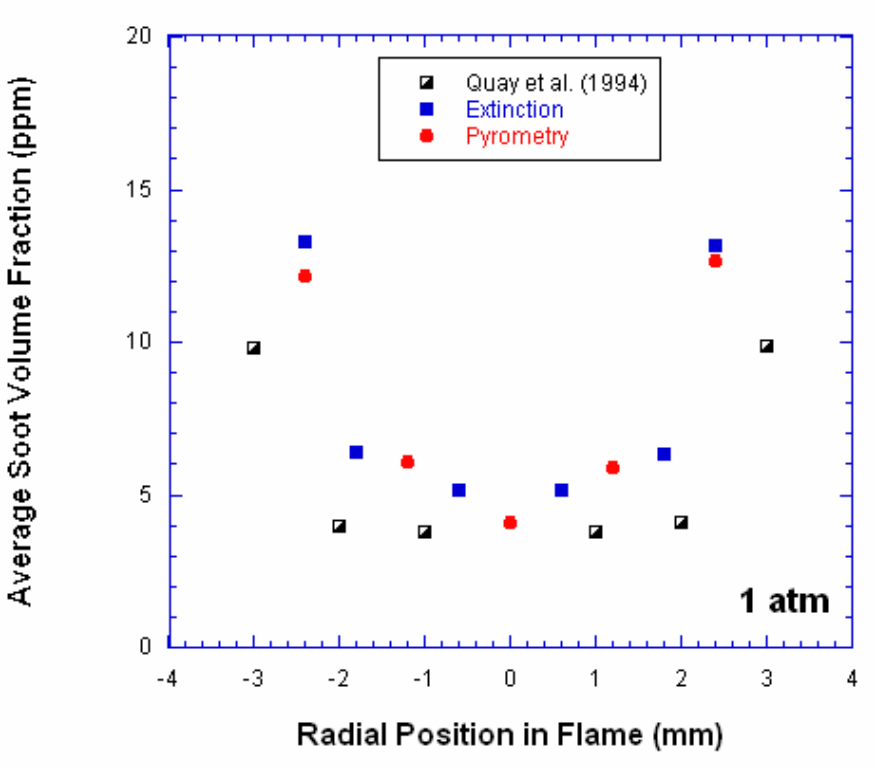


**Figure 7.2: Comparison of soot volume fraction measurements at 1 atmosphere**

Quay and Santoro also measured (in the same investigation) the soot volume fraction using laser induced incandescence (LII) and found that their extinction technique slightly over-predicts the soot volume fraction found using LII. Cignoli and co-workers (1994) measured soot volume fraction using pyrometry and extinction techniques and also observed the extinction measurements slightly over-predicting the pyrometry measurements for soot volume fraction values. As seen in Figure 7.2, it was also observed that the extinction technique slightly over-predicted the pyrometry technique for determining soot volume fraction. It should also be noted that, as expected, the higher soot volume fractions occurred at the "wings" of the flame with the lowest value of soot volume fraction occurring at the centerline of the flame. This has been shown by many researchers in the past, and agrees

with the theory that in diffusion flames the soot forms near the fuel side of the flame with the blue (soot-free) region extending along the centerline of the flame. Once it had been shown that the current techniques were valid in undiluted ethylene flames at atmospheric pressure, more flames (diluted 80% by volume) were investigated. The tomographic deconvolution of the flame changed the values of the soot volume fraction, measured using the extinction technique, mostly near the surface of the flame (in the "wings"), but changed the values through the center of the flame only slightly.

Figures 7.3a and 7.3b show the soot volume fraction values found using the pyrometry technique for the He and $CO_2$ diluted ethylene flames. Figures 7.3a shows the soot volume fraction field for He (left) and $CO_2$ (right) diluted flames at 1 atmosphere, and Figure 7.3b shows the temperature fields from the same flames, with the He diluted flame (left) having a peak temperature of 2300 K and the $CO_2$ diluted flame (right) having a peak temperature of 2240 K. The asymmetry of the $CO_2$ diluted flame can be explained by the lack of soot that exists in the flame. With such a small amount of soot present in the flame, the signal to background ratio is very small and therefore the image is affected.

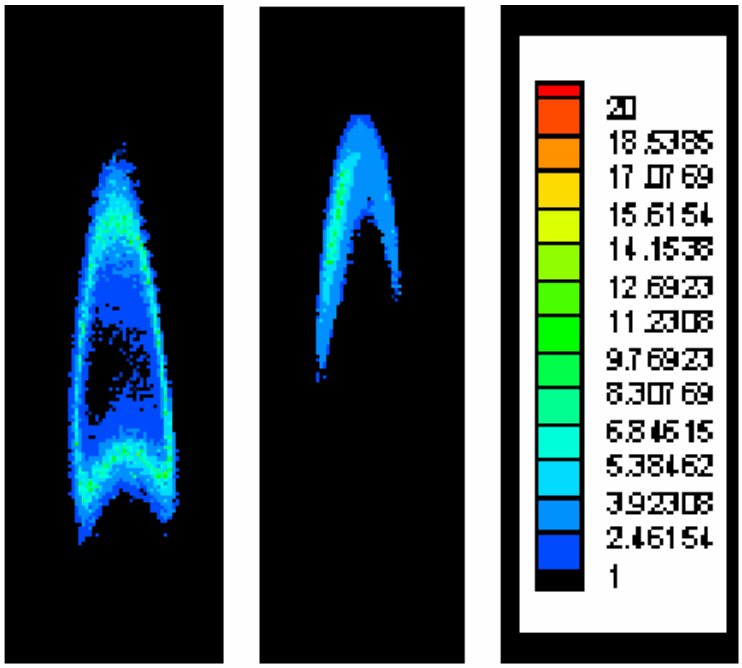


(a)

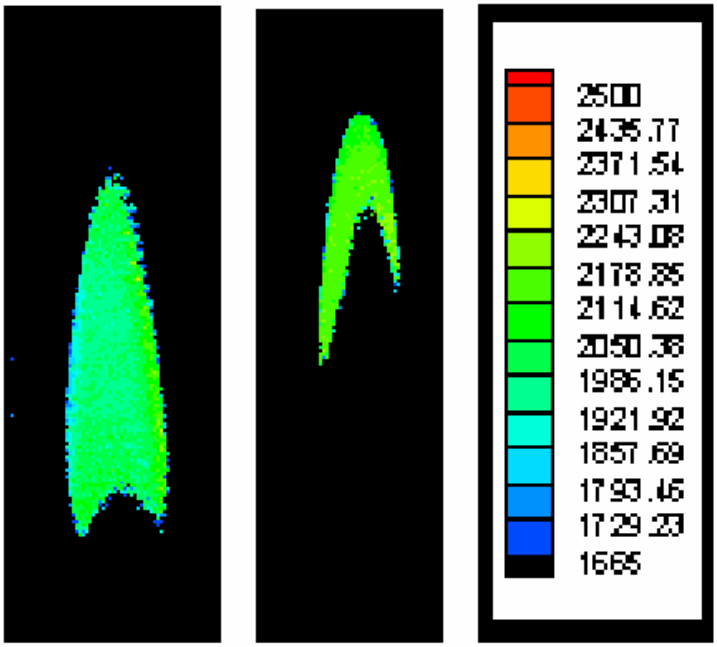


(b)

**Figure 7.3: Soot volume fraction (a), in ppm, and temperature (b), in Kelvin, profiles for He (left) and $CO_2$ (right) diluted flames at 1 atmosphere**

Figure 7.4 shows the soot volume fraction measured from each diluted flame at 1 atmosphere using the extinction technique as well as the extinction values obtained for the undiluted ethylene flame (at 1 atmosphere) as a point of reference. As expected, both of the diluted flames provided soot volume fractions less than that of the undiluted flame. Furthermore, the soot volume fraction of the $CO_2$ diluted flame is slightly lower than the soot volume fraction of the He diluted flame. The peak soot volume fraction values from the extinction measurements agree well with the peak values (at 65% of the flame height) from the pyrometry technique. From the pyrometry images, data was taken from 65% of the flame heights and inserted into the plot of soot volume fraction values from the extinction method. The extinction measurements yielded peak soot volume fraction values for He and $CO_2$ diluted flames of approximately 9.0 ppm and 6.9 ppm, respectively, while the pyrometry profiles yielded peak values of approximately 9.3 ppm and 7.6 ppm for He and $CO_2$ diluted flames, respectively.

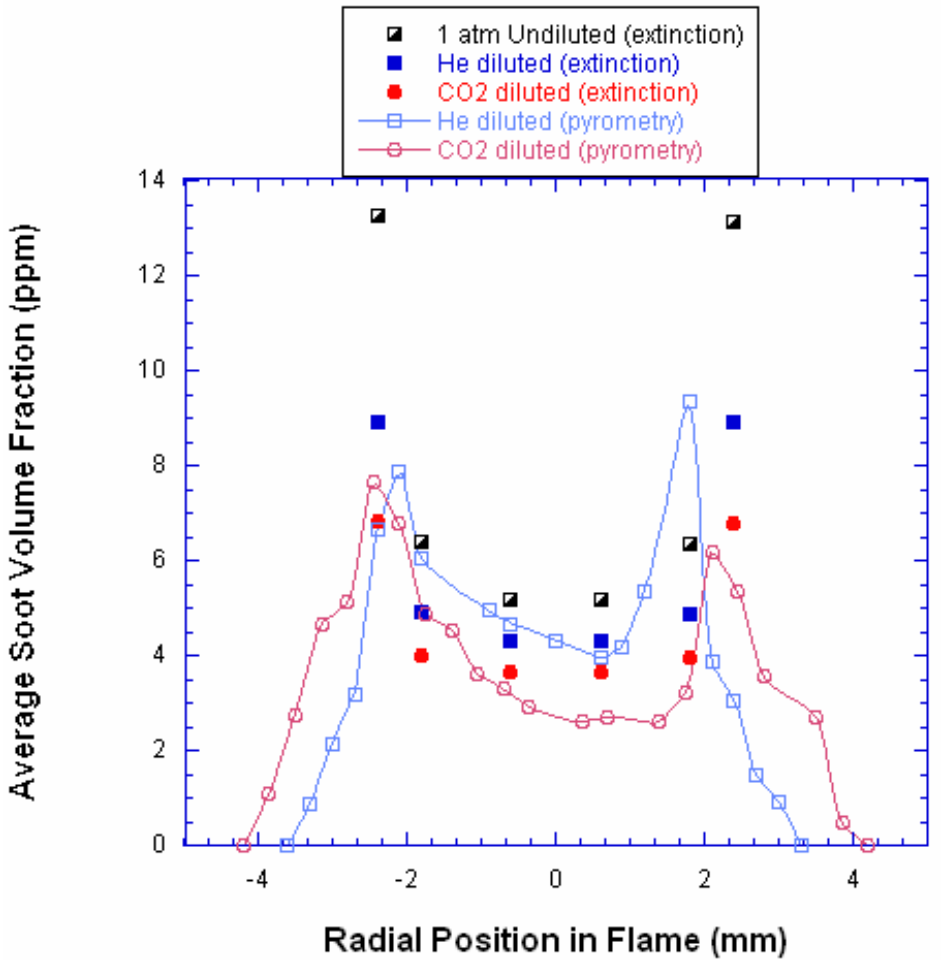


**Figure 7.4: Extinction measurements of soot volume fraction as a function of radial position at 1 atmosphere in diluted flames**

Figures 7.5a and 7.5b show the soot volume fraction and temperature fields, respectively, of the He diluted (left) and $CO_2$ diluted (right) flames.

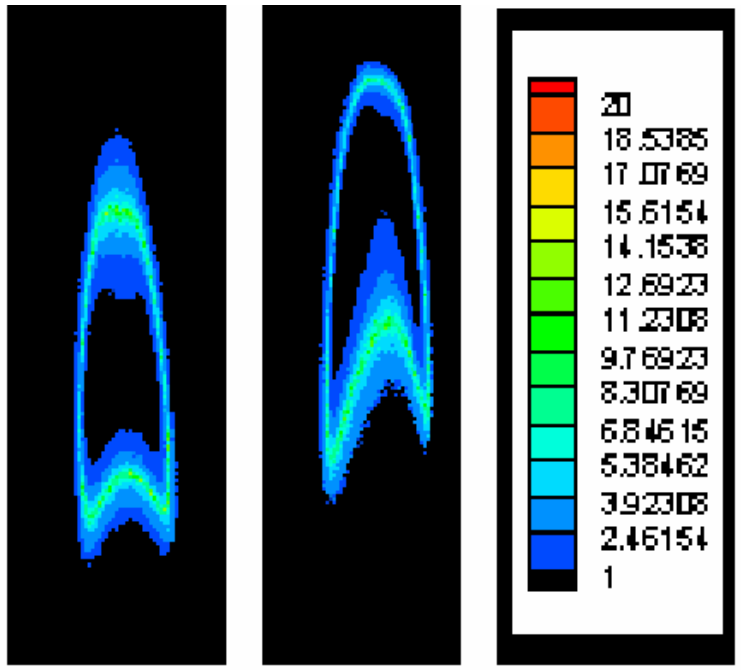


(a)

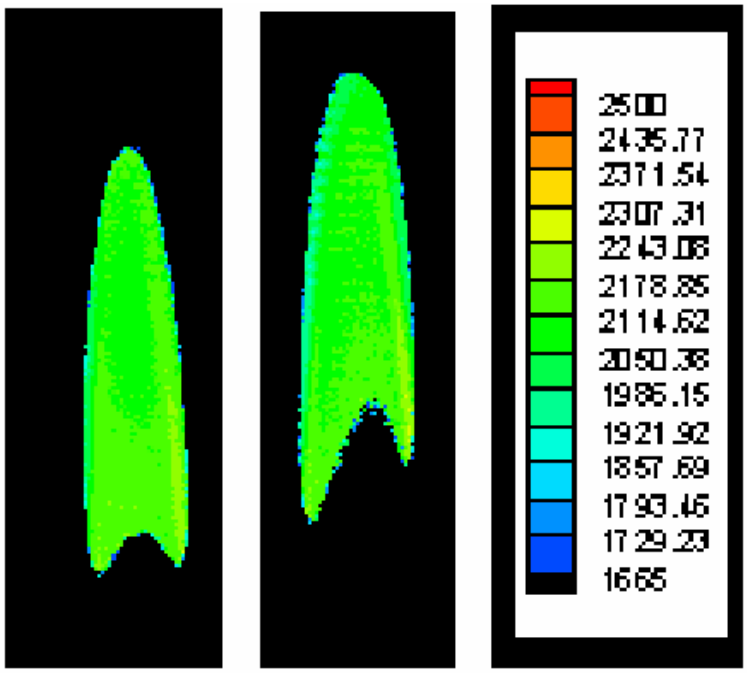


(b)

**Figure 7.5: Soot volume fraction (a), in ppm, and temperature (b), in Kelvin, profiles for He (left) and $CO_2$ (right) diluted flames at 2 atmospheres**

It should be noted that for all data of the soot volume fraction and temperature fields, the images were taken at the same burner height. Therefore, the $CO_2$ diluted flame is taller than the He diluted flame and the $CO_2$ diluted flame has a longer blue (soot free) region that is not imaged at the base of the flame (only the soot incandescence is possible to image). From Figure 7.5a it is observed that less soot is present in the $CO_2$ diluted flame than in the He diluted flame. Although it is difficult to see the immediate difference in the temperature fields of these two diluted flames from Figure 7.5b, the peak temperatures are quite different with the He diluted flame having a peak temperature of 2320 K and the $CO_2$ diluted flame having a peak of 2250 K. The temperatures at 2 atmospheres are slightly higher than the same diluted flames at 1 atmosphere, with an increase of 20 K for the He diluted flame and an increase of 6 K for the $CO_2$ diluted flame. In order to further consider the soot volume fraction within these two flames, extinction measurements were made (shown Figure 7.6).

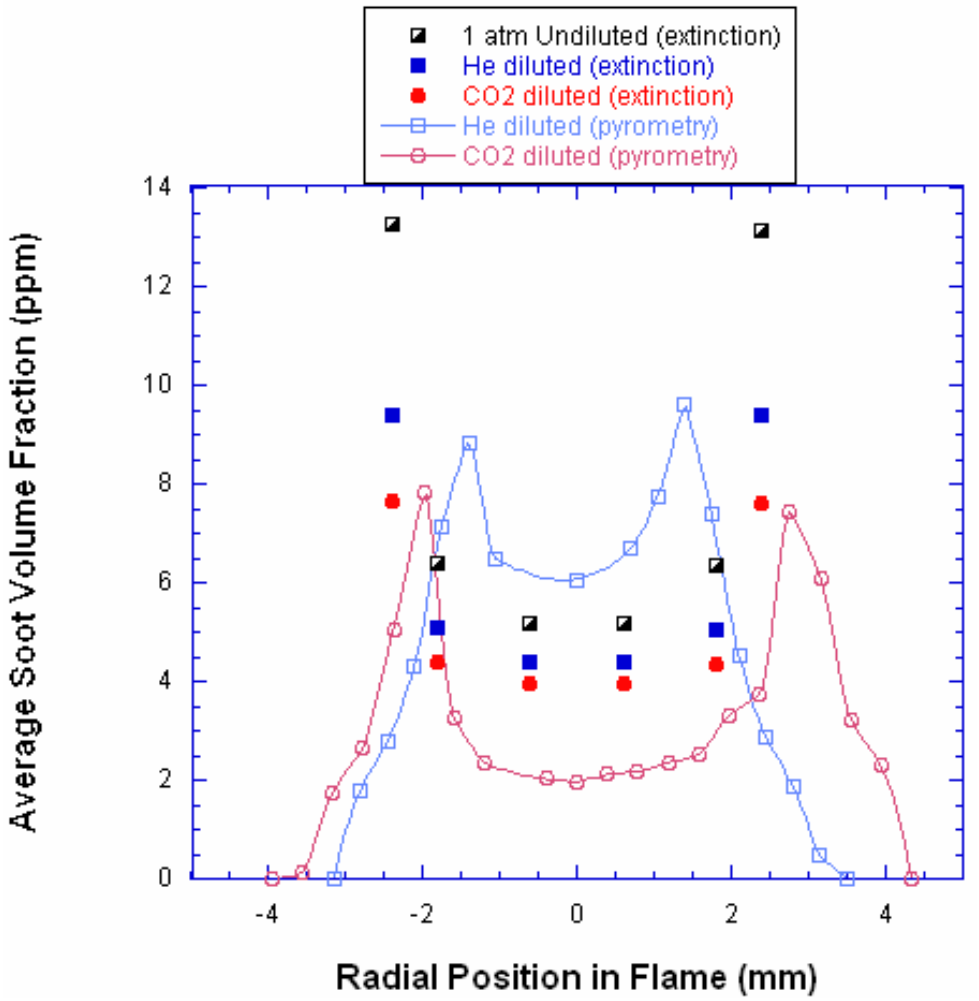


**Figure 7.6: Extinction measurements of soot volume fraction as a function of radial position at 2 atmospheres in diluted flames**

Again, with the extinction measurements, it is observed that the soot volume fractions of the He and $CO_2$ diluted flames at 2 atmospheres are slightly lower than the undiluted flame at 1 atmosphere, even with the pressure increase. However, at 2 atmospheres the difference in soot volume fraction between the He and $CO_2$ diluted flames is not as noticeable, with the He diluted flame peak (near the edge of the flame) at approximately 9.5 ppm and the $CO_2$ diluted flame peak at approximately 7.8 ppm. These peak values agree well with the pyrometry

values (at 65% of the flame height) in which the He diluted flame peaked (near the edge of the flame) at approximately 9.6 ppm and the $CO_2$ diluted flame at approximately 7.8 ppm.

Another increase in pressure (up to 4 atmospheres), while maintaining all other flame parameters, yields increased soot volume and temperatures as shown in Figure 7.7a and 7.7b, respectively. Again it is observed that the $CO_2$ diluted flame is taller than the He diluted flame and has a longer blue (soot free) region along the base of the flame. The peak temperatures within the flames increased with the pressure increase, with the He diluted flame peaking at 2390 K and the $CO_2$ diluted flame peaking at 2310 K. This was an increase in temperature from the peaks of the 2 atmosphere flames of 71 K for the He diluted flame and 60 K for the $CO_2$ diluted flame.

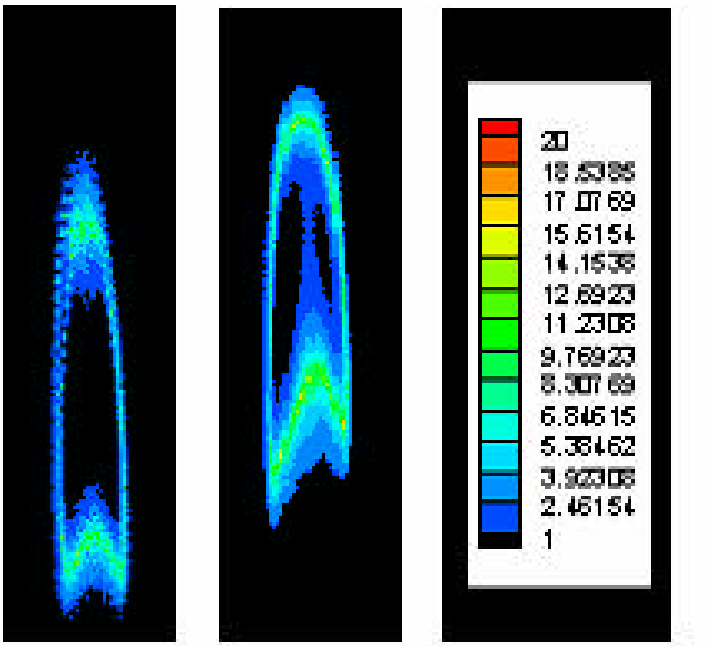


(a)

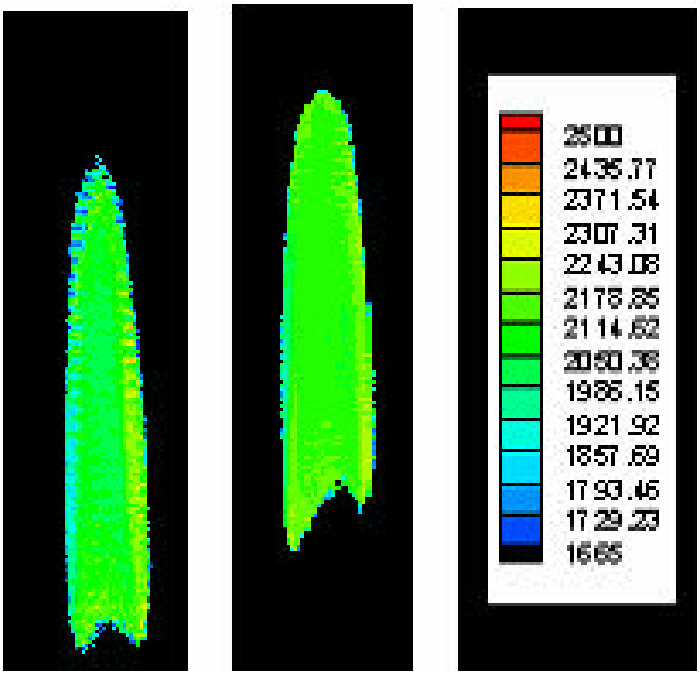


(b)

**Figure 7.7: Soot volume fraction (a), in ppm, and temperature (b), in Kelvin, profiles for He (left) and $CO_2$ (right) diluted flames at 4 atmospheres**

Next, the extinction measurements were made, in both diluted flames at 4 atmospheres, for comparison to the soot volume fraction measurements made through pyrometry (shown Figure 7.8). Again the peak soot volume fractions are observed to be at the edge of the flames, but with this increase in pressure the soot volume fractions at 4 atmospheres are approaching (but not overcoming) the soot volume fractions of the undiluted ethylene flame at 1 atmosphere. In these flames at 4 atmospheres, similar to the flames at 2 atmospheres, the soot volume fraction differences between the He and $CO_2$ diluted flames are minimal. The peak soot volume fraction in the He diluted flame is approximately 11.8 ppm and the peak for the $CO_2$ diluted flame is approximately 11 ppm. Again, when comparing to the peak soot volume fractions from 65% of the flame height with the pyrometry technique, the values are in agreement, with the He diluted flame peak of approximately 11.7 ppm and $CO_2$ peak of approximately 10.6 ppm.

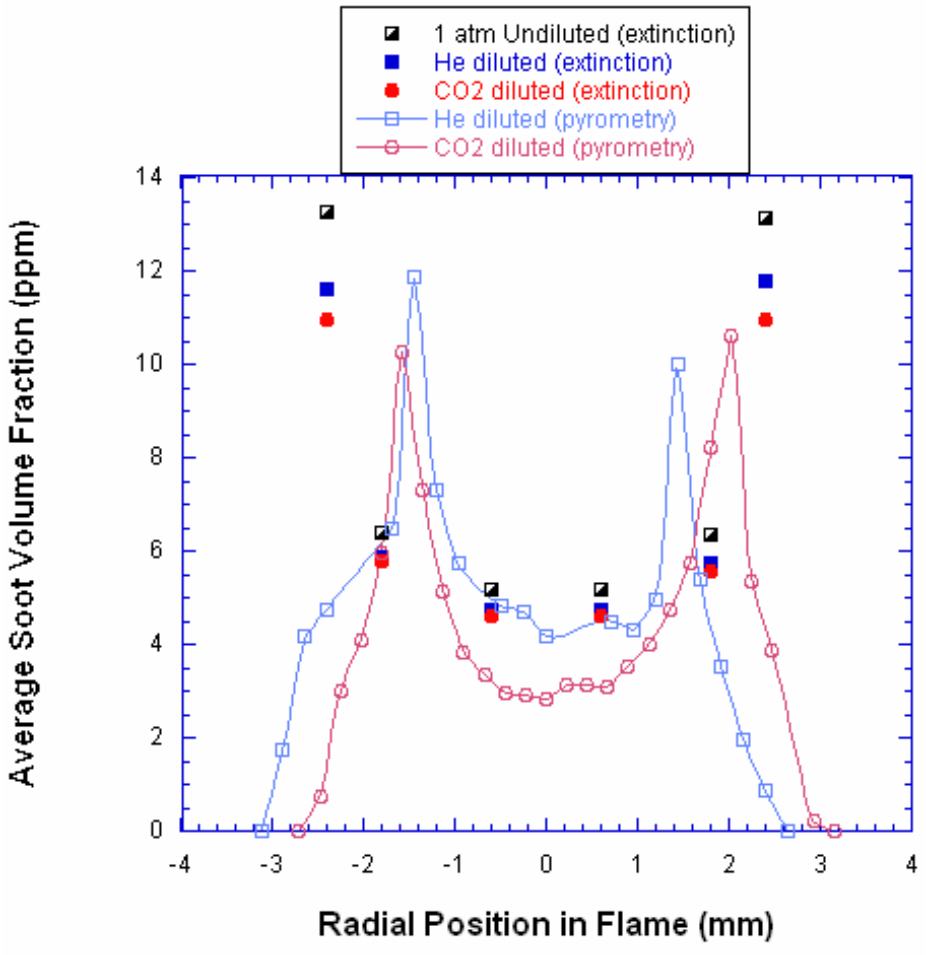


**Figure 7.8: Extinction measurements of soot volume fraction as a function of radial position at 4 atmospheres in diluted flames**

Finally, the diluted flames were investigated at 8 atmospheres for soot volume fraction and temperature fields. Figures 7.9a and 7.9b again show the soot volume fraction and temperature profiles, respectively. From these pyrometry images it is observed that there is no longer a blue (soot free) region in either of the diluted flames, and the heights of the two flames are nearly the same. The peak temperatures in each flame have again increased from the temperatures at 4 atmospheres, with the He diluted flame having a peak temperature of 2450 K and the $CO_2$ diluted flame having a peak temperature of 2380 K.

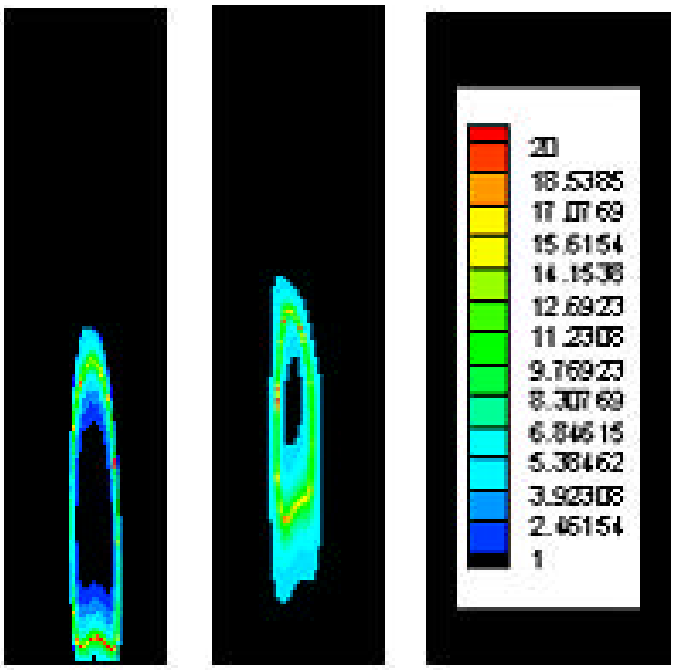


(a)

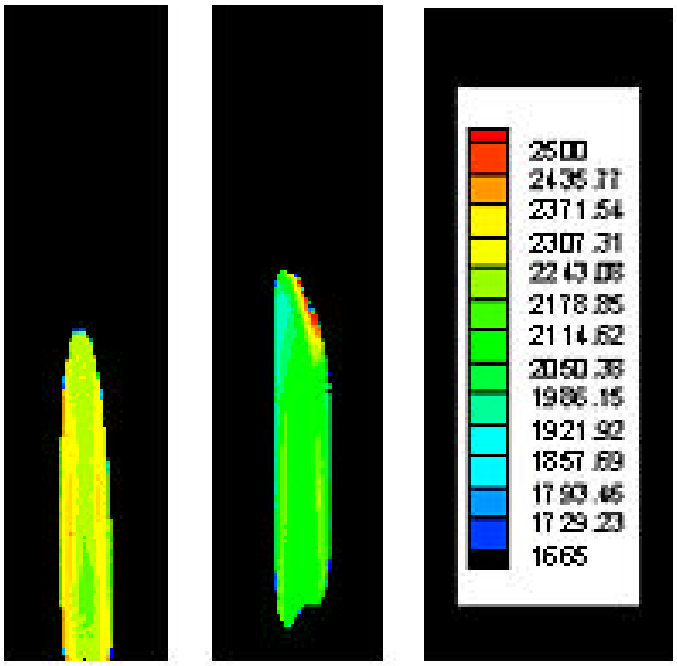


(b)

**Figure 7.9: Soot volume fraction (a), in ppm, and temperature (b), in Kelvin, profiles for He (left) and $CO_2$ (right) diluted flames at 8 atmospheres**

This is an increase of 62 K for the He diluted flame and an increase of 65 K for the $CO_2$ diluted flame from the same flames at 4 atmospheres. Therefore, overall difference in peak temperatures between the two flames has been on average 69 K for each increase in pressure, but the He diluted flame has increased peak temperature (from 1 to 8 atmospheres) 153 K, while the $CO_2$ diluted flame has increased peak temperature 137 K. In order to compare soot volume fraction values at 8 atmospheres, extinction measurements were made for both the diluted flames and plotted with the soot volume fraction from the 1 atmosphere undiluted ethylene flame, which is shown in Figure 7.10.

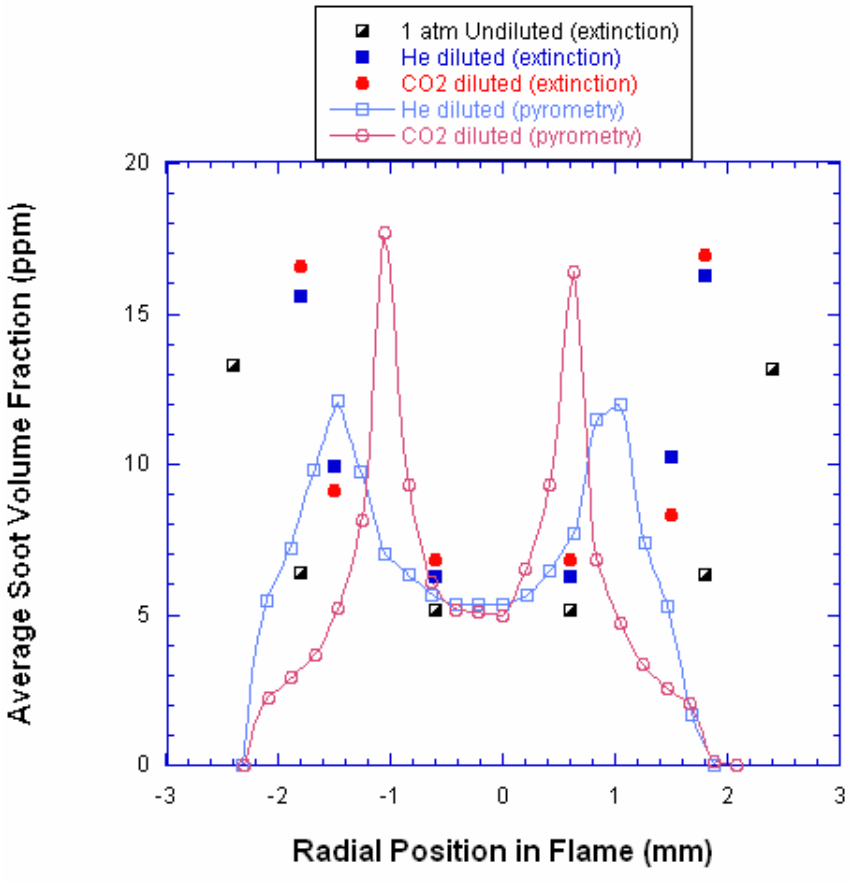


**Figure 7.10: Extinction measurements of soot volume fraction as a function of radial position at 8 atmospheres in diluted flames**

Here for the first time, at 8 atmospheres, the soot volume fractions for the diluted flames surpass the values from the undiluted ethylene flame at atmospheric pressure. The peak values from the extinction measurements agree relatively well (especially in trend) with the soot volume fraction profile peak values at 65% of the flame height, with the He diluted flame yielding 12.2 ppm (pyrometry technique) and 16.0 ppm (extinction technique) and the $CO_2$ diluted flame yielding 17.8 ppm (pyrometry technique) and 17.0 ppm (extinction technique). However, the agreement between the two techniques is not the observation that is most interesting. Here for the first time in the measurements of soot volume fraction, from

the He and $CO_2$ diluted flames, it is observed that at the wings of the flame (where the soot volume fraction has been the highest) the $CO_2$ diluted flame's soot volume fraction is greater than the He diluted flame's soot volume fraction. This is very interesting because at pressures below 8 atmospheres the peak soot volume fraction values has been in the "wings" of the flames, but at 8 atmospheres (from the pyrometry images) it is observed that the peak values occur towards the tip of the flame. Therefore, the reason that the $CO_2$ diluted flame has higher peak values at 65% of the flame height rather than the He diluted flame is that the soot volume has shifted towards the tip of the flame rather than remaining at 65% of the flame height. Achieving laminar, stable, attached flames that are diluted 80% by volume with He or $CO_2$ at elevated pressures greater than 8 atmospheres is not possible in the current burner configuration, and therefore measurements at higher pressures for comparison of the soot volume fraction trends with these two diluents were not attempted in the current investigation.

## 7.4 Soot Volume Fraction Conclusions

Measurement of temperature and soot volume fraction were made using an undiluted ethylene flame (at 1 atmosphere only) as well as He and $CO_2$ diluted ethylene flames from 1 to 8 atmospheres. Two different techniques for measuring soot volume fraction were utilized, pyrometry and extinction. With the pyrometry technique it was also possible to find temperature profiles for the flames investigated. The following observations were made through these experiments:

1. Pyrometry and extinction techniques are useful laboratory measurements for soot volume fraction and compliment each other by means of comparison and instilling confidence in the experimental data collected.

2. Soot volume fraction peak values exist at or near 65% of the flame height and near the flame's surface in the "wings" of the flame at 1 atmosphere but shifts from the "wings" of the flame toward the tip of the flame by 8 atmospheres.

3. As expected, soot volume fraction and temperature increase with increases in pressure, with He diluted flames increasing by approximately 7 ppm (peak at 65%) and 150 K (peak) from 1 to 8 atmospheres and $CO_2$ increasing by approximately 10 ppm (peak at 65%) and 135 K (peak) over the same range of pressure.

4. $CO_2$ proves to be a superior soot suppressant to He as a diluent in ethylene flames from 1 to 8 atmospheres but at 65% of the flame height at 8 atmospheres the peak values have shifted towards the tip rather than remaining in the "wings".

# 8 Investigation Conclusions

The overall goal of this investigation was to perform several individual experiments in order better understand soot production in hydrocarbon flames and to eventually analyze the applicability of the HACA soot growth mechanism at elevated pressures. Each of the experiments was completed in a co-flow diffusion flame burner, where all flames analyzed were laminar and stable. The majority of the experiments were completed utilizing ethylene, both pure and diluted (with He, $N_2$, Ar, and $CO_2$ individually), from 1 to 8 atmospheres and some experiments were completed with pure and diluted methane from 1 to 16 atmospheres.

Through several experiments within this investigation it was possible to measure the smoke point of pure and diluted ethylene and methane flames, show the effect of fuel exit velocity profile (plug versus parabolic) on a fuel's propensity to soot, show the effects of dilution, show the effect of choice of diluent (based on diffusivity, viscosity, and molecular weight), measure soot surface temperatures, analyze the major hydrocarbon species and the location of their peak concentrations, and measure soot volume fraction.

With each of these individual experiments, discussed in detail throughout the previous chapters, observations and conclusions were noted. Here the observations and conclusions of each experiment are considered together and the following overall conclusions can be drawn.

1. As pressure increases, the height of flames (where smoke is emitted) decrease and become thinner, as expected due to the increase in chemical reaction rates, but the addition of inert diluent increases the height of the flame where smoking begins.

2. When using a plug fuel exit velocity profile there is not a very pronounced effect on smoke point of the flame between use of different diluents; the most pronounced difference exist between $CO_2$ and He (which have very different diffusivities, viscosities, and molecular weights).

3. There is a noticeable difference in soot surface temperature, major hydrocarbon species concentration, and soot volume fraction when $CO_2$ and He are utilized. $CO_2$ proves to be superior to He as a soot suppressant. The concentrations of $C_2H_2$ and $C_6H_6$ (suggesting soot precursor and growth) were double and triple (respectively) the concentration in He flames than those diluted with $CO_2$ from 1 to 8 atmospheres.

4. Peak soot concentrations exist in the "wings" at approximately 65% of the flame height in flames at or slightly above 1 atmosphere, while at higher pressure (8 atmospheres) the peak concentrations exist at the tip of the flame.

5. The addition of inert diluent to the fuel stream causes not only a chemical effect but also a purely diffusion related effect, as seen in the concentrations of the $CO_2$ flame compared to the He flame, such that He diffuses out fastest of all species due to its molecular weight (lighter species diffuse out first). Furthermore, this diffusion effect does not occur in species that are heavier than $CO_2$ because by that point the $CO_2$ has diffused out. At elevated pressures, this diffusion effect is much more important as the diffusion rates increase with increases in pressure.

# 9 Future Work

It was the original intent of the current investigation to have two more phases of research including experiments to find the major non-hydrocarbon species concentrations as well as the radical species concentrations and then an overall analysis to in determine whether or not the Hydrogen Absorption Carbon Addition (HACA) mechanism is accurate at elevated pressures. These final two steps are discussed in some detail within this chapter.

## 9.1 Major Non-hydrocarbon and Radical Species Concentrations

In order to complete the analysis of the HACA mechanism it is necessary to know the concentrations of major hydrocarbon species, major non-hydrocarbon species (such as $H_2O$, CO, $CO_2$, $NO_x$, $O_3$), and the radical species (such as H, O, and OH). Therefore, the next logical phase for this investigation, to be carried out by another doctoral student, is to measure the major non-hydrocarbon species.

It has been shown by many researchers that CO, $CO_2$, $NO_x$ and $O_3$ can all be measured using gas chromatography, either directly or indirectly, with relative ease in laboratory scale experiments (Whalley et al., 2004; Klasson et al., 2003). Therefore, a method must be developed for the particular apparatus of the current investigation, but then these species concentrations can be determined using gas chromatography within the laboratory.

More difficulty is involved when measuring the concentration of $H_2O$ in the exhaust gases from flames. One technique that was mentioned for the current investigation was to

run each sample (being pulled from the flame) through a filter to catch moisture/condensation and then weight the filters to find the concentration of $H_2O$ in each sample at several locations within the flame. However, another method used by Wu and co-workers (2005) might have the capability of being scaled down to the co-flow burner used in the current investigation and yielding $H_2O$ concentrations. This method utilizes a tunable diode laser and can take concentration measurements from the "exhaust gas region above a laboratory burner" for CO and $H_2O$, as well as make temperature measurements.

With gas chromatography performing as a standard in many laboratory tests (as mentioned as being used for the above reference's experiments), it seems that most of these major species will be measured with relative ease. However, the water sampling and measurement of concentration may prove to be slightly more difficult as it seems to be a technique not used quite as often.

The more difficult, and very necessary, measurements will be those of radical species concentrations. Very few researchers have tackled these concentration measurements, and even fewer have attempted their methods at elevated pressures. Kim and Faeth (2004) were successful at measuring these species at sub-atmospheric pressures using the Lithium/Lithium Hydroxyl (Li/LiOH) Reversal Technique. The measurement of O, H, and OH radicals is accomplished by deconvoluted absorption following Li/LiOH atomic absorption. The method is explained in detail in the dissertation of Kim (2005); however, a brief explanation of the method is described here. Trace amounts of LiCl are seeded into the reactant flow and then undergoes a complete decomposition within the flame. Then a lithium hollow cathode lamp is used provide a wavelength of approximately 670 nanometers through

the flame and then the intensity of the light is measured with a photomultiplier tube. A calibration flame is used to provide the calculation of $[H]/[H]_{eq}$ as a function of height above the burner surface, and then knowing the concentration of $H_2O$ the concentration of H atom can be determined.

## 9.2 Analysis of the HACA Mechanism

The HACA mechanism is widely accepted as an explanation of soot growth in flames at atmospheric pressure. However, it has not been analyzed at elevated pressures, where most practical combustion devices operate, and a better understanding of its capabilities to predict soot growth at these higher pressures would greatly increase the pool of knowledge surrounding the combustion community. Therefore, a thorough investigation of the HACA mechanism's strengths and weaknesses at elevated pressure should take a bit of time. A great deal of data has been taken (and will continue to be taken) leading up to the analysis of the HACA mechanism and it would be a shame not to use every bit of the data to draw strong, interrelated conclusions to support or denounce its uses where it is most applicable to practical combustion devices, at elevated pressures.

# 10 References


Bento, D.S., Thomson, K.A., Gulder, O.L., "Soot formation and temperature field structure in laminar propane-air diffusion flames at elevated pressures," Combust. Flame **145**, 765-778 (2006).

Berry, T.L. and Roberts, W.L., "Measurements of smoke point in velocity-matched co-flow laminar diffusion flames with pure fuels at elevated pressures," Combust. Flame **145**, 571-578 (2006).

Boiarciuc, A., Foucher, F., Mounaim-Rousselle, C., "Soot volume fractions and primary particle size estimate by means of the simultaneous two-color-time-resolved and 2D laser-induced incandescence," Appl. Phys. B **83**, 413-421 (2006).

Burke, S.P. and Schumann, T.E.W., "Diffusion flames," Proceedings of the First and Second Symposium on Combustion, The Combustion Institute, 2-11 (c.1965).

Chang, H. and Charalampopoulos, T.T., "Determination of the wavelength dependence of refractive indices of flame soot," Proc. R. Soc. Lond. **430**, 577-591 (1990).

Cignoli, F., DeIuliis, S., Manta, V., Zizak, G., "Two-dimensional two-wavelength emission technique for soot diagnostics," Applied Optics **40**: 30, 5370-5378 (2001).

Comstock, M.L., "Diesel exhaust in the occupational setting – Current understanding of pulmonary health effects," Clinics in Lab. Med. **18** (1998).

D'Alessio, A., Beretta, F., Venitozzi, C., "Optical investigations on soot forming methane-oxygen flames, " Combust. Sci. Tech. **5**, 263 (1972).

Dai, Z. and Faeth, G.M., "Hydrodynamic suppression of soot formation in laminar co-flowing jet diffusion flames," Proceedings of the Combustion Institute **28**, 2085-2092 (2000).

Dalzell, W.H. and Sarofim, A.F., "Optical constants of soot and their application to heat-flux calculations," J. Heat Transfer **91**, 100 (1969).

DeIuliis, S., Barbini, S., Benecchi, F., Cignoli, F., Zizak, G., "Determination of the soot volume fraction in an ethylene diffusion falme by multiwavelength analysis of soot radiation," Combust. Flame **115**, 253-261 (1998).

DeIuliis, S., Migliorini, F., Cignoli, F., Zizak, G., "Peak soot temperature in laser-induced incandescence measurements," Appl. Phys. B **83**, 397-402 (2006).

Delichatsios, M.A., "A quantitative relationship between soot yield and smoke point measurements," Combust. Flame **63**, 349-358 (1986).

Drake, M.C., Correa, S.M., Pitz, R.W., Shyy, W., Fenimore, C.P., "Superequilibrium and thermal nitric oxide formation in turbulent diffusion flames," Combust. Flame **69**, 347-365 (1987).

Fischer, B.A. and Moss, J.B., "The influence of pressure on soot production and radiation in turbulent kerosene spray flames," Combust. Sci. and Tech. **138**, 43-61 (1998).

Flower, W.L., "The effect of elevated pressure on the rate of soot production in laminar diffusion flames, "Combust. Sci. and Tech. **48**, 31-43 (1986).

Flower, W.L. and Bowman, C.T., "Soot production in axisymmetric laminar diffusion flames at pressures from one to ten atmospheres," Twenty-first Symposium (International) on Combustion, The Combustion Institute, 1115-1124 (1986).

Frenklach, M., "Reaction mechanisms of soot formation in flames," Phys. Chem. Phys. **4**, 2028-2037 (2002).

Gaydon, A.G. and Wolfhard, H.G., *Flames: their structure, radiation and temperature*, 3rd ed., Chapman & Hall: London, 1970.

Glassman, I., "Soot formation in combustion processes," Twenty-second Symposium (International) on Combustion, The Combustion Institute, 295-311 (1988).

Glassman, I., *Combustion*, 3rd ed., Academic Press: Florida, 1996.

Glassman, I., "Sooting laminar diffusion flames: Effect of dilution, additives, pressure, and microgravity," Twenty-seventh Symposium (International) on Combustion, The Combustion Institute, 1589-1596 (1998).

Glassman, I. and Yaccarino, P., "The effect of oxygen concentration on sooting diffusion flames," Combust. Sci. and Tech. **24**, 107-114 (1980).

Glassman, I. and Yaccarino, P., "The temperature effect in sooting diffusion flames," Eighteenth Symposium (International) on Combustion, The Combustion Institute, 1175-1183 (1981).

Gomez, A., Sidebotham, G., Glassman, I., "Sooting Behavior in temperature-controlled laminar diffusion flames," Combust. Flame **58**, 45-57 (1984).

Gulder, O.L., Thomson, K.A., Snelling, D.R., "Effect of fuel nozzle material properties on soot formation and temperature field in coflow laminar diffusion flames," Combust. Flame **144**, 426-433 (2006).

Guo, H., Liu, F., Smallwood, G.J., Gulder, O., "A numerical study of the influence of transport properties of inert diluents on soot formation n a co-flow laminar ethylene/air diffusion flame," Twenty-ninth Symposium (International) on Combustion, The Combustion Institute, 2359-2365 (2002).

Guo, H., Liu, F., Smallwood, G.J., Gulder, O., "A numerical investigation of thermal diffusion influence on soot formation in ethylene/air diffusion flames," Int. J. Comput. Fluid Dynam. **18**:2, 139-151 (2004).

Hall, R.J. and Bonczyk, P.A., "Sooting flame thermometry using emission/absorption tomography," Applied Optics **29**:31, 4590-4598 (1990).

Heidermann, T., Jander, H., Wagner, H.G., "Soot particles in premixed $C_2H_4$-air flames at high pressures (P=30-70 bar)," Phys. Chem. Chem. Phys. **1**, 3497-3502 (1999).

Kadota, T., Hiroyasu, H., Farazandehmer, A., "Soot formation by combustion of a fuel droplet in high pressure gaseous environments," Combust. Flame **29**, 67 (1977).

Kanury, A.M., *Combustion Science and Technology, Vol. 2, Introduction to Combustion Phenomena*, Gordon and Breach, Langhorne, PA (1994).

Kennedy, I.M., Yam, C., Rapp, D.C., Santoro, R.J., "Modeling and measurements of soot and species in laminar diffusion flames," Combust. Flame **107**, 368-382 (1996).

Kent, J.H., "Quantitative relationship between soot yield and smoke point measurements," Combust. Flame **63**, 349-358 (1986).

Kim, C.H., El-Leathy, A.M., Xu, F., Faeth, G.M., "Soot surface growth and oxidation in laminar diffusion flames at pressures of 0.1-1.0 atm," Combust. Flame **136**, 191-207 (2004).

Kim, C.H., "Effects of pressure on the mechanisms of soot formation and oxidation in laminar diffusion flames," Univ. of Mich. - Ann Arbor, Dissertation (2005).

Kim, C.H., Xu, F., Faeth, G.M., "Soot surface growth and oxidation at pressures up to 8.0 atm in laminar nonpremixed and partially premixed flames," Combust. Flame **152**, 301-316 (2008).

Klasson, K.T., Jones, S.A., Walker, A.B., "Research Note: Measurement of ozone via indirect gas chromatography method," Ozone-Science and Engineering **25**:2, 155-158 (2003).

Li, Y., "Applications of transient grating spectroscopy to determine temperature and transport properties measurements in high-pressure environments," NC State Univ., Dissertation (2001).

Lin, K-C. and Faeth, G.M., "Hydrodynamic suppression of soot emissions in laminar diffusion flames," J. Prop. Power **12**:1, 10-17 (1996).

Liu, F., Guo, H., Smallwood, G.J., Gulder, O., "The chemical effects of carbon dioxide as an additive in an ethylene diffusion flame: implications for soot and $NO_x$," Combust. Flame **125**, 778-787 (2001).

McArragher, J.S. and Tan, K.J., "Soot formation at high pressure: a literature review," Combust. Sci. Tech. **5**, 257 (1972).

McCrain, L.L. and Roberts, W.L., "Soot volume fraction measurements in high pressure jet diffusion flames," Combust. Flame **140**, 60-69 (2005).

McEnally, C.S. and Pfefferle, L.D., "Comparison of non-fuel hydrocarbon concentrations measured in coflowing nonpremixed flames fueled with small hydrocarbons," Combust. Flame **117**, 362-372 (1999).

McEnally, C.S., Pfefferle, L.D., Schaffer, A.M., Long, M.B., Mohammed, R.K., Smooke, M.D., Colket, M.B., "Characterization of a coflowing methane/air non-premixed flame with computer modeling, Rayleigh-Raman imaging and on-line mass spectroscopy," Twenty-eighth Symposium (International) on Combustion, The Combustion Institute, 2063-2070 (2000).

McLintock, I.S., "The effect of various diluents on soot production in laminar ethylene diffusion flames," Combust. Flame **12**, 217-225 (1968).

Millberg, M.E., "Carbon formation in an acetylene-air diffusion flame," J. Phys. Chem. **63**, 578 (1959).

Miller, I.M. and Maahs, H.G., "High pressure flame system for pollution studies with results for methane-air diffusion flames," NASA Report No. TND-8407 (1977).

Newman, J.S. and Wiecsorek, C.J., "Chemical flame heights," Fire Safety J. 39, 375-382 (2004).

Quay, B., Lee, T-W., Ni, T., Santoro, R.J., "Spatially resolved measurements of soot volume fraction using laser-induced incandescense," Combust. Flame **97**, 384-392 (1994).

Rapp, D.C., "Soot formation: species measurements and analysis in laminar coannular diffusion flames," Penn. State Univ., Dissertation (1996).

Richter, H. and Howard, J.B., "Formation of polycyclic aromatic hydrocarbons and their growth to soot – a review of chemical reaction pathways," Prog. Energy Combust. Sci. **26**, 565-608 (2000).

Roper, F.G., "The prediction of laminar jet diffusion flame sizes: Part 1 Theoretical model," Combust. Flame **29**, 219-226 (1977).

Roper, F.G., Smith, C., Cunningham, A.C., "The prediction of laminar jet diffusion flame sizes: Part 2 Experimental verification," Combust. Flame **29**, 227-234 (1977).

Santoro, R.J., Semerjian, H.G., Dobbins, R.A., "Soot particle measurements in diffusion flames," Combust. Flame **51**:2, 203-218 (1983).

Schalla, R.L., Clark, T.P., McDonald, G.E., "Formation and combustion of smoke in laminar flames," NASA Report **1186**, 657-677 (1954).

Schalla, R.L. and McDonald, G.E., "Mechanisms of soot formation in diffusion flames," Fifth Symposium (International) on Combustion, The Combustion Institute, 316 (1955).

Scheepers, P.T.J. and Bos, R.P., "Combustion of diesel fruel from a toxicological perspective 2 toxicity," Int. Arch. Occup. Environ. Health **64**, 163-177 (1992).

Schug, K.P., Manheimer-Timnat, Y., Yaccarino, P., Glassman, I., "Sooting behavior of gaseous hydrocarbon diffusion flames and the influence of additives," Combust. Sci. Tech. **22**, 235-250 (1980).

Smooke, M.D., Long, M.B., Connelly, B.C., COlket, M.B., Hall, R.J., "Soot formation in laminar diffusion flames," Combust. Flame **143**, 613-628 (2005).

Smooke, M.D., McEnally, C.S., Pfefferle, L.D., Hall, R.J., Colket, M.B., "Computational and experimental study of soot formation in a coflow, laminar diffusion flame," Combust. Flame **117**, 117-139 (1999).

Sydbom, A., Blomberg, A., Parina, S., Stenfors, N., Sandstrom, T., Dahlem, S.E., "Health effects of diesel exhaust emissions," European Respiratory J. **17**, 733-746 (2001).

Thomson, K.A., Gulder, O.L., Weckman, E.J., Fraser, R.A., Smallwood, G.J., Snelling, D.R., "Soot concentration and temperature measurements in co-annular, nonpremixed $CH_4$/air laminar flames at pressures up to 4 MPa," Combust. Flame **140**, 222-232 (2005).

Urban, D.L., Yuan, Z.G., Sunderland, P.B., Lin, K-C., Dai, Z., Faeth, G.M., "Smoke point properties of non-buoyant round laminar jet diffusion flames," Twenty-eighth Symposium (International) on Combustion, The Combustion Institute, 1965-1972 (2000).

Wagner, H.G., ed. Siegla, D. and Smith, G., "Soot formation – an overview," *Particulate Carbon Formation During Combustion*, Plenum: New York (1981).

Whalley, L.K., Lewis, A.C., McQuaid, J.B., Purvis, R.M., Lee, J.D., Stemmler, K., Zellweger, C., Ridgeon, P., "Two high-speed portable gas chromatography systems designed fort he measurement of non-methane hydrocarbons and PAN: Results from the Jungfraujoch High Altitude Observatory," J. Environ. Monitoring **6**:3, 234-241 (2004).

Wu, Q., Thomson, M.J., Chandra, A., "Tunable diode laser measurements of CO, $H_2O$, and temperature near 1.56 microns for steelmaking furnace pollution control and energy efficiency," Metallurgical Material Transaction B-Process Metallurgy and Materials Processing Science **36**:1, 53-57 (2005).

Xu, F., El-Leathy, A.M., Kim, C.H., Faeth, G.M., "Soot surface oxidation in hydrocarbon/air diffusion flames at atmospheric pressure," Combust. Flame 132:1-2, 43-57 (2003).

# 11 Appendices

## 11.1 MATLAB Code for Two Color Pyrometry

**Main Body of Code**

```
%function[] = TStuff()

% Program to determine temperature from two images taken from different
% filters.

%  Input first image, second image and output file name:
[fname,pname] = uigetfile('*.tif', 'Select Numerator Image');
Bp = [pname,fname];
T1 = fname(1,1);
[fname,pname] = uigetfile('*.tif', 'Select Denominator Image');
Ap = [pname,fname];
[fname,pname] = uiputfile('*.dat', 'Select name to save techplot file');
Tp = [pname,fname,'.dat'];
Tp2 = [pname,fname,'Poly.dat'];

% Convert the images from unit8 to double precision:
A = double(imread(Ap));
B = double(imread(Bp));

%--------------------------------------------------------------------------
% Perform division if denominator is above threshold described below:
%--------------------------------------------------------------------------
Thresh = 50;
%--------------------------------------------------------------------------
%--------------------------------------------------------------------------
h2 = waitbar(0,'Processing...');
k = 0;
for i = 1:size(A,1)
   for j = 1:size(A,2)
      k = k + 1;
      if A(i,j) < Thresh
         R(i,j) = 0;
      else
         R(i,j) = B(i,j)/A(i,j);
      end
      if T1 == ['A'];     % Temperature determined from ratio
         R(i,j) = R(i,j)*0.4319;
         T(i,j) = -8551.5*R(i,j)^4 + 13789*R(i,j)^3 - 8097.9*R(i,j)^2 + 4885.3*R(i,j) +
802.85;
      else
```

```
            R(i,j) = R(i,j)*0.4037;
            T(i,j) = -706.74*R(i,j)^4 + 2580.8*R(i,j)^3 - 2004.1*R(i,j)^2 + 2900.2*R(i,j) +
658.83;
        end
    end
    waitbar(k/size(A,1)/size(A,2),h2);
end
close(h2);

%-----------------------Polyline----------------------------------------
%------------Specify locations for polylines (in percent of flame height):
h1 = 33;
h2 = 66;
%---------------------------------------------------------------------------
%---------------------------------------------------------------------------
D = str2double(inputdlg('Enter Pixel Displacement','Input',1,{'00'}));
% Find height of flame for placement of polyline:
for i = 1:size(R,1)
    if sum(R(i,:)) > 0
        Bs = i;
        break
    end
end
 for i = size(R,1):-1:1
    if sum(R(i,:)) > 0
        Ts = i;
        break
    end
end
H1 = (Ts-Bs) - round((Ts-Bs)*h1/100) + Bs;
H2 = (Ts-Bs) - round((Ts-Bs)*h2/100) + Bs;
%H1 = size(R,1) - (round((Ts-Bs)*h1/100) + Bs); % Position of first line
%H2 = size(R,1) - (round((Ts-Bs)*h2/100) + Bs); % position of second line

% Find left and right boundaries at first polyline y-coordinate.
for i = 1:size(R,2)
    if R(H1,i) > 0
        Ls = i;
        break
    end
end
for i = size(R,2):-1:1
    if R(H1,i) > 0
        Rs = i;
```

```
        break
    end
end
Z = floor(mean([Rs,Ls]));       % Index of zero
X = -Z+1:(size(R,2)-Z);         % Array of x-coordinate
P = [X',T(H1,:)',T(H2,:)'];     % Combined data
T = flipud(T);                  % Flip temp array for display and saving

%-------------------------------------------------------------------------
%------------------------Save Data----------------------------------------
%-------------------------------------------------------------------------

Da=1:128;Da=(Da'*Da)/128;
h3 = msgbox('Saving Data','Please Wait','custom',Da,hot(64));
T2(:,3) = reshape(T,size(T,1)*size(T,2),1);
T2(:,2) = reshape((1:size(T,1))'*ones(1,size(T,2)),size(T,1)*size(T,2),1);
T2(:,1) = reshape(ones(size(T,1),1)*(1:size(T,2)),size(T,1)*size(T,2),1);

%-------------------------2D field-----------------------------------------
fid = fopen(Tp,'w');
head = ['ZONE I=',num2str(size(T,1)),' J=',num2str(size(T,2)),' \n'];
fprintf(fid,head);
for i = 1:length(T2)
    fprintf(fid,' %5f %5f %5f \n',T2(i,1) + D,T2(i,2),T2(i,3));
end
fclose(fid);

%-------------------------Polyline Data------------------------------------
fid = fopen(Tp2,'w');
head2 = ['VARIABLES= "X", "',num2str(h1),'%%", "',num2str(h2),'%%"  \n'];
fprintf(fid,head2);
for i = 1:length(P)
    fprintf(fid,' %5f %5f %5f \n',P(i,1),P(i,2),P(i,3));
end
fclose(fid);

close(h3);
figure; contourf(T,5); colorbar;  hold on; plot(1:640,ones(1,640)*(size(R,1)-
H1),1:640,ones(1,640)*(size(R,1)-H2)); hold off;
figure; plot(P(:,1),P(:,2),P(:,1),P(:,3));
%return
```

**Sub-program for Ratio of Images**

```
function [R,T] = Tdivision(A,B,T1,Thresh)

h2 = waitbar(0,'Processing Image...');
k = 0;
for i = 1:size(A,1)
   for j = 1:size(A,2)
      k = k + 1;
      if A(i,j) < Thresh
         R(i,j) = 0;
      else
         R(i,j) = B(i,j)/A(i,j);
      end
      if T1 == ['A'];     % Temperature determined from ratio
         R(i,j) = R(i,j)*0.4319;
         T(i,j) = -8551.5*R(i,j)^4 + 13789*R(i,j)^3 - 8097.9*R(i,j)^2 + 4885.3*R(i,j) +
802.85;
      else
         R(i,j) = R(i,j)*0.4037;
         T(i,j) = -706.74*R(i,j)^4 + 2580.8*R(i,j)^3 - 2004.1*R(i,j)^2 + 2900.2*R(i,j) +
658.83;
      end
   end
   waitbar(k/size(A,1)/size(A,2),h2);
end
close(h2);
```

## 11.2 MATLAB Code for Temperature and Soot Volume Fraction

```
function[T,fv_632,fv_766,R] = SootTemp()

% Program to determine temperature from two images taken from different
% filters with the option of combining two separate positions of the images

Thresh = 35;
str = ['One';'Two'];
ImgNum = listdlg('PromptString','Select Number of Images',...
            'SelectionMode','single',...
            'ListSize',[130,40],...
            'ListString',str);
if ImgNum == 2
   D = str2double(inputdlg('Enter Pixel Displacement of Tip Image','Input',1,{'00'}));
end
if ImgNum == 1
   %  Input first image, second image and output file name:
   [fname,pname] = uigetfile('*.*','Select Numerator Image');
   Bp = [pname,fname]; cd(pname);
   T0 = fname(1,1);
   [fname,pname] = uigetfile('*.*','Select Denominator Image');
   Ap = [pname,fname];

   [fname,pname] = uiputfile('*.dat','Select name to save techplot file');
   Tp  = [pname,fname,'.dat'];
   Tp2 = [pname,fname,'Poly.dat'];

   % Convert the images from unit8 to double precision:
   A = double(imread(Ap));
   B = double(imread(Bp));

   % The denominator threshold is 160% of the mean field value:
   %Thresh = mean(mean(B))*3.0;

   %--------------------------------------------------------------------------
   % Perform division if denominator is above threshold described in 'Thresh'
   %--------------------------------------------------------------------------
   [T,fv_632,fv_766] = Tdivision(B,A,Thresh);

elseif ImgNum == 2
   [fname,pname] = uigetfile('*.*','Select Numerator of Base Image');
   Bp = [pname,fname];
   T0 = fname(1,1);
```

```
[fname,pname] = uigetfile('*.*','Select Denominator of Base Image');
Ap = [pname,fname];

% Convert the images from unit8 to double precision:
A = double(imread(Ap));
B = double(imread(Bp));

[fname,pname] = uigetfile('*.*','Select Numerator of Tip Image');
Bp = [pname,fname];
[fname,pname] = uigetfile('*.*','Select Denominator of Tip Image');
Ap = [pname,fname];

[fname,pname] = uiputfile('*.dat','Select name to save techplot file');
Tp  = [pname,fname,'.dat'];
Tp2 = [pname,fname,'Poly.dat'];

% Find the height to cut images from tip image
Olap = round((size(A,1)-D)*0.5);

% The denominator threshold is 300% of the mean field value:
%Thresh = mean(mean(B))*3.0;

% Process the base image:
[T1,fv_632_1,fv_766_1] = Tdivision(A,B,Thresh);

% Find the left side of the base image
for i = 1:size(R,2)
   if R(Olap,i) > 0
      Ls1 = i;
      break
   end
end

% Convert the images from unit8 to double precision:
A = double(imread(Ap));
B = double(imread(Bp));

% The denominator threshold is 300% of the mean field value:
%Thresh = mean(mean(B))*3.0;

% Process the tip image:
[T2,fv_632_2,fv_766_2] = Tdivision(A,B,Thresh);

% Find the left side of the tip image
```

```
    for i = 1:size(R,2)
        if R(size(A,1)-Olap,i) > 0
            Ls2 = i;
            break
        end
    end

    h2 = waitbar(0,'Combining Images...');
    T = T2;
    fv_632 = fv_632_2;
    fv_766 = fv_766_2;

    if Ls1 > Ls2
        % Base image edge is left of tip edge
        for i = 1:size(T2,1)
            if i == (size(T2,1)-Olap)
                for j = (Ls1-Ls2):size(T2,2) - (Ls1-Ls2)
                    T(i:i+size(T1(Olap:end,:),1)-1,j) = T1(Olap:end,j + (Ls1-Ls2));
                    fv_632(i:i+size(T1(Olap:end,:),1)-1,j) = fv_632_1(Olap:end,j + (Ls1-Ls2));
                    fv_766(i:i+size(T1(Olap:end,:),1)-1,j) = fv_766_1(Olap:end,j + (Ls1-Ls2));
                    waitbar(j/(size(T2,2) - (Ls1-Ls2)),h2);
                end
            end
        end
    else
        % Tip edge is left of base edge
        for i = 1:size(T2,1)
            if i == (size(T2,1)-Olap)
                for j = (Ls2-Ls1):size(T2,2) - (Ls2-Ls1)
                    k = k + 1;
                    T(i:i+size(T1(Olap:end,:),1)-1,j) = T1(Olap:end,j - (Ls2-Ls1));
                    fv_632(i:i+size(T1(Olap:end,:),1)-1,j) = fv_632_1(Olap:end,j - (Ls2-Ls1));
                    fv_766(i:i+size(T1(Olap:end,:),1)-1,j) = fv_766_1(Olap:end,j - (Ls2-Ls1));
                    waitbar(j/(size(T2,2) - (Ls1-Ls2)),h2);
                end
            end
        end
    end
    close(h2);
else
    disp('Aborted by user');
    return
end
```

```
T = flipud(T);                % Flip temp array for display and saving
fv_632 = flipud(fv_632);
fv_766 = flipud(fv_766);

%-------------------------------------------------------------------------
%-------------------------Save Data---------------------------------------
%-------------------------------------------------------------------------

Da=1:128;Da=(Da'*Da)/128;
h3 = msgbox('Saving Data','Please Wait','custom',Da,hot(64));
T3(:,3) = reshape(T,size(T,1)*size(T,2),1);
T3(:,2) = reshape((1:size(T,1))'*ones(1,size(T,2)),size(T,1)*size(T,2),1);
T3(:,1) = reshape(ones(size(T,1),1)*(1:size(T,2)),size(T,1)*size(T,2),1);
T3(:,4) = reshape(fv_632,size(T,1)*size(T,2),1);
T3(:,5) = reshape(fv_766,size(T,1)*size(T,2),1);
%-------------------------2D field-----------------------------------
fid = fopen(Tp,'w');
head = ['VARIABLES= "X", "Y", "Temp", "fv_632", "fv_766" ZONE
I=',num2str(size(T,1)),' J=',num2str(size(T,2)),' \n'];
fprintf(fid,head);
for i = 1:length(T3)
   fprintf(fid,' %5.2f %5.2f %5.2f %5.2f %5.2f\n',T3(i,1),T3(i,2),T3(i,3),T3(i,4),T3(i,5));
end
fclose(fid);

close(h3);
figure; contourf(fv_632,10); colorbar;
figure; contourf(fv_766,10); colorbar;
figure; contourf(T,5); colorbar;

return

%-------------------------------------------------------------------------
%-----------------------Temperature Subroutine----------------------------
%-------------------------------------------------------------------------

function [T,fv_632,fv_766] = Tdivision(E_632,E_766,Thresh)

% Input for flame width:
W = str2double(inputdlg('Enter Flame Width in mm','Input',1,{'00'}))*1000;

h2 = waitbar(0,'Calculating Image Ratio...');
k = 0;
for i = 1:size(E_632,1)
```

```
   for j = 1:size(E_632,2)
      k = k + 1;
      % Evaluate Ratio of images:
      if E_766(i,j) < Thresh
         R(i,j) = 0;
         E_766(i,j) = 0;
         E_632(i,j) = 0;
      else
         R(i,j) = E_632(i,j)/E_766(i,j);  %*0.4319;
      end
      if R(i,j) > 1.267
         R(i,j) = 0;
      end
      Rc(i,j) = 0.2324*R(i,j) + 0.0378;
      %Rc(i,j) = -418.92*R(i,j)^3 + 390.49*R(i,j)^2 - 119.8*R(i,j) + 12.182;

      % Temperature determined from ratio:
      T(i,j) = -8551.5*Rc(i,j)^4 + 13789*Rc(i,j)^3 - 8097.9*Rc(i,j)^2 + 4885.3*Rc(i,j) +
802.85;

   end
   waitbar(k/size(E_632,1)/size(E_632,2),h2);
end
%R = sparse(R);


% Calculate soot volume fraction (in ppm):
fv_632 = -0.147646/W*log(1-0.99*(E_632./43.66.*exp(-6.626e-34/0.632*(1/1323.15 -
1./T))))*1e6;
fv_766 = -0.184353/W*log(1-0.99*(E_766./151.02.*exp(-6.626e-34/0.766*(1/1323.15 -
1./T))))*1e6;
close(h2);

return
```

## 11.3 Quartz Chimney Modifications for Concentration Measurements

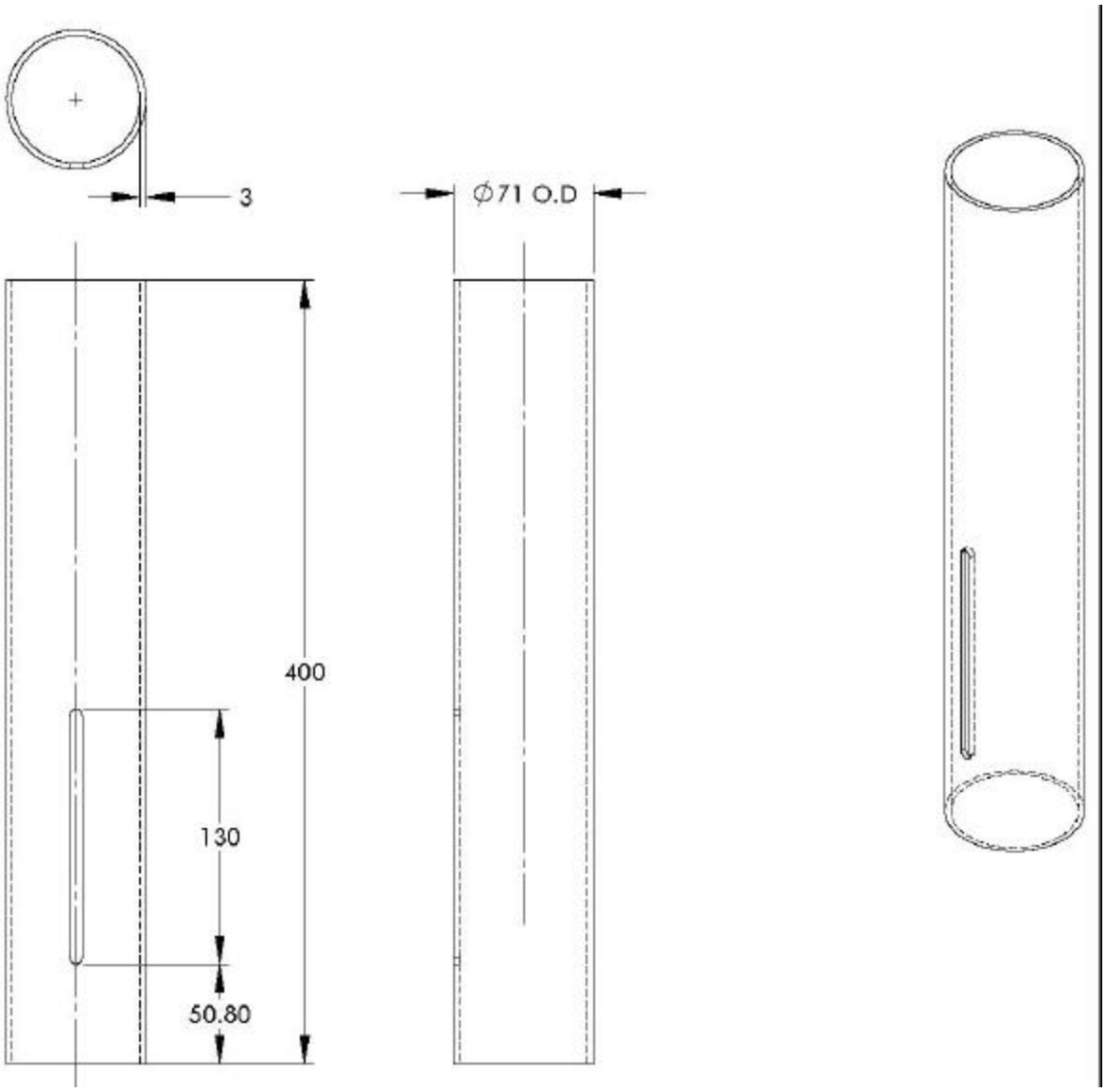

## 11.4 Quartz Sleeve for Concentration Measurements

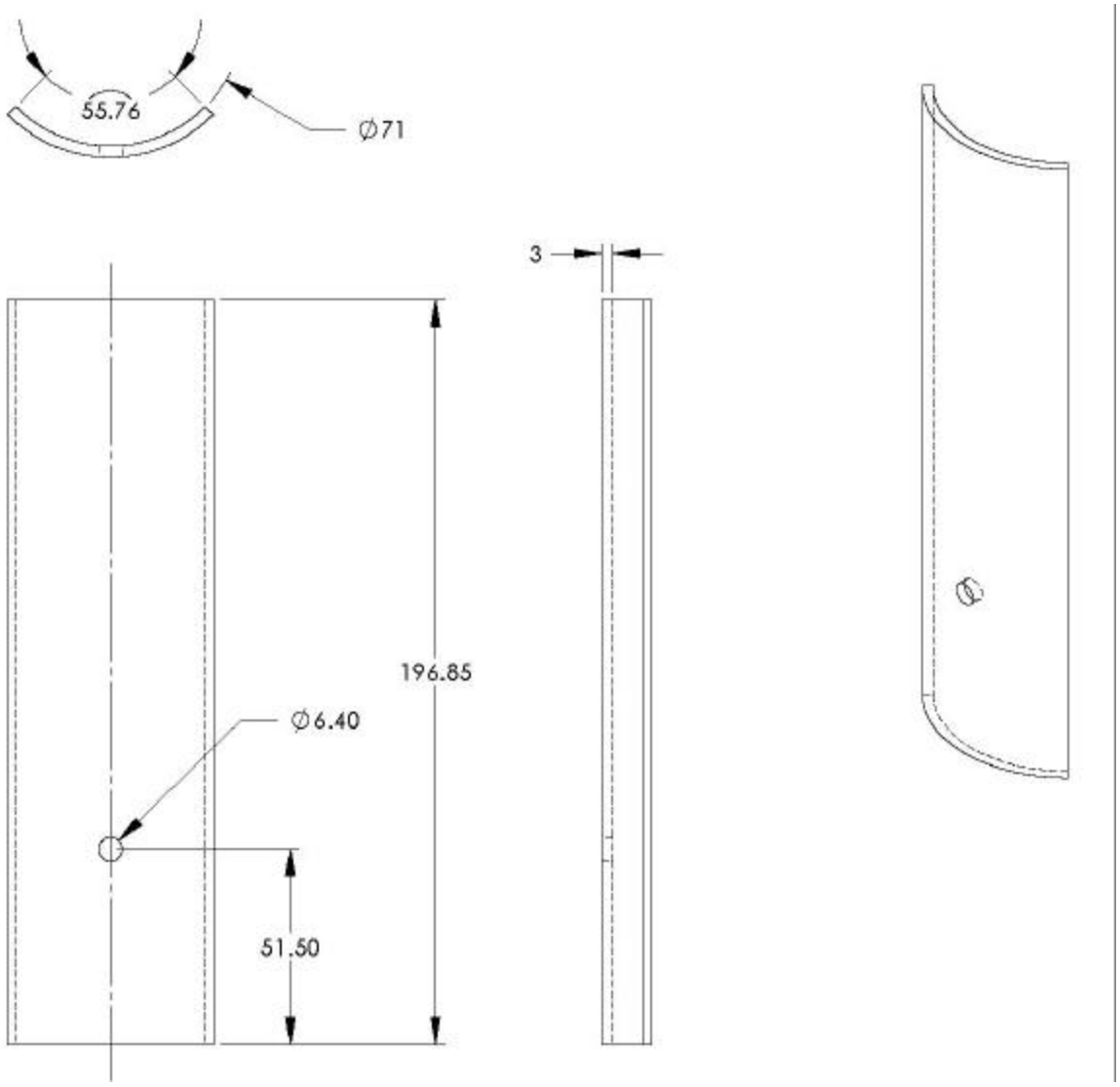

## 11.5 Threaded Rod for Microprobe Use in Pressure Vessel

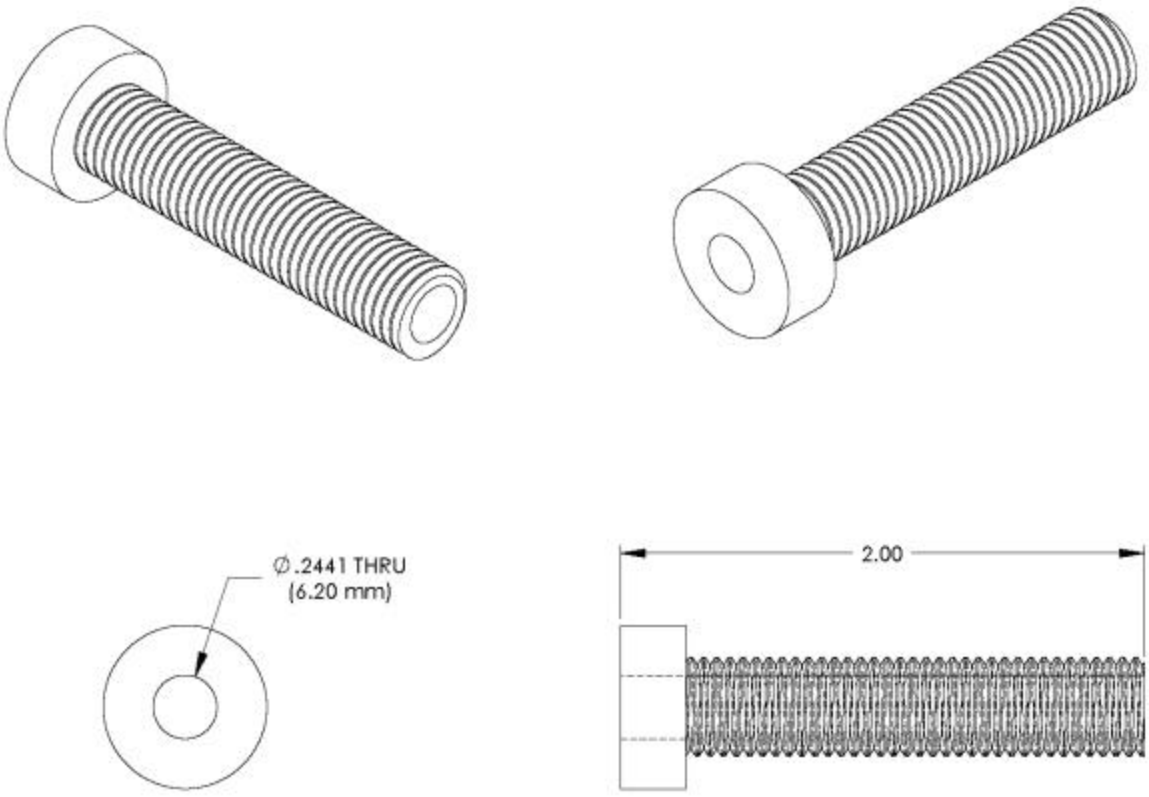

## 11.6 Quartz Chimney Modifications for Soot Volume Fraction